1-1-2001

Polymers on nanoperiodic, heterogeneous surfaces.

Lee D. Rockford
University of Massachusetts Amherst

POLYMERS ON NANOPERIODIC, HETEROGENEOUS SURFACES

A Dissertation Presented

By

LEE D. ROCKFORD

Submitted to the Graduate School of the
University of Massachusetts Amherst in partial fulfillment
of the requirements for the degree of

DOCTOR OF PHILOSOPHY

February 2001

Polymer Science and Engineering

POLYMERS ON NANOPERIODIC, HETEROGENEOUS SURFACES

A Dissertation Presented

by

LEE D. ROCKFORD

Approved as to style and content by:

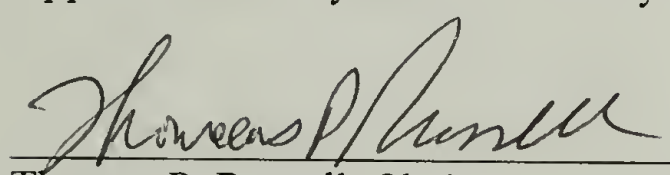

Thomas P. Russell, Chair

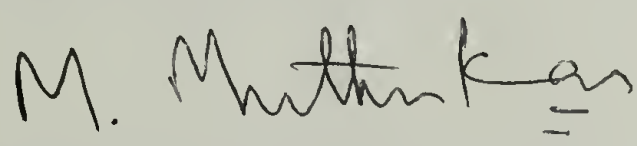

Murugappan Muthukumar, Member

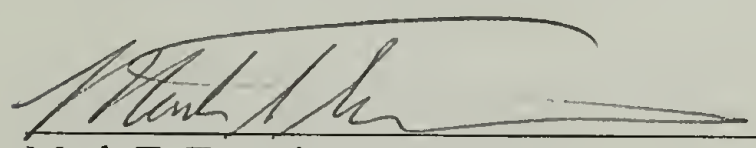

Mark T. Tuominen, Member

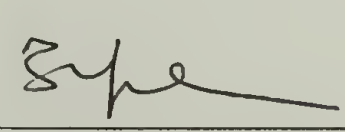

Thomas J. McCarthy, Department Head
Polymer Science and Engineering

To Julius, Bea, Izzy, and Sayde

ACKNOWLEDGEMENTS

My education at the University of Massachusetts Amherst in the Polymer Science Department has been nothing but exemplary. The faculty, students, staff, and the facilities they support and maintain are among the best I've ever had the pleasure to work with. It has made me proud every day of my graduate career to be a part of, and educated in, one of the finest polymer research facilities in the world. I would like to thank anyone and everyone who has taken the time to dedicate some part of themselves to the Polymer Science department, for their efforts have been greatly appreciated.

I would like to thank my thesis advisor Dr. Tom Russell for setting the standard. I have met few people in this world with such a complete, and at times selfless dedication to all aspects of his position. He is an advisor, a teacher, a professor, a scientist, a representative to the scientific community, a parent, a friend, and occasionally a pain in the ass. He has taught me as much by his actions as by his words, and I have benefited greatly from the experience of having him for my advisor. I would like to thank him for all of his efforts, his confidence in me and my abilities, and his unfaltering support of my work.

I would like to thank my thesis advisors Muthu and Mark Tuominen for our valuable discussions and their excellent advice, as well as their help and efforts in seeing my thesis through to completion. I've appreciated their genuine concern for not only my research but for myself, and my growth as a scientist.

Research is not a singular effort, but a collaboration of many hands and minds. I would like to thank the scientists and technicians, without which this thesis could not have been completed. I owe a great debt to Mirang Yoon for her efforts in teaching me

the finer details of facetted silicon substrate preparation, which went from hands-on instruction at MIT, to nick-of-time email support while I was locked away in the halls of the APS in Argonne. I would like to thank Dr. Simon Mochrie for his generous offer of the use of his laboratory equipment at both MIT and APS, which enabled the preparation of the facetted silicon substrates. Larry Lurio and Harold Gibson at the IMM-CAT at the APS were invaluable in helping me assemble the high vacuum chamber for substrate preparation. Elizabeth Shaw at MIT's surface analysis facility provided useful insight into the operation and interpretation of data from the Atomic Force Microscope. Christopher Stafford from UMass and Jimmy Mays from the University of Alabama at Birmingham prepared numerous block copolymer samples that were essential to my work and I thank them for their efforts. Moustafa Bal collaborated on a couple nanoscopic structures projects with me, and his E-Beam lithography efforts were a great help and I thank him for them. I would also like to thank Alan Waddon for our numerous and educational discussions about Xray experimentation, and data analysis and interpretation, as well as for hands-on assistance with maintaining the refelctometer on the Rotating Anode in the Russell Labs. Louis Raboin's FESEM experience and help has been essential in this last year of my thesis, and I appreciate his advice on sample preparation which helped me bring my work form nanoscopic to macroscopic in bright, sharp detail. Our department's sysadmin Andrew Melcuk has been extremely helpful in curing my computer ailments these past years, including my hard drive failure three chapters into this thesis, and I thank him a GB. Finally, I would like to thank Jack Hirsh not only for assistance with XPS, but for helping me bail out in rapid fashion from the numerous snafus that plague every research operation, and for showing me the generous friendship

and consideration that he nurtures with all of the students he works with in the Department.

Advisorship is not limited to professors. I've learned a great deal from our group's post doctoral fellows Paul Mansky, Yun Liu, Thomas-Thurn Albrecht, Ho-Cheol Kim, and Tobias Kerle, as well as the visiting scientists Shenda Baker and InJoo-Chin, and I've appreciated the opportunity to learn and research with them. They have demonstrated a level of scientific excellence that I've respected and aspired to. Many of the students in the department have been teachers in their own right, helping me advance my work with our discussions, and I thank them for their time and friendship. Elbert Huang and Heather Hayes have been great colleagues and even better friends, and I'm looking forward to sharing a future with them in our field of research.

This thesis is dedicated to my grandparents, whom unfortunately I can no longer thank. Without their efforts from two generations past I would not have been able to complete this work financially, and without their memory I would have not have had the inspiration to begin in the first place. I've been fortunate enough to be raised by a family that plans for its future, cares for its children, and respects and supports all of the choices they make in their lives. I have benefited from the efforts of my parents greatly, and I thank Wendy and Larry for all of their love and support and encouragement through these many years of study. I would like to thank my wife Kyra, the truest friend I have ever known, for her boundless love, encouragement, and understanding. She has made these past years of graduate school some of the best of my life, and I know the best is yet to come!

ABSTRACT

POLYMERS ON NANOPERIODIC, HETEROGENEOUS SURFACES

FEBRUARY 2001

LEE D. ROCKFORD, B.S. MASSACHUSETTS INSTITUTE OF TECHNOLOGY

M.S., UNIVERSITY OF MASSACHUSETTS AMHERST

Ph.D., UNIVERSITY OF MASSACHUSETTS AMHERST

Directed By: Professor Thomas P. Russell

Herein we establish a relationship between controlled nanoscale surface interactions and subsequent macromolecular ordering. Chemically heterogeneous striped surfaces of polar silicon oxide and non polar gold are generated over large areas, via glancing angle evaporation on facetted silicon substrates. The processing conditions required for generation of stripe widths comparable to the size of a polymer molecule are outlined. Substrates with 20-30 nm metal linewidths and 40-60 nm stripe periods are prepared.

Spin and solution casting of incompatible polymer mixtures of polystyrene (PS) and polymethylmethacrylate (PMMA) on heterogeneous surfaces are found to generate films with unique, substrate directed morphologies dependant on the kinetics of the casting process. Spin cast films posses a surface adsorbed layer of blended composition due to rapid polymer adsorption from solution, while solution cast films phase separate at the substrate/polymer interface on a molecular level. Preferential adsorption of PS to the non polar gold stripes and PMMA to polar silicon oxide stripes is observed at the substrate beneath the macroscopically phase separated domains of the blend components.

Preferential adsorption occurs over a large molecular weight range, with a molecular weight dependence on the morphology of the adsorbed polymer lines found.

Solution cast films of the symmetric copolymer poly(styrene-block-methylmethacrylate), P(S-b-MMA), on heterogeneous surfaces show lamellar microdomain orientations perpendicular to the substrate plane, parallel to the striping. Commensurability of the block copolymer and substrate stripe periods is found to be essential for producing such a surface directed morphology. The commensurability window depends inversely on the degree of confinement of the morphology, with unconfined films requiring more stringent conditions for surface directed morphology reorientation. The distance over which the orientation of the microdomains persists in thick films is found to depend on the ordering kinetics, scaling with copolymer molecular weight. Confinement effects such as tension and compression and defects in the lateral long range orientation of surface directed lamellar morphologies are observed for slightly incommensurate morphologies, with the amount of strain and defect concentration found to increase with the loss of commensurability.

TABLE OF CONTENTS

Page

ACKNOWLEDGEMENTS v

ABSTRACT viii

LIST OF TABLES xiii

LIST OF FIGURES xiv

CHAPTER

1 PREPARATION OF NANOPERIODIC, CHEMICALLY HETEROGENEOUS SURFACES 1

Introduction 1
Experimental 4

Grooved Substrates 4
Gradient Substrates 10
Substrate Metallization 11
Substrate Characterization 17

Results and Discussion 19

Reconstructed Si Substrates 19
Substrate Metallization 25

Conclusion 29
References 30

2 MORPHOLOGY OF HOMOPOLYMER BLEND THIN FILMS ON HOMOGENEOUS AND HETEROGENEOUS SURFACES 31

Introduction 31
Experimental 35

Substrates 35
Thin Film Preparation 37
Characterization 39

Results 40

Spin Cast and Annealed Films 40
Selective Solvent Etching 48

Complimentary Solvent Etching 55
Solution Casting 61

Conclusion 68
References 70

3 BLOCK COPOLYMER ULTRA THIN FILMS ON NANOPERIODIC, HETEROGENEOUS SURFACES 72

Introduction 72
Experimental 75

Substrates 75
Thin Film Preparation 76
Characterization 77

Results and Discussion 78

Surface Directed Orientation 78
Strain 89
Defects 93

New Polymer System 95
Conclusion 97
References 99

4 PROPAGATION OF NANOPATTERNED SUBSTRATE TEMPLATED ORDERING OF BLOCK COPOLYMERS IN THICK FILMS 101

Introduction 101
Experimental 103

Polymers 103
Heterogeneous Surfaces 104
Film Preparation 105
Characterization 106

Results and Discussion 106
Conclusion 118
References 119

5 SUGGESTIONS FOR FUTURE WORK 122

Introduction 122
Facetted Surfaces 122
Strength of Surface Interactions 125

Structure of Defects 127
Window of Commensurability 128
Conclusion 129
References 130

BIBLIOGRPAHPY 131

LIST OF TABLES

Table Page

1.1. Substrate and annealing parameters used for grooved substrate preparation 7

1.2. Evaporation thickness required at normal incidence to produce 1 or 2 nm thick films at incident angle θ..... 13

1.3. Summary of surface statistics derived from measurements on AFM height images of grooved substrates 20

1.4. Substrate and annealing parameters used for gradient grooved substrate preparation 20

1.5. In-situ surface temperature measurement at points indicated by the diagram on a 1.3° miscut gradient substrate during anneal..... 23

1.6. In-situ surface temperature measurement at points indicated by the diagram on a 1.1° miscut gradient substrate during anneal..... 24

1.7. Summary of metallization conditions used to prepare substrates for experiments with homopolymer blends and blocks in subsequent chapters 26

2.1. Preparation data and characterization information for substrates used in solution and spin casting experiments 37

2.2. Polymers used in thin film casting experiments 38

2.3. Fractional surface coverage area of polystyrene upon spin casting and annealing determined from image analysis of solvent etched homopolymer blend films. ... 55

3.1. Polymers used in thin film casting experiments 76

4.1. Summary of the p(S-b-MMA) copolymers used in experiments 104

LIST OF FIGURES

Figure Page

1.1. Sketch of silicon wafer as received from Semiconductor Processing Co. Crystallographic orientations are indicated by short arrow vectors 5

1.2. Orientational phase diagram for miscut Si (113) wafers 8

1.3. Plot of peak period (length Å) and corresponding wavevector as a function of annealing time 9

1.4. Schematic showing geometry of a surface (dark gray) with symmetric grooves of period l and height h 13

1.5. Stripe width of evaporated metal on symmetric grooves of 60 nm period as a function of evaporation angle 14

1.6. AFM height images of Cr metal lines evaporated from 1.5° incident angle on facetted silicon substrates 15

1.7. Schematic showing effect of decreased thickness of evaporation as a function of evaporation angle 16

1.8. AFM height images of grooved substrate in false perspective 18

1.9. Plot of measured groove period as a function of substrate width along a gradient substrate prepared from a 1.3° miscut wafer. 22

1.10. Plot of measured groove period as a function of substrate width along a gradient substrate prepared from a 1.1° miscut wafer. 24

1.11. Plot of groove peak height after Cr metallization to a normal incidence thickness equivalent measured on the crystal thickness monitor 27

1.12. Plot of groove peak height after Au metallization of a Cr lined substrate 28

2.1. Schematic of the selective solvent etching technique 36

2.2. AFM height image of PMMA thin film spin cast onto a) gold. b) silicon oxide 41

2.3. AFM height image of PS thin film spin cast onto a) silicon oxide. b) gold 43

2.4. AFM height image of PS+PMMA blend thin film spin cast onto a) silicon oxide b) gold 45

2.5. AFM height image of PS+PMMA blend thin film spin cast onto heterogeneous substrates 47

2.6. AFM height images of PS+PMMA blend thin film spin cast onto SiOx and annealed 49

2.7. AFM height images of PS+PMMA blend thin film spin cast onto gold and annealed 51

2.8. AFM height images of PS+PMMA blend thin film spin cast onto heterogeneous surfaces and annealed 53

2.9. Schematic cross-sectional morphology of spin-cast and annealed blend films on different substrates, based on initial solvent-selective etch. 54

2.10. AFM height images of SiOx and Au surfaces after a complimentary solvent etch to remove remaining polymer. 56

2.11. AFM height images of heterogeneous surfaces after initial and complimentary solvent etch to remove remaining polymer 59

2.12. Schematic cross-sectional morphology of spin-cast and annealed blend films on different substrates, as reconstructed from all solvent-selective etches 60

2.13. AFM height image of 30.3 kMw PS/27 kMw PMMA solution cast blend thin film after cyclohexane etch to remove the PS 62

2.14. AFM height images of the nm length scale heterogeneous surface morphology after blend solution casting and selective solvent etching 63

2.15. AFM height images of the PS remaining on the gold lines of the heterogeneous substrate after solution casting and acetic acid etching 65

2.16. RMS roughness of polystyrene remaining on heterogeneous surface after acetic acid etch 67

2.17. Comparison of schematic cross-sectional morphology of a) spin-cast, b) solution cast blend films on heterogeneous substrates, as reconstructed from all solvent-selective etches 67

3.1. AFM tapping mode phase images of the free surface of p(S-b-MMA) films cast from 0.1 wt% toluene solution over 30 minutes onto 52 nm heterogeneous substrates 79

3.2. AFM tapping mode phase images of the free surface of p(S-b-MMA) films cast from 0.1 wt% toluene solution over 30 minutes onto 52 nm heterogeneous substrates 80

3.3. AFM phase images of the free surface of p(S-b-MMA) 113 kMw thin films solution cast from 0.1 wt% toluene on a) SiOx. b) Au 82

3.4. Orientation function f as a function of degree of commensurability for solution cast block copolymer thin films on 52 nm heterogeneous substrates. 82

3.5. AFM tapping mode phase images of the free surface of p(S-b-MMA) films cast from 0.1 wt% toluene solution over 30 minutes onto 42 nm heterogeneous substrates. 84

3.6. AFM tapping mode phase images of the free surface of p(S-b-MMA) films cast from 0.1 wt% toluene solution over 30 minutes onto 42 nm heterogeneous substrates. 85

3.7. Orientation function f as a function of degree of comensurability for solution cast block copolymer thin films on 42 nm heterogeneous substrates 87

3.9. Block copolymer period as a function of molecular weight 90

3.10. Strain in lamellar period at free surface as a function of the degree of commensurability, δ. 92

3.11. AFM height images of common defect structures observed in the lamellar morphology of solution cast block copolymer thin films on heterogeneous surfaces 94

3.12. AFM images of 100k p(S-b-2VP) thin films solution cast from 0.1 wt% toluene onto various substrates 96

4.1. FESEM cross-sectional images of copolymers on homogeneous substrates 108

4.2. FESEM cross-sectional images of a) 53 k [δ= 0.65]. b) 73 k [δ = 0.80], on 42 nm heterogeneous surface 111

4.3. FESEM cross-sectional images of a) 84 k [δ= 0. 88]. b) 107 k [δ= 1.03], on 42 nm heterogeneous surface 112

4.4. FESEM cross-sectional images of a) 113 k [δ= 1.07]. b) 121 k [δ= 1.11], on 42 nm heterogeneous surface 113

4.5. FESEM cross-sectional images of a) 177 k [δ= 1.43]. b) 214 k [δ= 1.61], on 42 nm heterogeneous surface 114

4.6. FESEM cross-sectional images of a) 107 k, 1 μm scale bar. b) 113 k, 1 μm scale bar, on 42 nm heterogeneous surfaces 117

CHAPTER 1

PREPARATION OF NANOPERIODIC, CHEMICALLY HETEROGENEOUS SURFACES

Introduction

Surfaces and interfaces play a dominant role in affecting change in the local chain conformation and the macroscopic morphology of polymeric materials. Surface roughness or topography will perturb the chain conformation away from the lowest energy state seen in the bulk affecting its entropy[1,2], while surface chemistry results in specific interactions between local groups along the chain backbone, which can force a specific conformation of the chain at the surface[3-5]. Since both entropy and enthalpy play a role in surface control, a variety of tailored surfaces can be generated to impart a specific response from the polymer, and hence tailor the equilibrium state of the material[6,7]. To date, however, no studies have attempted to investigate the effect of molecular length scale surface heterogeneity on polymer morphology, since controlled chemical surface patterning on the nm length scale has been difficult to achieve. In this chapter we will discuss the preparation of novel, chemically heterogeneous, nanoperiodic surfaces for the study of such interfacial interactions.

Current technologies for preparing heterogeneous surfaces are limited either in feature resolution or total patterning area. Serial processes such as electron beam lithography dominate in ultimate resolution, with state of the art processes approaching 10 nm line resolution. Beam writing must be done line by line however, and large areas are time intensive to produce. To study polymer/surface interactions and morphology effectively, a surface must be large enough to span the range of polymer length scales

from molecular to micron, making any serial process unfeasible. Parallel processes such as optical lithography can generate patterns over large areas, but are limited to tenth micron features, an order of magnitude larger than the biggest synthetic linear macromolecules. To date there is no established parallel process for large area patterning of nanometer length scale chemically distinct features, which would be necessary for studying polymers on a molecular level. While combined techniques are in development, such as nanoimprint lithography, they still rely on an initial serial process for mask patterning and are consequently area limited [8]. Mochrie et. al., however, have developed a surface reconstruction technique which enables the topographic patterning of a silicon substrate with facets (grooves) having periods ranging from 10s to 1000s of nm and amplitudes from 1 to 100s of nm[9]. Combination of this process with glancing angle metal evaporation has allowed us to prepare large area surfaces with chemical heterogeneities that are periodic on molecular length scales.

Facetted silicon substrates are prepared by a high temperature anneal of a single crystal wafer with a surface that is miscut slightly from a selected, indexed cleavage plane, which results in a reorganization of the surface atoms into a low energy state. All cut crystal facets have a particular surface energy dependent on the number of unsatisfied bonds formed from cleaving a single crystal. Certain facets are so high in energy that at elevated temperatures they are in equilibrium with an arbitrarily cut surface through the lattice. Hence annealing such a particularly cut surface just below the material's melting temperature promotes enough atomic mobility to generate an atomic reorganization, and a new topography and minimum surface free energy state is achieved. This new surface state, due to the equivalence of free energy of miscut and facetted atomic planes, results

in a periodically ordered atomic structure, or facetted surface. Unlike the flattening of the surface of a polymer melt to minimize free energy, these surfaces evolve from a flat, polished face, to one striped with parallel crystal facets with a topography like an atomic staircase. Depending on the annealing temperature and the initial miscut of the surface, the period and amplitude of the facets can be varied over a large range.

The staircase, or grooved surface topography, now allows one to impart some chemical heterogeneity via a glancing angle metal evaporation whereby the grooves are shadowed by the metal. A surface consisting of alternating stripes of substrate oxide and the evaporated metal is then produced. The nature of the metal evaporated will dictate the type of interactions presented to the polymer. Choice of the appropriate evaporate such as chromium, used as an adhesion layer to the native oxide present on the facetted silicon's free surface, followed by gold, a non polar metal, produces a chemically heterogeneous polar/non polar striped surface. The appropriate choice of initial cut silicon surface to yield a grooved substrate with low amplitude, nanometer periodicity, coupled with the controlled metal evaporation, allows one to produce a surface that enables the study of the effect of molecular length scale chemical heterogeneity on polymer morphology. A simple calculation shows that the increase in groove amplitude from metallization is small enough to impart a negligible effect on polymer chain conformation, with respect to a flat surface[10].

Here we present the preparation of a variety of such heterogeneous surfaces using facetted silicon substrates with 40-60 nm periodicity and sub 1 nm amplitude, and their use in fabrication of chemically heterogeneous metallized surfaces with 4-5 nm amplitude. We present a statistical analysis of groove morphology dependent on process

conditions, and discuss attempts at experimental design for substrates with a gradient in groove period from 10s to 100s of nm continuously over a single substrate. Finally we will show the conditions necessary for appropriate metallization, and characterization of metallized surfaces.

Experimental

Grooved Substrates

Silicon wafers were purchased from Semiconductor Processing Co. with miscuts of 1.3° or 1.1° +/- 0.5° from the (113) pole towards the (001)/(-1-10) poles. Substrate front sides were mechanically polished to 6 Å RMS roughness while the backside was left rough. Samples with dimensions 1 cm x 3 cm were cleaved from the wafers as described in Figure 1.1, with the long side parallel to the major flat (-110). Chevrons ">" were inscribed on the rough side of each sample pointing towards the major flat such that the crystallographic orientation of the substrates could be identified. Prior to mounting in the vacuum chamber for annealing, the substrates were wiped clean using a lint-free fabric cloth soaked with acetone, and then again with a second cloth soaked in methanol.

The details of the sample chamber and the annealing steps required to produce the grooved surface morphology are published elsewhere [11], but an outline of the processing steps will be mentioned here for completeness. A sample was mounted in the high vacuum chamber with the electrodes attached such that the current would flow "downhill" in the direction of the miscut. Current flow would result in sample heating due to the resistivity of the silicon. The chamber was then evacuated over several hours to bring the pressure down to 10^{-9} torr through the use of heating tapes to bake-out the

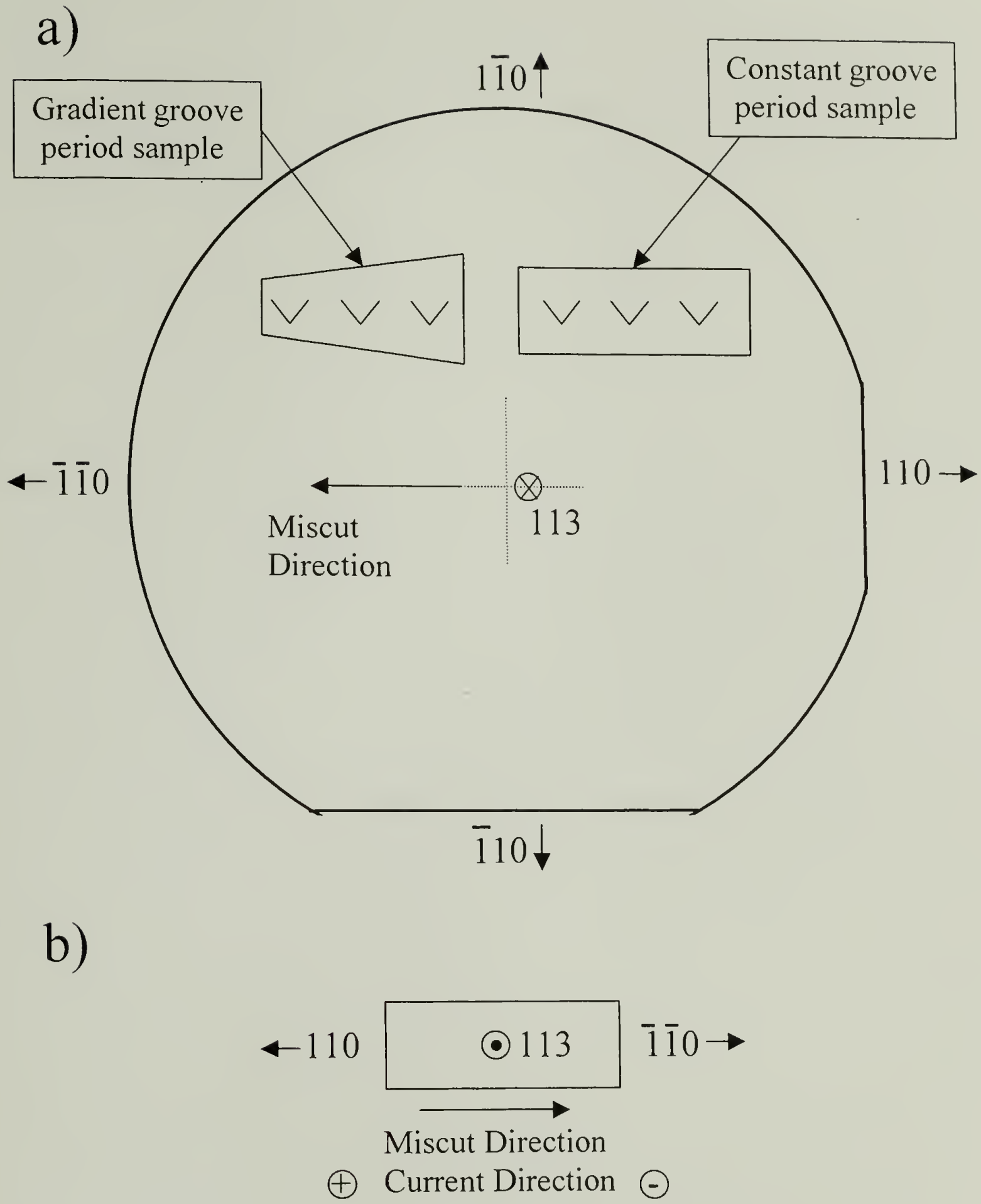

Figure 1.1. Sketch of silicon wafer as received from Semiconductor Processing Co. Crystallographic orientations are indicated by short arrow vectors. a) 1.1° miscut (113) silicon wafer back side with outline of smaller sample shapes cleaved from the wafer for annealing. Chevrons are scribed on the wafer backside to indicate the direction towards the major flat (-110). b) Front side of sample cleaved from wafer for annealing. Current flow direction during resistive heating is indicated.

chamber and a combination of a turbomolecular and ion pump. Next the sample was subjected to a sequence of processing steps, called "flashes", within the chamber to clean the silicon surface and remove the oxide layer. The sample was resistively heated via electrical current to near the melting point, or "flash" temperature of 1523° K, and held there for one minute. The sample was then quenched to 1235° K, just above the facetting point, or 'two-phase region' in the orientational phase diagram of the miscut silicon surface, shown in Figure 1.2. The surface was then slowly cooled to 1135° K, just above the triple point in the phase diagram over the course of 1.5 hours, and then brought back to 1235° K over the course of another 2 hours. The cycle was then repeated a minimum of 8 times to burn off the oxide layer and any impurities, exposing the bare silicon. The substrate temperature was measured by a calibrated optical pyrometer, a Minolta/Land Cyclops 152. After the final flash and quench to 1235°K the sample was quenched to the desired anneal temperature, for a set amount of time from 10s to 1000s of seconds. Figure 1.3 plots, for a 1.3° miscut, the substrate groove period (length λ) as a function of quench time for 2 quench temperatures as determined from Xray scattering data [12]. Upon completion of the anneal period the current was switched off, and the sample allowed to cool before removing it from the vacuum chamber. Samples were then stored in atmosphere in Fluoroware containers. The flash and anneal parameters used for the samples prepared in this study are summarized in Table 1.1. An anneal temperature of 1180° K was chosen to obtain a groove spacing of 60 nm with a 100 second quench for 1.3° miscut samples, and a groove spacing of 42 nm with a 10 second. The same temperature was used for the 1.1° miscut samples in an effort to achieve a 42 nm period with a 100 second anneal.

The 1 cm x 3 cm samples were cut into smaller pieces before metallization. 2-4 mm wide strips were cut off of the 1 cm wide edge by scribing the sample backside and breaking the strips off over a glass slide edge. 10-15 samples could be prepared from each grooved substrate in this manner. The sample backside was marked with a smaller chevron, again pointing toward the substrate major flat as a point of reference for metal evaporation.

Table 1.1. Substrate and annealing parameters used for grooved substrate preparation.

Date	Sample	Miscut Angle	Flash' Cycles	Anneal Temp ° K	Anneal Time (sec)
Oct-96	1	1.3	> 8	1180	10
	2	1.3	> 8	1180	100
	3	1.3	> 8	1185	10
Aug-97	1	1.3	> 8	1182	10
	2	1.3	> 8	1179	10
	3	1.3	> 8	gradient	10
Mar-98	1	1.3	8	1171	10
May-98	1	1.1	13	1180	10
	2	1.1	>8	1180	10
	3	1.1	>8	1180	100
	4	1.1	>8	1180	1800
	5	1.1	> 8	gradient	10
	6	1.1	> 8	gradient	1800
Oct-99	3	1.1	> 8	1180	100
	4	1.1	8	1180	100
	5	1.1	8	1180	100
	6	1.1	9	1180	100
	7	1.1	9	1180	100

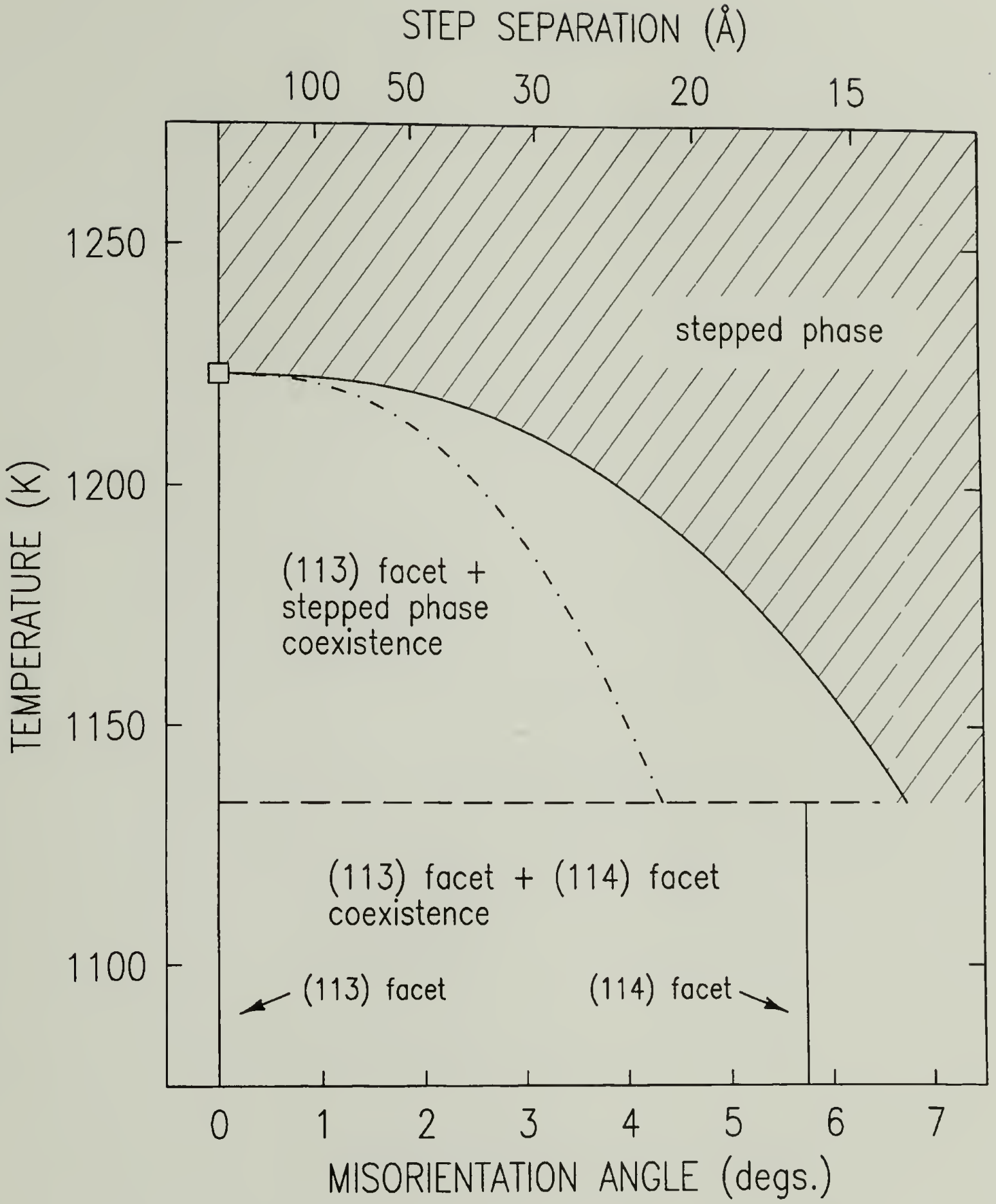

Figure 1.2. Orientational phase diagram for miscut Si (113) wafers. The 'two phase' region begins below 1225° K, the triple point is as 1134° K. Data taken courtesy of reference [12].

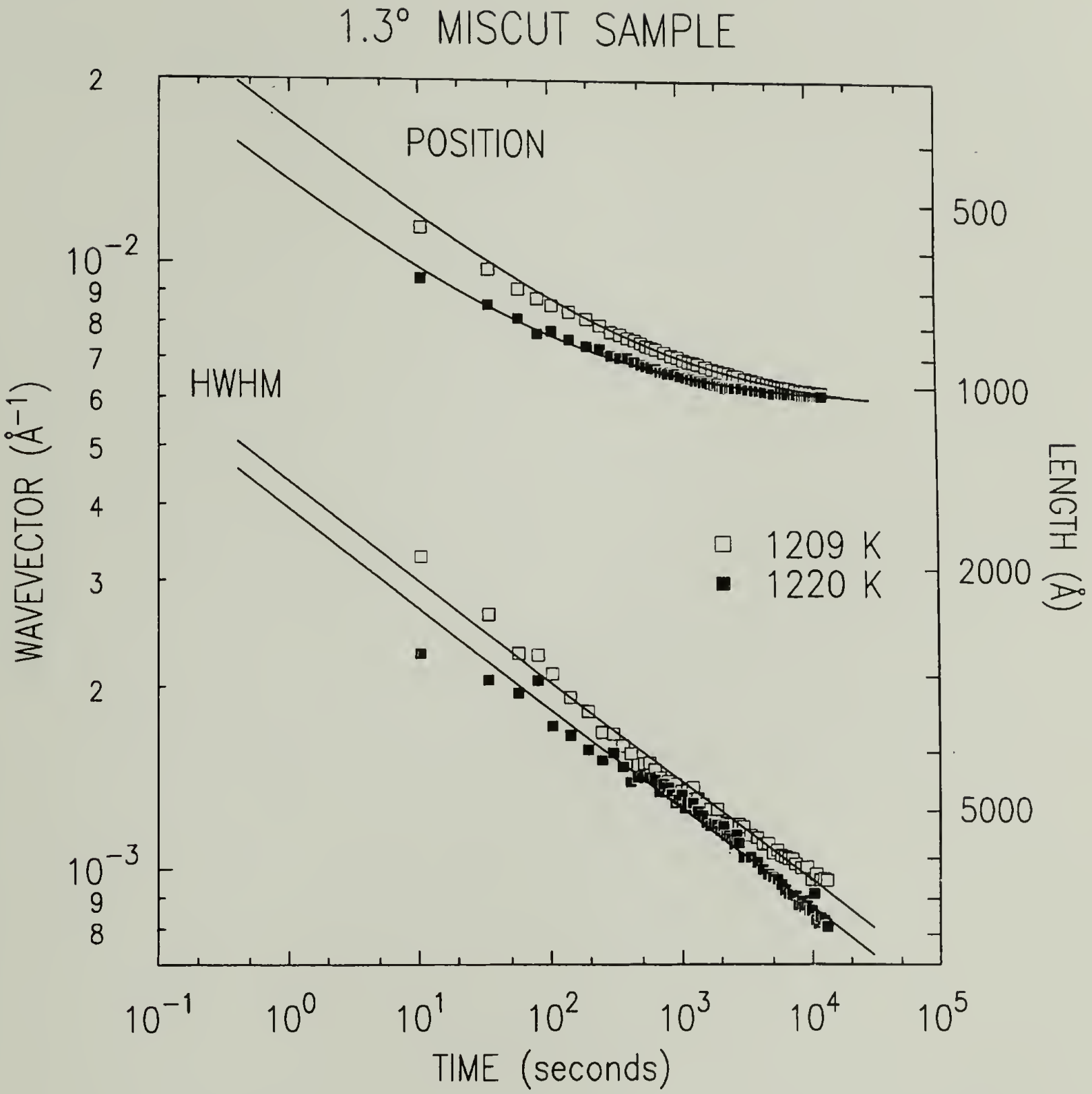

Figure 1.3. Plot of peak period (length Å) and corresponding wavevector as a function of annealing time. Measured via in situ XRay scattering on 1.3° miscut silicon substrates at two annealing temperatures, 1209, and 1220° K. Data taken courtesy of reference [12].

Gradient Substrates

Gradient surfaces were prepared in a similar fashion out of trapezoidal shaped substrates as shown in Figure 1.1. Under the UHV preparation conditions, only two modes of thermal dissipation are available to the substrate, conduction and radiation. Given the small area of contact between the sample heating electrodes and the substrate, as well at the lower thermal conductivity of the silicon semiconductor material relative to a metallic surface, thermal dissipation via infrared radiation should dominate. Therefore a larger radiating surface, given constant heat input, results in a lower surface temperature. Additionally, with constant resistivity, the larger cross-section of the substrate's wider end will heat up less per square than the narrower. These two factors contribute to the development of a thermal gradient along the length of the substrate, which could be directly correlated to an approximate groove period based on data from Song et. al.[12]. The temperature gradient was monitored in situ via optical pyrometer, and the temperature adjusted via current changes to shift the resulting range of surface period to shorter or longer wavelengths. Based on the data in Figure 1.3, a higher anneal temperature would yield a longer surface period.

Flash and anneal cycles were modified slightly to account for the surface gradient. The flash temperature was set at the narrow end, which prevented the wide end from achieving flash temperature. Flashing the wider end would have raised the narrow end above the melting temperature and destroyed the sample. Likewise, the triple point was set at the wide end to keep the entire substrate within the two-phase region in the phase diagram. Finally, the anneal temperature was set so that some region of the substrate

annealed at the 1180° K/60 nm period window, yet the narrow end was below the facetting temperature at 1225° K such that facets were sure to develop over the entire surface region.

Substrate Metallization

Samples were metallized in a dual electrode thermal evaporator (Thermionics, Inc.) with a custom substrate mount designed to vary substrate orientation with respect to the metal source. Metal sources were purchased from Electronic Space Products International (ESPI). Gold purity was quoted at 99.9999 and Chromium at 99.95. Evaporation boats were purchased from R. D. Mathis Co. Gold was evaporated from flat, 1/2" wide dimpled tungsten boats, while chromium was evaporated inside a tungsten baffled box which prevented a direct line-of-sight between the metal pellets and the substrate surface to minimize large-particle contamination of the substrate by chromium. The vacuum chamber was evacuated to a maximum of $4x10^{-6}$ torr before evaporation started. Evaporation was monitored in situ by a quartz crystal microbalance sensor (Maxtek) which was mounted in the chamber below the sample holder. The crystal sensor was water cooled to prevent thickness measurement drift that could arise from infrared radiation heating from the metal sources. The difference in path length between the evaporation source and the sensor crystal and the source and sample necessitated an ex-situ calibration measurement. Metal was evaporated on a partially shuttered flat substrate and the AFM used to measure the evaporated thickness. This value was used to correct the 'tooling factor' of the sensor crystal such that the sensor reading during evaporation indicated the actual thickness of material deposited at the sample location.

Grooved substrates were mounted such that the incident metal atoms arrived at a glancing angle to highlight only the facing facet edges. The mounting angle required for shadowing was initially determined from the geometric diagram in Figure 1.4. Assuming a symmetric groove morphology with a period λ and an amplitude h, evaporated metal atoms incident on the surface at angle θ would cover a strip of length w on the facing facets. Calculation of $w(\theta)$ for $l = 60$ nm and $h = 1$ nm is shown in Figure 1.5. From this calculation an initial substrate orientation setting of 1.5° was chosen. Because of the real asymmetry of the grooves, however, initial evaporations were done with two substrates together. Both were mounted at the same angle with the grooves running perpendicular to the incident metal atoms, but the chevron scribed on the backside of the two samples had opposite orientation. Chevrons pointing left '<' with respect to the incident metal atoms resulted in metallization of the narrower, rough stepped groove side while chevrons pointing right '>' were metallized on the wider, flat, (113) facet groove side. The diagram in Figure 1.6 describes this asymmetry in orientation and metallization. After the initial evaporation and measurement of each substrate, the appropriate angle and chevron orientation were determined empirically through a series of experiments on new substrates with varied mounting conditions to optimize stripe width and uniformity.

The thickness of evaporated metal required was determined through a similar geometric argument outlined in Figure 1.7. While the crystal sensor could be used to measure the thickness of material deposited on a flat substrate (angle = 90°) 'd', the same amount of material projected onto a surface of incident angle θ would result in a thickness 't'. Therefore to achieve the desired metallization 't' of 1 nm Cr and 2 nm Au, believed sufficient to meet the requirements of uniform chemistry and minimum

thickness perturbation, the calculated thickness d(θ) is presented in table 1.2. Again, after initial evaporation and AFM measurement of the metallized substrates, the appropriate evaporation thickness was determined empirically from this starting point.

Table 1.2. Evaporation thickness required at normal incidence to produce 1 or 2 nm thick films at incident angle θ.

incident angle θ	Cr(t) 1 nm d nm	Au(t) 2 nm d nm
0.5	114.5	229.2
1	57.2	114.5
1.5	38.2	76.4

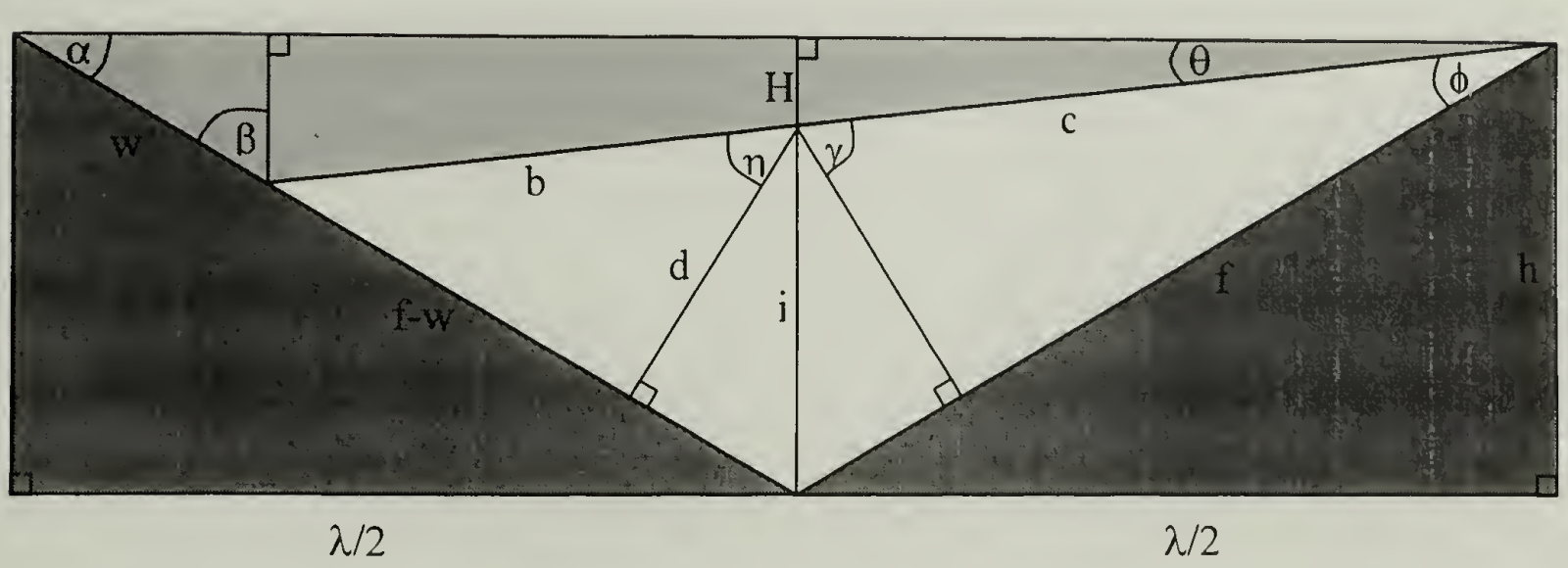

Figure 1.4. Schematic showing geometry of a surface (dark gray) with symmetric grooves of period l and height h. Metal atoms incident on surface during evaporation at an angle q from surface parallel (light gray) will deposit on a strip of width w on facing facet.

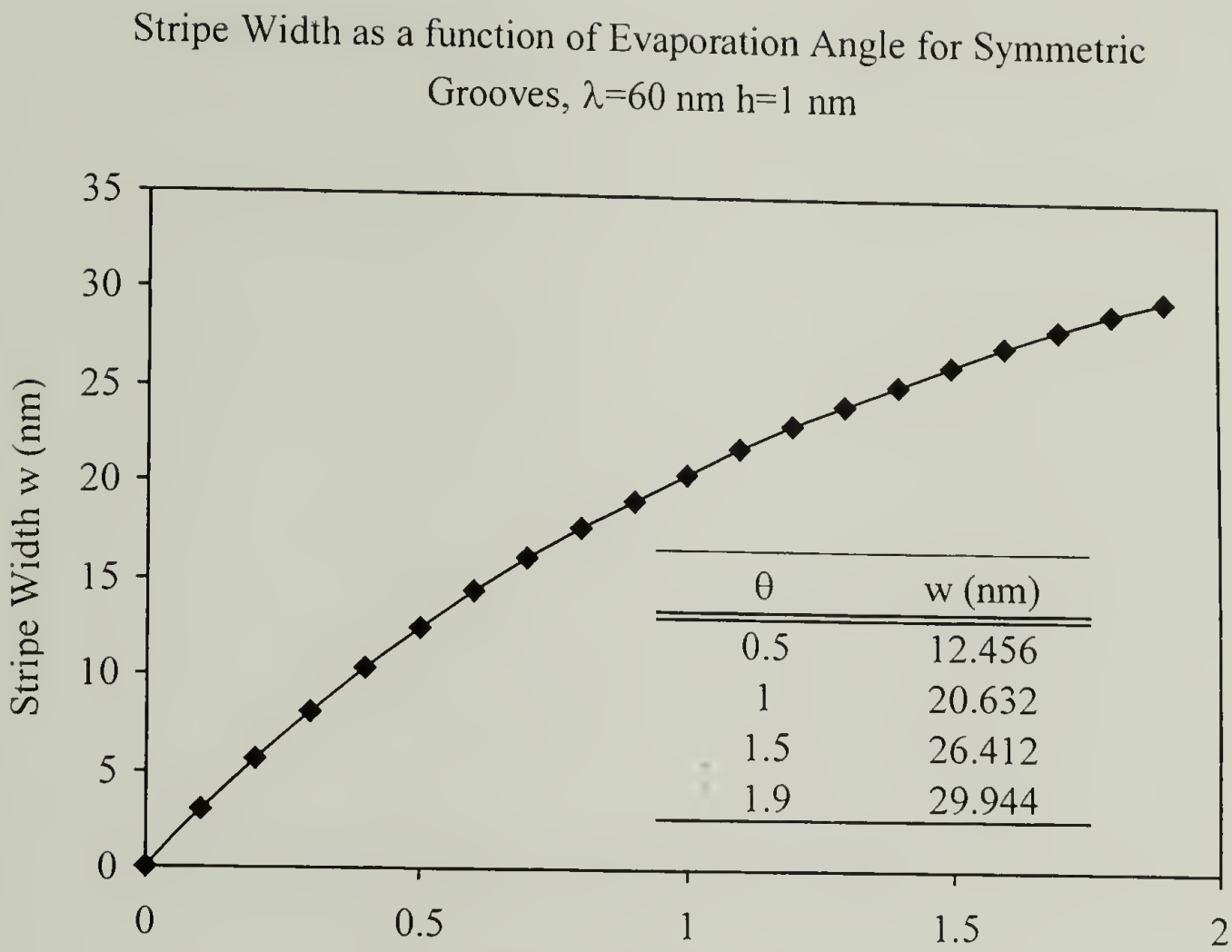

Figure 1.5. Stripe width of evaporated metal on symmetric grooves of 60 nm period as a function of evaporation angle. Inset table lists values for specific angles.

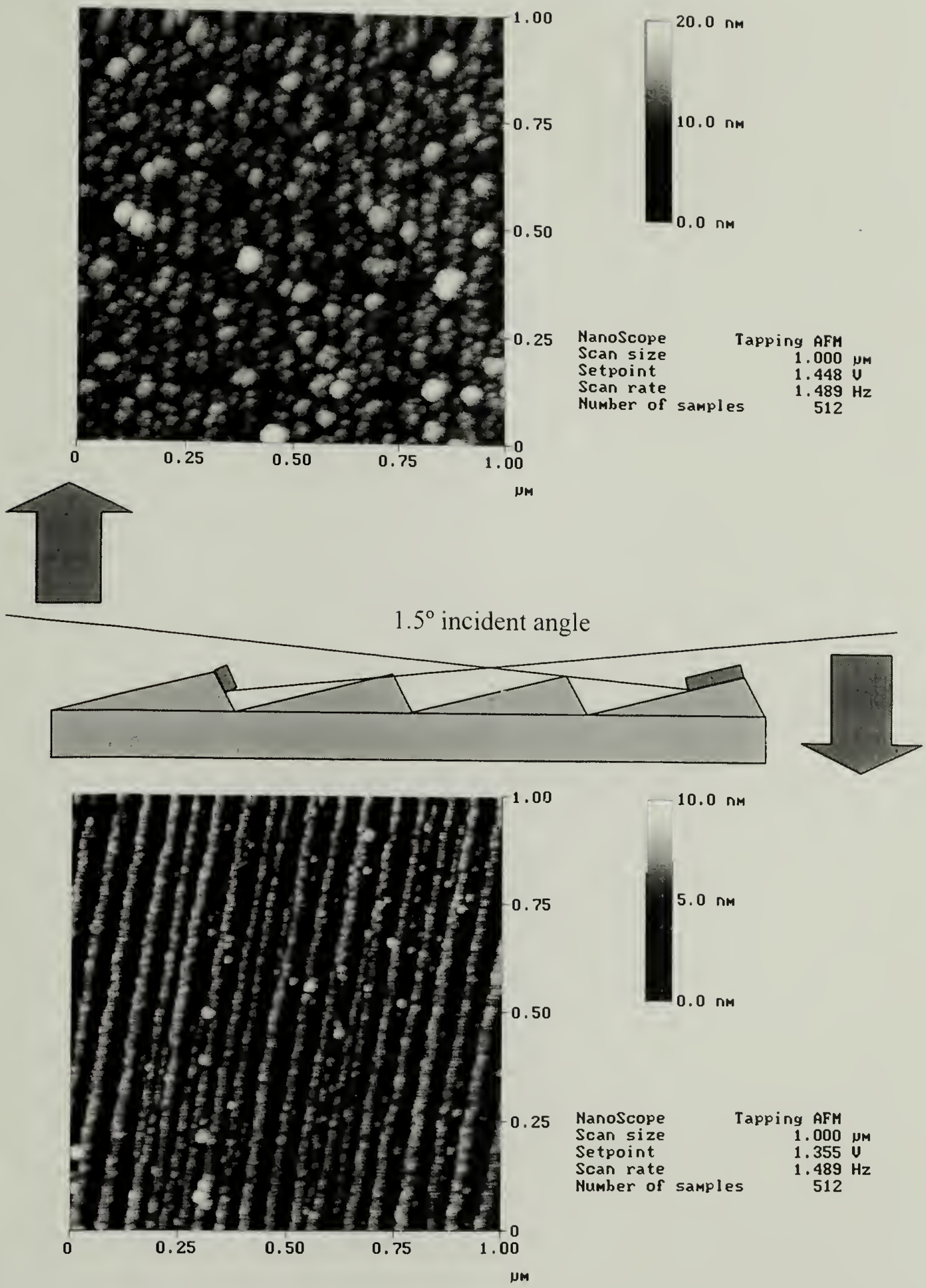

Figure 1.6. AFM height images of Cr metal lines evaporated from 1.5° incident angle on facetted silicon substrates. Facets are not symmetric resulting in stripe width differences depending on direction of incidence. Top, Cr incident on substrate with major flat (-110) pointing right, bottom, left.

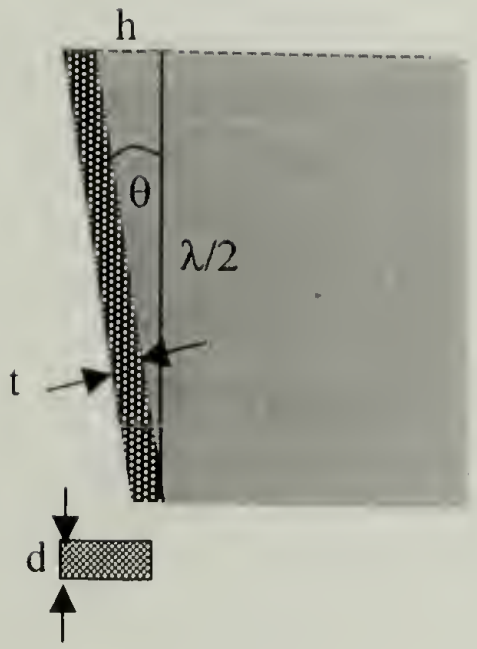

Figure 1.7. Schematic showing effect of decreased thickness of evaporation as a function of evaporation angle. A film of thickness d evaporated at normal incidence will produce a film of thickness t when the substrate is inclined at angle θ from normal.

Evaporation of Cr and Au were initially done in separate steps such that the thickness of Cr metallization could be determined independently from that of Au for a given evaporation condition. Exposure of Cr to atmosphere for AFM measurement prior to Au evaporation, however, would generate a finite degree of Cr oxidation. Au deposition on an oxide surface, whether SiOx or CrOx, results in less uniform Au lines due to nonwetting of the oxide by the gold and a beading up and surface migration of the deposited gold particles. This reduced the fidelity of the deposited lines and made the surfaces unacceptable for use in polymer experiments as truly periodic heterogeneous substrates. To take advantage of the use of Cr as an adhesion layer for Au, metal evaporation has to be done consecutively in a single vacuum evaporation step. Thus the deposited Cr is a metal, not an oxide, and favorably wet by Au to produce more uniform lines. After the appropriate conditions for individual Cr and subsequent Au evaporation were determined, all evaporations were done consecutively in one step to produce the chemically heterogeneous periodic surfaces.

Substrate Characterization

Facetted silicon substrates were characterized by tapping mode atomic force microscopy (AFM) performed on a Digital Instruments 3100 nanoscope. A typical AFM image of a 60 nm period substrate is shown in Figure 1.8. The uniformity of the grooves is apparent, as well as the fluctuation in groove period. The image shows an average groove period of 62 nm from the inset spectrum, a measure of the surface period via fast Fourier transform (FFT). The small arrowheads on the inset topography trace indicate an

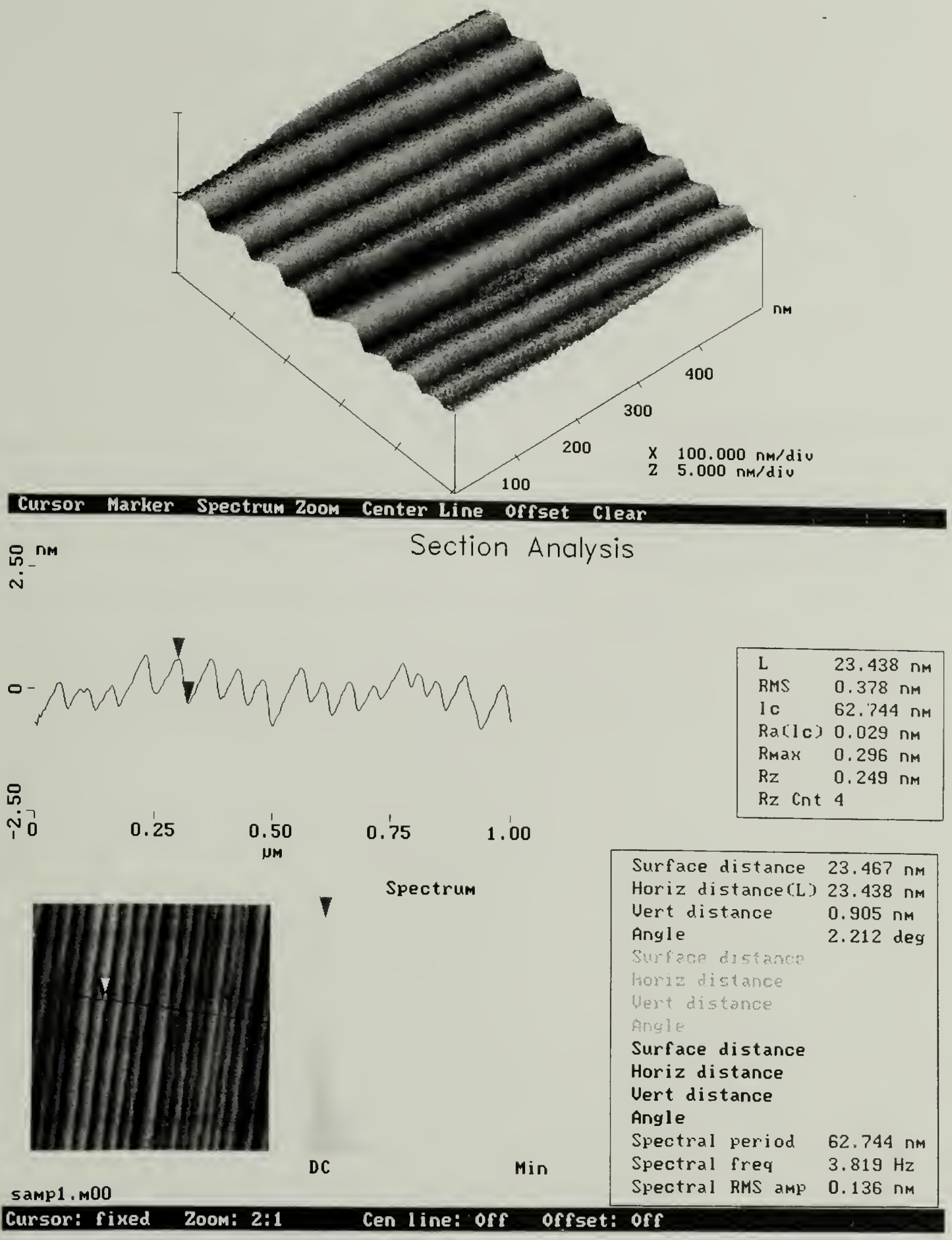

Figure 1.8. AFM height images of grooved substrate in false perspective (top) and cross-section (bottom). Cross-section shows sub nm groove height and 10s of nm groove period.

amplitude of only 0.9 nm. Thus the aspect ratio is small, and the actual roughness of the sample minute, despite the apparent amplification of the roughness from the scale of the topography trace.

Samples were imaged at different locations along the surface, and the AFM image analysis software was used to determine absolute and RMS average peak-to-peak spacing, called the substrate period, λ. From this data the standard deviation in groove period was calculated as well. The groove amplitude distribution was also measured to determine a baseline groove height that could be used in determining the enhancement of line thickness from metallization.

Metallized substrates were characterized by the same technique, and line height and width were determined. Metal line width was characterized by the full width at half maximum of the peaks measured from AFM line sections of metallized substrates.

Results and Discussion

Reconstructed Si Substrates

A summary of the groove data measured from 1.3° and 1.1° miscut substrates is presented in Table 1.3. 1.3° miscut samples produced a longer groove period, measuring approximately 52 nm on average for a 10 second anneal, and 95 nm for a 100 second anneal. 1.1° samples annealed for 100 seconds produced groove periods on average 42 nm. (Note that the data show only shorter period samples that were measured before metallization, other 1.1°/100 second samples produced slightly larger periods but were only measured post-metallization and are not included in the table.) Groove amplitude was found to decrease with groove period, ranging from 4 to 10 angstroms depending on

period. Period and amplitude distribution decreased with annealing time, in accordance with the data of Song et. al.[12].

Table 1.3. Summary of surface statistics derived from measurements on AFM height images of grooved substrates. σ indicates the standard deviation for the measurement.

Miscut Angle	Anneal Time (sec)	Period L (RMS) nm	σ (nm)	Amplitude (RMS) nm	σ (nm)
1.3	10	64.05	6.26	0.68	0.24
1.3	100	95.79	5.85	0.87	0.35
1.3	10	47.18	14.69	0.58	0.21
1.3	10	51.92	13.79	0.48	0.19
1.1	100	33.51	7.45	0.37	0.12
1.1	100	33.77	7.68	0.42	0.12
1.1	100	39.97	8.30	0.42	0.17
1.1	100	38.12	8.41	0.53	0.13

Gradient substrates were prepared from 1.3° and 1.1° miscut substrates for short and long annealing times as shown in Table 1.4. While short annealing times produced smaller groove periods, the period distribution was large, and a very long anneal time 1.1° substrate was prepared in an attempt to prepare a surface with a more uniform local groove period.

Table 1.4. Substrate and annealing parameters used for gradient grooved substrate preparation.

Sample	Miscut Angle	Flash' Cycles	Anneal Temp ° K	Anneal Time (sec)
3	1.3	> 8	gradient	10
5	1.1	> 8	gradient	10
6	1.1	> 8	gradient	1800

The in-situ surface temperature of the 1.3° miscut sample is shown in Table 1.5. Small circles on the associated diagram represent temperature measurement locations, which correlate to the row/column location in the table. Surface temperature ranged from 1180 to 1235 K. The predicted surface groove period is calculated for those temperature measurements based on the data in Figure 1.3, and ranged from 60 to 80 nm from low to high temperature. Figure 1.9 plots the results of AFM measurement of the surface period as a function of substrate width. The data points represent the average groove period measured at each location, while the error bars cover +/- one standard deviation in the measured period distribution. It is evident that the groove period distribution for any given point is much larger than any gradient in average groove period that could have developed over the length of the surface. The brief, 10 second anneal is responsible for that large period distribution, and therefore a longer anneal was designed into preparation of a 1.1° gradient sample. The line on the graph is a guide to the eye for a 20 nm average period gradient that developed over the center of the substrate. Nonuniformity in temperature at the sample edges due to thermal conduction to the sample mount and limited electrode contact area may be the reason for the deviation from this gradient at the sample edges. The measured gradient in average groove period covers both a different range (35 to 55 nm vs. 60 to 80) and a different slope than predicted from Table 1.5. Groove period was found to be larger for the wider and cooler sample region and shorter for the narrow hot region, counter to the predicted trend from previous data [12]. No explanation can be given for this result without further experimentation, which is outside the scope of this work.

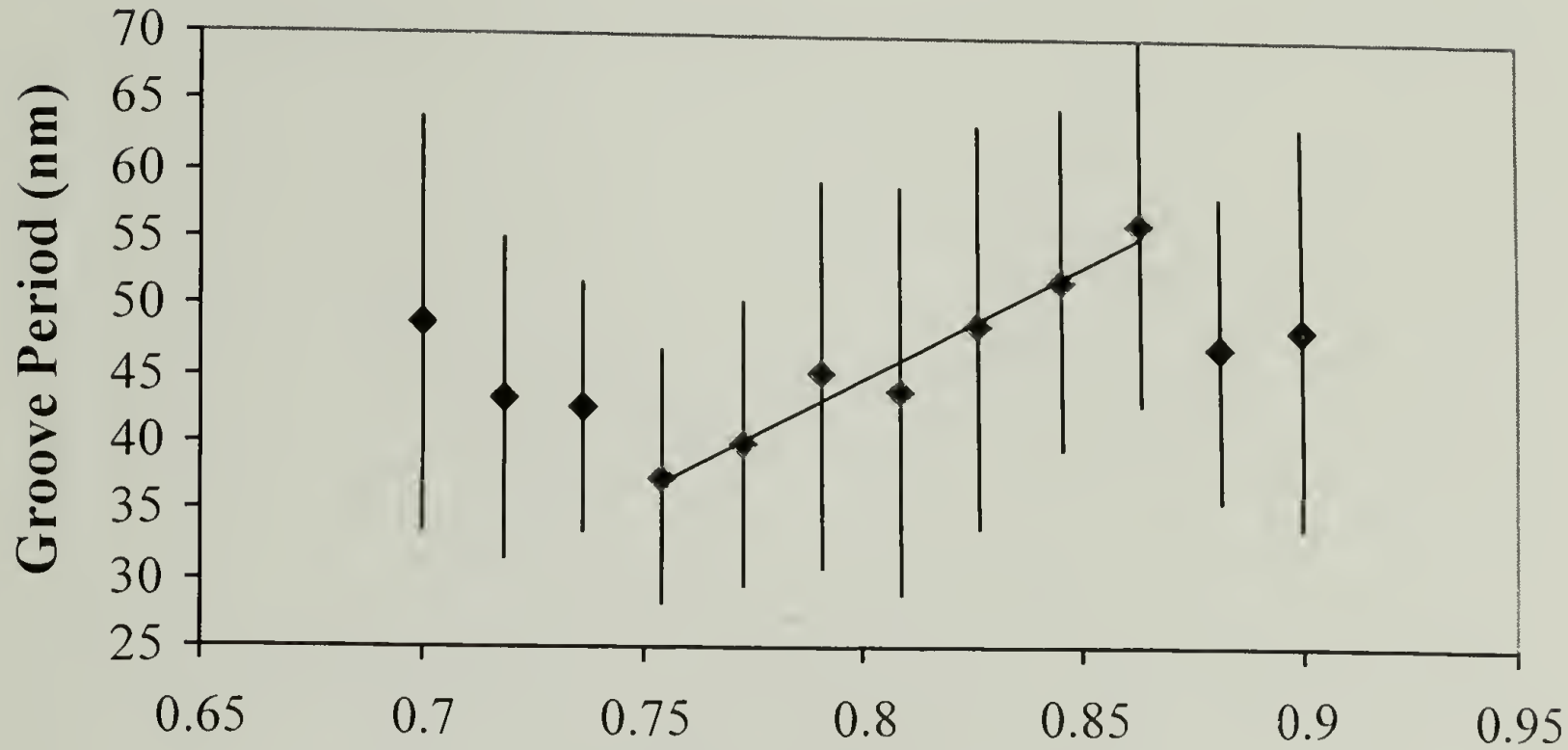

Figure 1.9. Plot of measured groove period as a function of substrate width along a gradient substrate prepared from a 1.3° miscut wafer. Line is a guide to the eye to indicate trend borne out by excluding edges from measurement. Error bars are +/- one standard deviation in groove period measured at each point.

Table 1.5. In-situ surface temperature measurement at points indicated by the diagram on a 1.3° miscut gradient substrate during anneal. Predicted surface period arising at measurement points is shown as well.

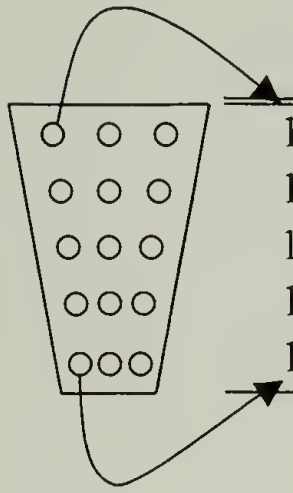

Surface Temp °K			Surface Period, nm (predicted)		
1198	1189	1168	66.04	62.21	53.28
1189	1186	1179	62.21	60.94	57.96
1194	1196	1192	64.34	65.19	63.49
1208	1212	1212	70.29	71.99	71.99
1224	1234	1235	77.09	81.35	81.77

Table 1.6 shows the measured surface temperature and predicted groove period for a 1.1° miscut sample annealed for 1800 seconds. Figure 1.10 plots the measured groove data and reveals a similar result to the 1.3° sample in spite of the extended annealing time. Groove period distribution for a given location is still much larger than the gradient in average period, and the trend in temperature dependant period is still inverse to that predicted from previous data. Additionally, a previous 10 second anneal experiment on a different 1.1 degree miscut sample produced a similar distribution in groove period at each point along the surface with no discernable gradient in period. Unfortunately, in spite of improvements made to the experimental procedure based on the initial gradient experiments, a substrate with a gradient in average groove period in excess of the local period distribution could not be produced. Further experimentation would be needed to produce such a surface.

Table 1.6. In-situ surface temperature measurement at points indicated by the diagram on a 1.1° miscut gradient substrate during anneal. Predicted surface period arising at measurement points is shown as well.

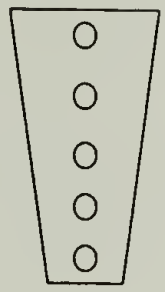

Surface Temp °K	Surface Period, nm (predicted)
1134	38.8
1155	47.8
1158	49.0
1177	57.1
1176	56.7

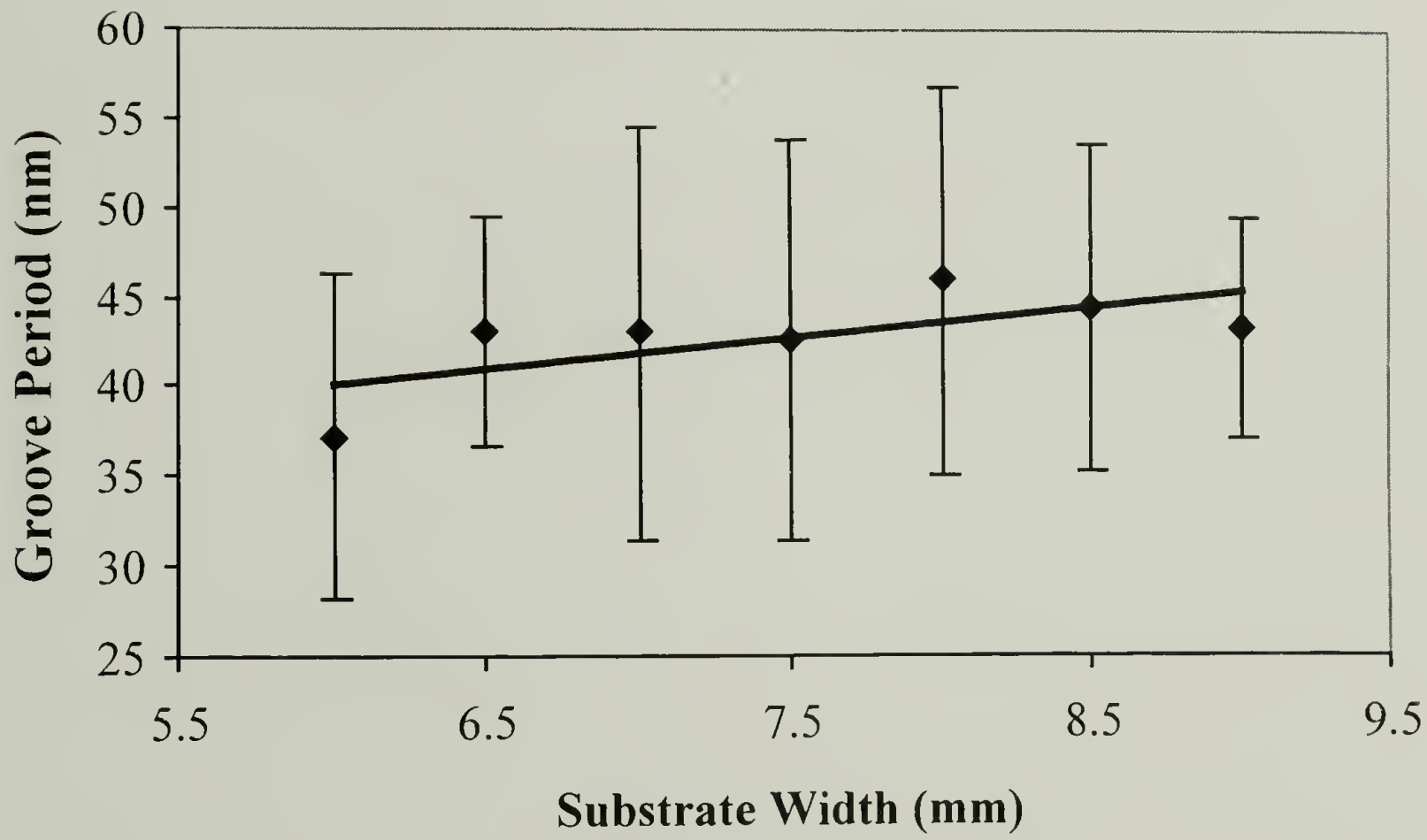

Figure 1.10. Plot of measured groove period as a function of substrate width along a gradient substrate prepared from a 1.1° miscut wafer. Line is a guide to the eye to indicate trend borne out by excluding edges from measurement. Error bars are +/- one standard deviation in groove period measured at each point.

Substrate Metallization

AFM images taken of a 60 nm substrate metallized with Cr at 1.5° as prescribed by the initial geometric calculations are shown in Figure 1.6. The top image shows the sample with a chevron-right ">" orientation, and the bottom image chevron-left "<". Due to the asymmetry in the grooves, the width of the metal stripe deposited for the different orientations varies for the single incident angle. The ">" orientation results in metal deposition on the wider (113) facet side of the groove producing wider, discontinuous metal stripes with narrow oxide channels. The "<" orientation produces narrow, continuous metal lines with distinct oxide stripes. Use of the ">" orientation would thus require prohibitively small angles to shadow a narrow enough strip to produce distinct lines, and therefore for all experiments the "<" left orientation was used.

To determine the optimum conditions for Cr metallization on a 60 nm grooved substrate, a range of incident angles and evaporated metal thicknesses were used. Figure 1.11 shows a plot of the AFM results of measurements made on these substrates. It is clear that the "<" orientation showed no strong angular dependence on groove peak height, however, AFM images on higher angles showed slightly wider lines which were preferred, and therefore 6° was used for 60 nm substrates. The amount of metal deposited was clearly the critical factor, and had to be kept in the range of 125 Å on the crystal thickness sensor such that the groove peak height remained below 1.5 nm.

Optimum Au metallization conditions were determined in a similar fashion, as shown in Figure 1.12. Again, 6° was determined as the appropriate shadowing angle, while an evaporation thickness of 175Å was found to yield an average increase in the thickness of the Cr metal lines of only 2.5 nm. Thus, periodic, distinct metal lines could

be produced with an average thickness of 4.5 nm, by consecutive deposition of 125 Å of Cr followed by 175 Å of Au at an incident angle of 6° onto a 60 nm grooved substrate.

This process was repeated for grooved substrates prepared with different miscut angles and average groove periods so that optimum conditions could be established for each substrate. Table 1.7 lists the evaporation conditions used for preparation of the heterogeneous substrates used in polymer studies described later in this thesis. For the samples shown, and all others prepared for polymer experimentation, Cr and Au were evaporated consecutively without breaking vacuum. The AFM measured characteristics after metallization as well as the peak FWHM, or average metal linewidth, are noted in the table as well. Samples with similar groove morphologies were repeatedly prepared using identical conditions.

Table 1.7. Summary of metallization conditions used to prepare substrates for experiments with homopolymer blends and blocks in subsequent chapters.

Metal	Angle	Substrate Period (nm)	Evap. Thick XTM (Å)	Avg. Peak Height (nm)	peak FWHM (nm)
Cr/Au	6	60	100/120	3.5	23.63
Cr/Au	2	40	100/125	4.35	25.70
Cr/Au	4	40	100/150	5.5	26.68

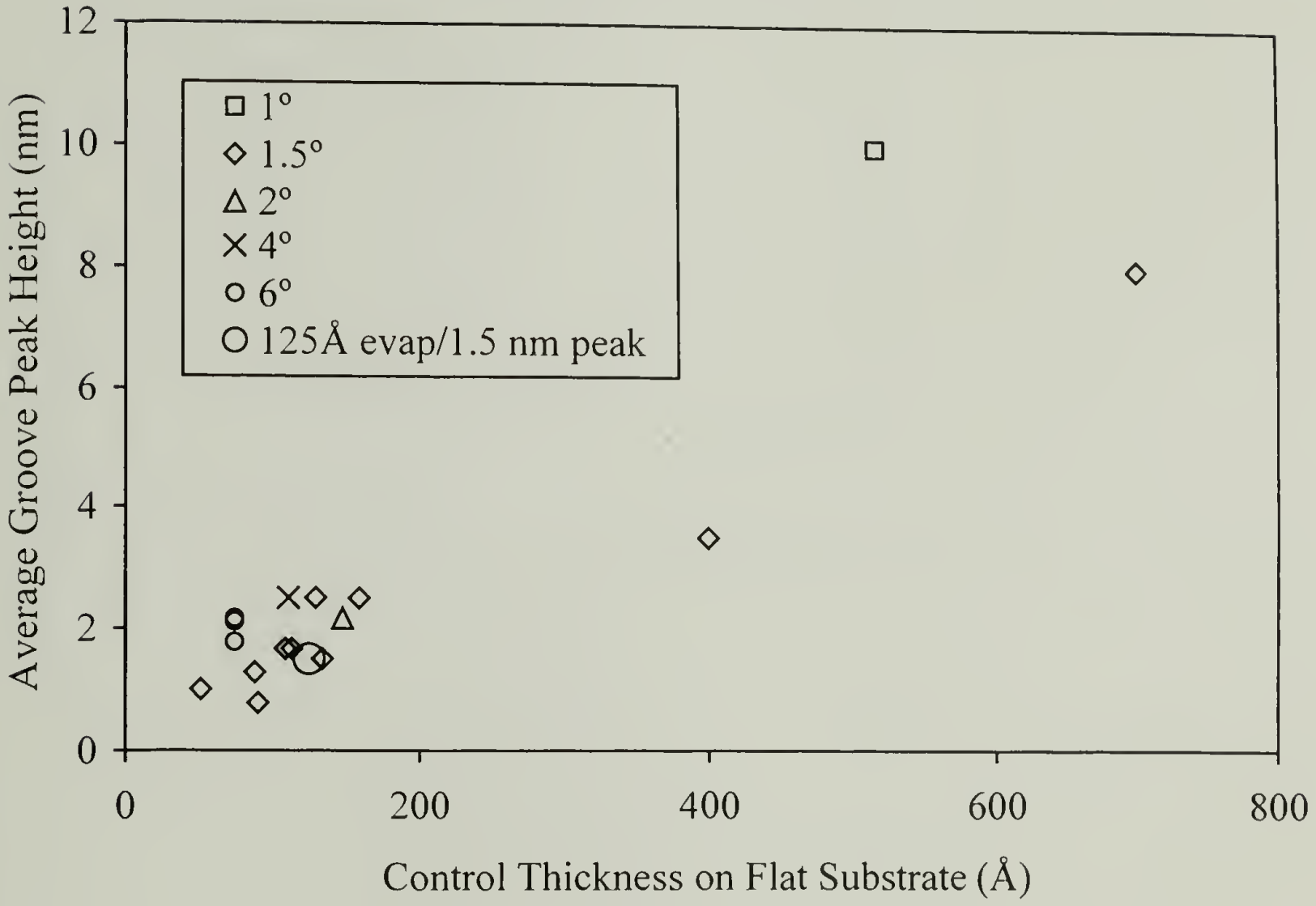

Figure 1.11. Plot of groove peak height after Cr metallization to a normal incidence thickness equivalent measured on the crystal thickness monitor. Legend indicates incident angle used for evaporation. Large circle denotes optimum evaporation conditions determined from graph.

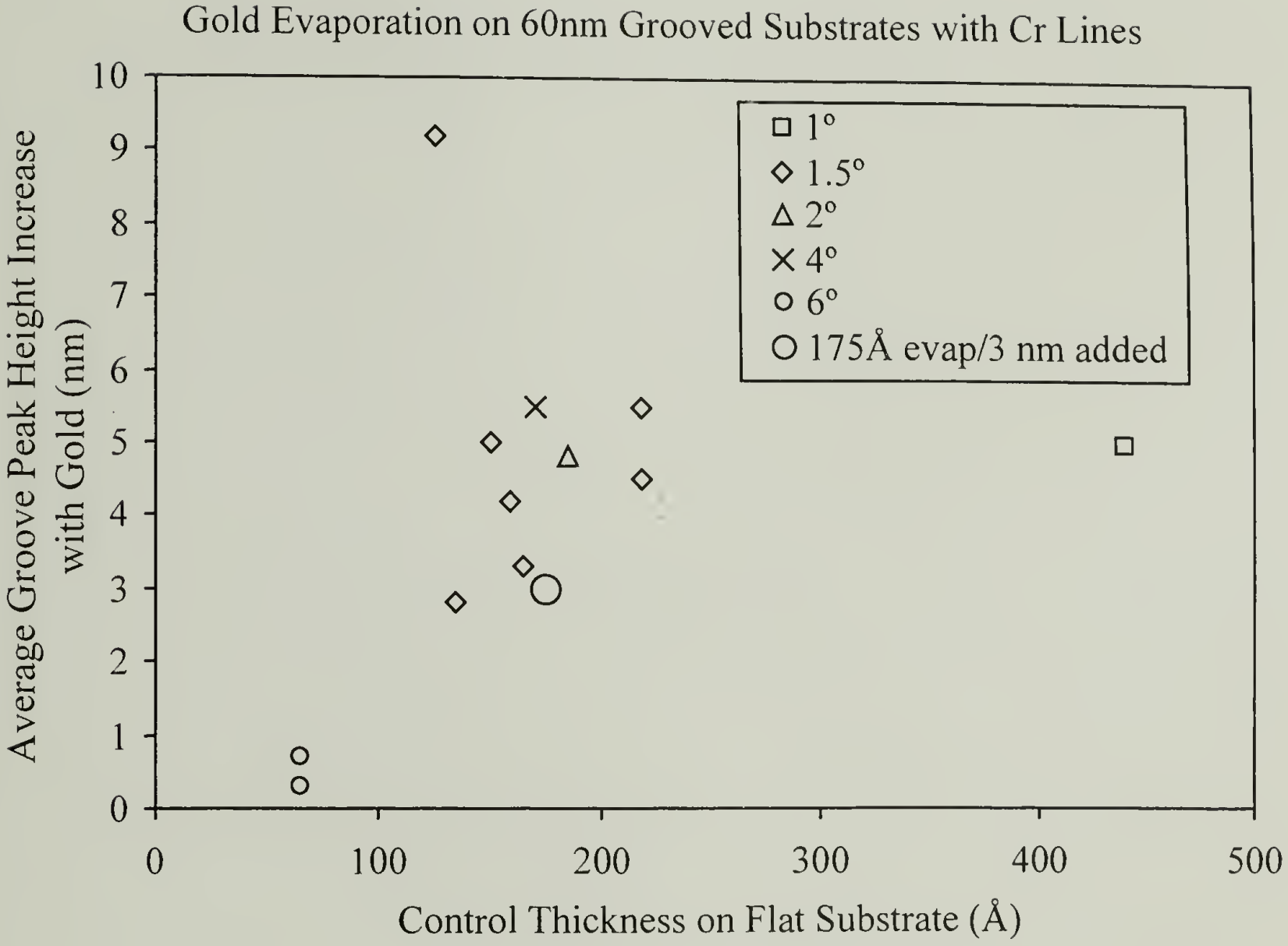

Figure 1.12. Plot of groove peak height after Au metallization of a Cr lined substrate. Au evaporation to a normal incidence thickness equivalent measured on the crystal thickness monitor. Legend indicates incident angle used for evaporation. Large circle denotes optimum evaporation conditions determined from graph.

Conclusion

Nanoperiodic, chemically heterogeneous surfaces have been prepared for use in thin film studies of polymer phase separation and morphology. The technique of surface reconstruction has been used on miscut (113) silicon wafers to generate substrates with a grooved surface topography. Grooves can be generated uniformly over a 3 cm^2 surface with 40 – 100 nm periodicity and .4 –1.0 nm amplitude, depending on the chosen preparation conditions. Groove period distribution is found to be +/- 20% of the average groove period and arises out of the need for using short annealing times to achieve small groove periods. The appropriate conditions for glancing angle metal evaporation of Cr and Au on grooved silicon have been determined, and used to prepare metal lines with an average height of 4.5 nm and linewidths of 25 nm. Substrate chemical heterogeneity thus arises from the alternation of polar SiOx and nonpolar Au on a length scale commensurate with the chain dimensions of homopolymers and the phase separated morphology of block copolymers. Grooved surfaces with a gradient in the average period have been prepared as well. However, the conditions used were not sufficient to generate a macroscopic gradient in excess of the local distribution in groove period, and consequently such substrates were not metallized for use in polymer experimentation.

References

1. Lepine, Y. & Caille, A. The Configuration of a Polymer Chain Interacting with a Plane Interface. *Canadian Journal of Physics* 56, 403-408 (1977).

2. Baumgatrner, A. & Muthukumar, M. Effect of Surface Roughness on Absorbed Polymers. *Journal of Chemical Physics* 94, 4062-4070 (1991).

3. Bijsterbosch, H. D., Cohen Stuart, M. A. & Fleer, G. J. Adsorption of Graft Copolymers onto Silica and Titania. *Macromolecules* 31, 8981-8987 (1998).

4. Lipatov, Y., Chornaya, V. & Todosijchuk, T. Adsorption from Two-Phase Solution of Polymer Blends. *Journal of Colloid and Interface Science* 188, 32-38 (1996).

5. Semenov, A. N., Bonet-Avalos, J., Johner, A. & Joanny, J. F. Adsorption of Polymer Solutions onto a Flat Surface. *Macromolecules* 29, 2179-2196 (1996).

6. Fasolka, M. J., Harris, D. J., Mayes, A. M., Yoon, M. & Mochrie, S. G. J. Observed Substrate Topography-Mediated Lateral Patterning of Diblock Copolymer Films. *Physical Review Letters* 79, 3018-3021 (1997).

7. Böltau , M., Walheim, S., Mlynek, J., Krausch, G. & Steiner, U. Surface Induced Structure Formation of Polymer Blends on Patterned Substrates. *Nature* 391 (1998).

8. Chou, S. Y., Krauss, P. R. & Renstrom, P. J. Nanoimprint Lithography. *Journal of Vacuum Science Technology B* 14, 4129-4133 (1996).

9. Mochrie, S. G. J., Song, S., Yoon, M., Abernathy, D. L. & Stephenson, G. B. Facetting of Stepped Silicon (113) Surfaces: Self Assembly of Nanoscale Gratings. *Physica B, Condensed Matter* 221, 105-125 (1996).

10. Pickett, G. T., Witten, T. A. & Nagel, S. R. Equilibrium Surface Orientation of Lamellae. *Macromolecules* 26, 3194-3199 (1993).

11. Yoon, M., Mochrie, S. G. J., Tate, M. W., Gruner, S. M. & Eikenberry, E. F. Periodic Facetting of a Si (113) surface miscut towards (1-10). *Surface Science* 411, 70-85 (1998).

12. Song, S., Mochrie, S. G. J. & Stephenson, G. B. Facetting Kinetics of Stepped Si(113) Surfaces: A Time-Resolved X-Ray Scattering Study. *Physical Review Letters* 74, 5240-5243 (1995).

CHAPTER 2

MORPHOLOGY OF HOMOPOLYMER BLEND THIN FILMS ON HOMOGENEOUS AND HETEROGENEOUS SURFACES

Introduction

The study of polymer thin film morphology generated by various processing conditions such as solution casting, spin casting, and annealing, has great relevance to technological applications requiring both processing speed and control over thin film structure. Polymer thin films used in microlithography, optical[1,2], and material applications[3] require a component of thin film processing for their production. These films possess specific functionalities, chemistries, and structures on a variety of length scales, and knowledge of the processing conditions required to generate a given film morphology is essential. Consequently, numerous studies have investigated the morphology of spin cast films produced from homopolymer[4] and blend films[1], the effect of phase separation on spin cast morphologies[5], the effect of surface chemistry[6], and the equilibrium morphology of these films generated after annealing[7,8].

Spin casting is a common technique used for rapidly generating homopolymer films of uniform thickness over large areas from dilute solution. It is a highly non equilibrium process, however, as solvent evaporation during spinning causes continual changes in both solution concentration and temperature. The rapid material flow and collapse can also result in non Gaussian chain conformations which require an annealing step to relax out[4]. Solution-substrate interfacial energies dominate at low polymer concentrations, enabling a polymer with an unfavorable substrate interaction to be spin coated from a solvent that favorably wets the spinning substrate[1]. Polystyrene (PS) spin

coated from a toluene solution onto a silicon wafer is a typical example. While a uniform film can be prepared from spin casting, subsequent annealing of the PS film above the glass transition results in dewetting, due to unfavorable interactions with the substrate's native oxide layer[9,10]. Likewise, dewet structures can arise during spin casting from unfavorable solvent-surface interactions. When dewetting occurs concurrently with the spinning process, the morphology of the film produced can be highly discontinuous. Small domains remain in a mosaic pattern after all solvent has evaporated, having become glassy before the flowing polymer solution is ejected from the spinning surface.

The morphology of spin cast homopolymer blend solutions is even more complex due to phase separation, which occurs during film formation. As solvent evaporates during spinning, the screening of unfavorable polymer-polymer interactions is reduced to the point where spinodal phase separation occurs. The phases formed can have different viscosities due to differences in molecular weight or preferential solvency, as well as different surface and interfacial energies[1]. When the surface and interfacial energies of the phase separated domains are similar, the resulting film morphology is directed solely by the spinodal phase separation process. Interconnected domains of both polymers, microns in size, extend from the substrate to the film's free surface. Preferential solvency of one phase however, may lead to asymmetry in the final morphology with the more highly solvated component composing the matrix or major phase, with both components remaining present at the substrate and free surface. Increasing the difference in surface energy between the two solutions can result in either subsumed or exposed domains of one phase at the air surface, while similar differences in interfacial energy between solution and substrate can dictate the fraction of polymer present at the substrate. Thus, a

wide range of morphologies driven by competing energies and solvency can develop in these heterogeneous polymer systems.

Studies by Walheim and Böltau on the morphology of spin cast blend films on homogeneous and heterogeneous surfaces exemplify the control over morphology one can obtain through tailored polymer solution/surface interaction[6]. Böltau showed that chemically patterning a substrate in two dimensions on the micron length scale could direct the final phase separated morphology of a spin cast film explicitly, by coupling the natural length scale of spinodal phase separation with preferential solution/substrate interactions. Fukunaga et. al. showed that randomly chemically patterned surfaces with nanometer length scales could be used to significantly reduce the lateral dimensions of phase separated domains upon spin casting[11]. Preferential solution-surface interactions interfered with coarsening during the spinodal phase separation process by pinning concentration fluctuations on shorter length scales, reducing the overall domain sizes in spin cast films. The final domain sizes, however, while smaller than those occurring on non patterned surfaces, were still far larger than the substrate's patterned length scale. The process of spinodal phase separation, which precludes the generation of concentration fluctuations on nm length scales for high molecular weight polymers, is likely the limiting factor in miniaturizing domain size.

As an alternative to spin casting for thin film preparation, dilute solution casting can be a more controlled process. Due to the significantly reduced time scale of adsorption versus phase separation as a means to generate concentration fluctuations, as well as the tunable rate of solvent evaporation[12,13], the conformation of chains at the substrate can possess a structure closer to equilibrium. In dilute solution, chains have

ample time to recognize surface chemistry and organize according to preferential interactions[14,15]. Subsequent collapse of the adsorbed layer by adding a non solvent to the system or evaporating the solvent that is present will not perturb the relative chain concentrations at the interface, when adsorption from a blend solution is performed. High solvent evaporation rates can lead to free surface roughness, however, and preferential solvency among the phase separated domains will still dictate the structure of the free surface morphology[16].

Here we have prepared homopolymer and blend films on homogeneous and heterogeneous substrates by both spin and solution casting routes to compare the two techniques from the standpoint of preferential length scales and surface interactions. With the natural length scale of phase separation in spin casting being of order microns, yet that of adsorption from solution casting being of molecular order, substrate heterogeneity on a molecular length scale should result in a distinct film morphology dependent on the casting process. Heterogeneous surfaces have been prepared, composed of polar/non polar stripes of silicon oxide and gold, by glancing angle metal evaporation on facetted (113) silicon substrates[17,18]. The stripes are nearly symmetric in width, with an average periodicity of 52 nm. Hence the substrate periodicity is two orders of magnitude smaller than the natural length scale of polymer blend phase separation, yet is of order the size of the radius of gyration of linear macromolecules in solution. Polystyrene and polymethylmethacrylate (PMMA) will serve as the model polymers for these experiments, as previous work has shown that PS interacts favorably with a non polar gold surface, while PMMA wets the polar native oxide layer of a silicon substrate[10,19,20].

Characterization of blend morphology in the thin films will be facilitated by a selective solvent etch process. While films will be spun from toluene, a favorable solvent for both polymers, acetic acid and cyclohexane will be used to etch PMMA and PS, respectively. Rinsing cast films in selective solvents will remove the domains from one phase, leaving the domains of the unsolvated phase in relief, as shown in Figure 2.1. This will allow explicit identification of the size and distribution of both phases. Rinsing off upper surface phases will also expose buried interfaces and domains, allowing characterization of the domain morphology at the substrate. Thus a complete cross sectional morphology of the cast films can be reconstructed by piecing together images, and an effective comparison made of the morphologies generated by different casting processes.

Experimental

Substrates

Homogeneous silicon substrates were purchased from Semiconductor Processing and used as-received if new, or if used, cleaned in sulfuric acid and nochromix, followed by a deionized water rinse and isopropanol reflux. Substrate cleanliness was monitored by ellipsometry to confirm the absence of surface contamination. A value of the ellipsometric parameter Δ greater than 172.8 was required. Silicon substrates were cleaned in bulk, and stored in Fluoroware containers prior to use. Homogeneous gold substrates were prepared from silicon wafers by metal evaporation in a thermal evaporator (Thermionics Inc.). Chromium was evaporated first, as an adhesion layer to

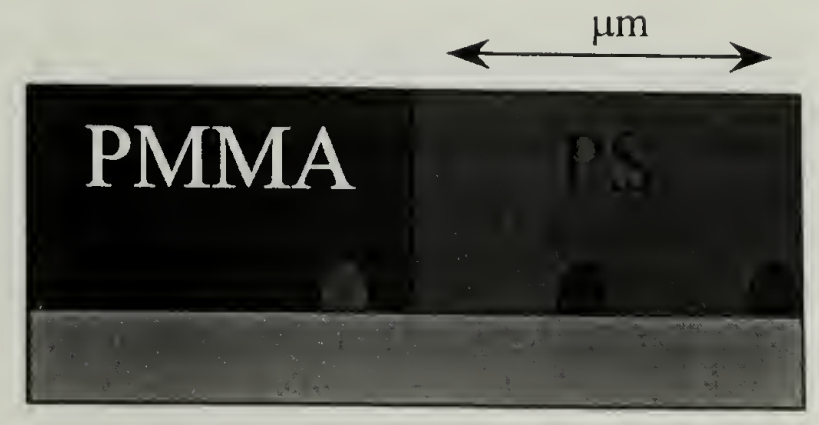

Cyclohexane Acetic Acid

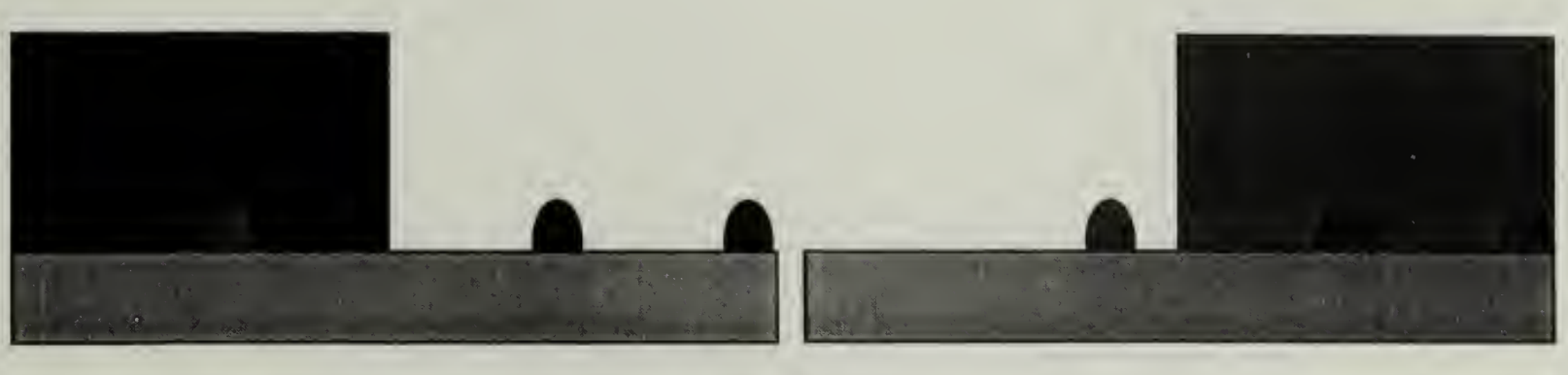

Figure 2.1. Schematic of the selective solvent etching technique. Phase separated thin films possess micron sized domains extending from the substrate up to the free surface. Exposure of the film to a solvent selective for one phase will remove it entirely from the surface, leaving the other polymer untouched.

the native oxide present on the silicon substrates, to a thickness of 150 Å, followed by 300 Å of gold. Films were cast immediately on the gold surfaces after evaporation to prevent ambient contamination from adsorbing to the gold surface.

Heterogeneous substrates were prepared as outlined in Chapter 1. Substrates with a 50-60 nm average periodicity and a 3-4 nm average amplitude after metallization were used. Table 2.1 notes substrate preparation parameters and characterization data for two representative surfaces. Two sets of substrates were used for the experiments, one for spin casting, another for solution casting. Samples were reused after film characterization, having been rinsed thoroughly in toluene in an ultrasound bath after each experiment to remove the previous polymer layer.

Table 2.1. Preparation data and characterization information for substrates used in solution and spin casting experiments.

Metal	angle	Evap. Thick XTM (Å)	Average Peak Height (nm)	Standard Dev. (nm)	peak FWHM (nm)
Cr/Au	6	100/120	3.9	1.8	
Cr/Au	6	100/120	3.16	1.49	23.625

Thin Film Preparation

Homopolymer solutions were prepared in toluene from 0.5 wt% polymer, using the polymers listed in Table 2.2. Polymers were used as-received from Polymer Labs, or synthesized anionically. Blend solutions of 0.25 wt% were prepared by mixing symmetric volumes of homopolymer solutions, or by direct preparation.

Table 2.2. Polymers used in thin film casting experiments

Polymer	Mw kg/mol	PDI
PS	30.3	1.03
PMMA	27	1.11
PS	52	1.03
PMMA	53	1.04
PS	66	1.03
PMMA	64	1.09
PS	95	1.04
PMMA	96	1.04
PS	127	1.05
PMMA	125	1.08

Spin casting was performed in a laminar flow hood, to minimize particulate contamination, on a Headway Research spin coater. Spin acceleration was set to maximum, and spin speed was set by an external digital controller. Homogeneous substrates were placed directly on the vacuum chuck for spinning, while the smaller 0.25 cm^2 heterogeneous substrates were mounted on larger wafers with Scotch brand double stick tape underneath, or Scotch brand transparent tape over the sample edges. Substrates were spun at 3000 rpm and rinsed with toluene prior to film casting, and once dry the chosen spin speed was set on the controller before stopping the spinning. Solution was applied via micropipette to the static substrate with enough solution to wet the center of the substrate, before spinning commenced. Films spun from homopolymer solutions were transparent and colored due to optical interference between the reflective substrate and polymer film free surface. Blend films were opaque due to the microphase separation that occurred during spinning. Film thickness after spinning was measured by ellipsometry on homopolymer films cast on silicon wafers, and by AFM on blend films.

Solution casting was performed in a closed glass crystallization dish in the presence of excess solvent, in an effort to control the rate of solvent evaporation and promote an equilibrium morphology [13]. Substrates were placed within a 600 ml aluminum foil covered glass crystallization dish. Inside the casting container was an additional small dish filled with toluene, to saturate the vapor pressure inside and mediate solvent evaporation from the substrate. A syringe inserted through a small, 0.3 cm^2 hole in the foil covering allowed for wetting of the substrates with polymer solution, as well as controlled evaporation. The substrates were wet entirely, but the solution prevented from spilling over the substrate edge due to surface tension. Solvent evaporated completely over the course of 30 minutes. While homogeneous solutions produced transparent films, blends produced opaque films of nonuniform thickness due to macroscopic phase separation.

Characterization

Substrate immersion in a solvent bath followed by blow drying with compressed nitrogen allowed for selective film etching. A 5 minute bath in heated cyclohexane was used to remove the PS, while acetic acid followed by a quick rinse in deionized water removed the PMMA. Some samples were subsequently etched in the complimentary solvent after characterization to reveal the phase morphology beneath the unetched domains.

Surface morphology was characterized by atomic force microscopy (AFM) in tapping mode on a Digital Instruments Di3100. Images were analyzed using either the bundled AFM software package or ImageSXM, a modified version of NIH Image designed to handle AFM files.

Results

Spin Cast and Annealed Films

Homopolymer films of 95 kMw PS and 96 kMw PMMA were spin cast onto homogeneous gold and silicon oxide surfaces at 3500 rpm from a 0.5 wt% toluene solution. As cast, all films were transparent and uniform in color, indicating completely wet films with little thickness variation. Ellipsometry showed film thickness to be 260 nm on the SiOx substrate. To determine equilibrium wetting properties of the polymers on each substrate, films were annealed for 4 days at 160° C in a vacuum oven and then imaged with the AFM. Figure 2.2 shows height images of the free surface of the PMMA films on both substrates. PMMA remained wet on both silicon oxide and gold, while PS films dewet both surfaces, leaving micron sized droplets in a mosaic pattern as shown in figure 2.3.a. From purely numerical arguments this is an unexpected result, as both polymers should completely wet both substrates to minimize surface tension[21,22]. The surface tension of the polymers of order 30 dyne/cm is far less than that of either substrate, 44.0 dyne/cm for gold[23] versus 36.5 for SiOx. The price PS must pay in interfacial energy, however, drives dewetting on both surfaces, while PMMA interfacial energies are low enough to allow spreading. Favorable polar interactions between PMMA and SiOx can explain the low interfacial energy for the oxide surface, yet gold is a non polar metal and should not lower the interfacial tension significantly or promote wetting. Without any specific PMMA/Au interaction however, Young's surface tension argument holds, and the PMMA should, and does, wet gold. For PS, a non polar polymer, unfavorable interaction with SiOx should increase interfacial energy and promote dewetting, while on non polar gold without any specific interaction, it would be expected

a)

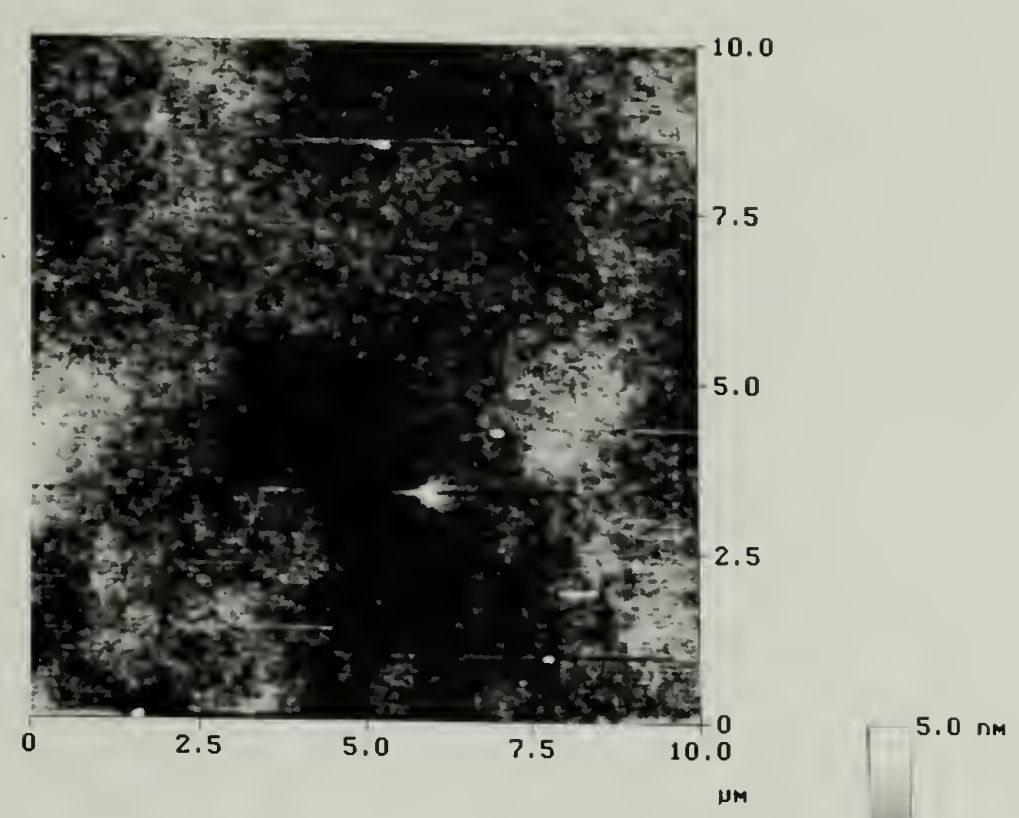

b)

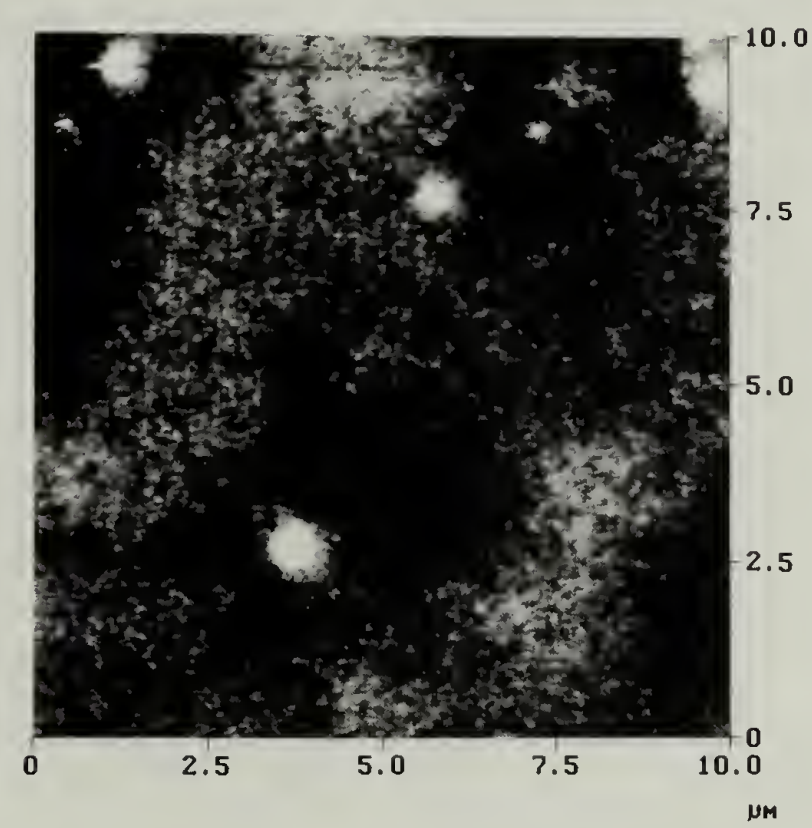

Figure 2.2. AFM height image of PMMA thin film spin cast onto a) gold. b) silicon oxide. Then annealed for 4 days at 160° C under vacuum. Films remained completely wet on substrate.

to wet. This is not the case, however, and some unknown is driving dewetting of PS on Au. Droplet contact angles for PS on both surfaces averaged 20°, which in the context of Young's equation based purely on surface tension, yields a higher interfacial energy for PS on gold than on SiOx, in spite of the polar/non polar interaction between PS and the oxide surface. Previous work in block copolymers found a preference for PS wetting gold over PMMA, indicating a lower interfacial energy for gold, which is not borne out in these experiments [19]. However, the AFM image of PS on the gold substrate on the micron length scale in Figure 2.3.b shows a morphology indicative of 'partial wetting' whereby many tiny droplets remain on the surface after mesoscopic dewetting has occurred. Muller-Buschbaum et. al. found a similar nano-dewetting morphology[7] with PS on certain oxide surfaces and attributed it to a favorable Hamaker constant for the substrate-polymer-air system, which served to stabilize a several nm thick film at elevated temperatures. When quenched in air upon removal of the annealed film from the oven, spinodal dewetting in the nm thick film occurred instantaneously, with a length scale limited by the film thickness, forming nm sized droplets. As this morphology is not present on the SiOx surface in this work, its presence on gold indicates a favorable short-range interaction for PS. Thus, in the context of short-ranged interactions, we find a slight preference for PS on gold versus SiOx. It may in fact be such short range interactions that stabilize the PS wetting layer on Au in p(S-b-MMA) block copolymer systems[19], although the Hamaker constant spreading argument breaks down on length scales as large as the half-period of a phase separated block copolymer[22]. Calculation of the spreading coefficients for these copolymer materials is beyond the scope of this work, and will not be made in support of this argument.

a)

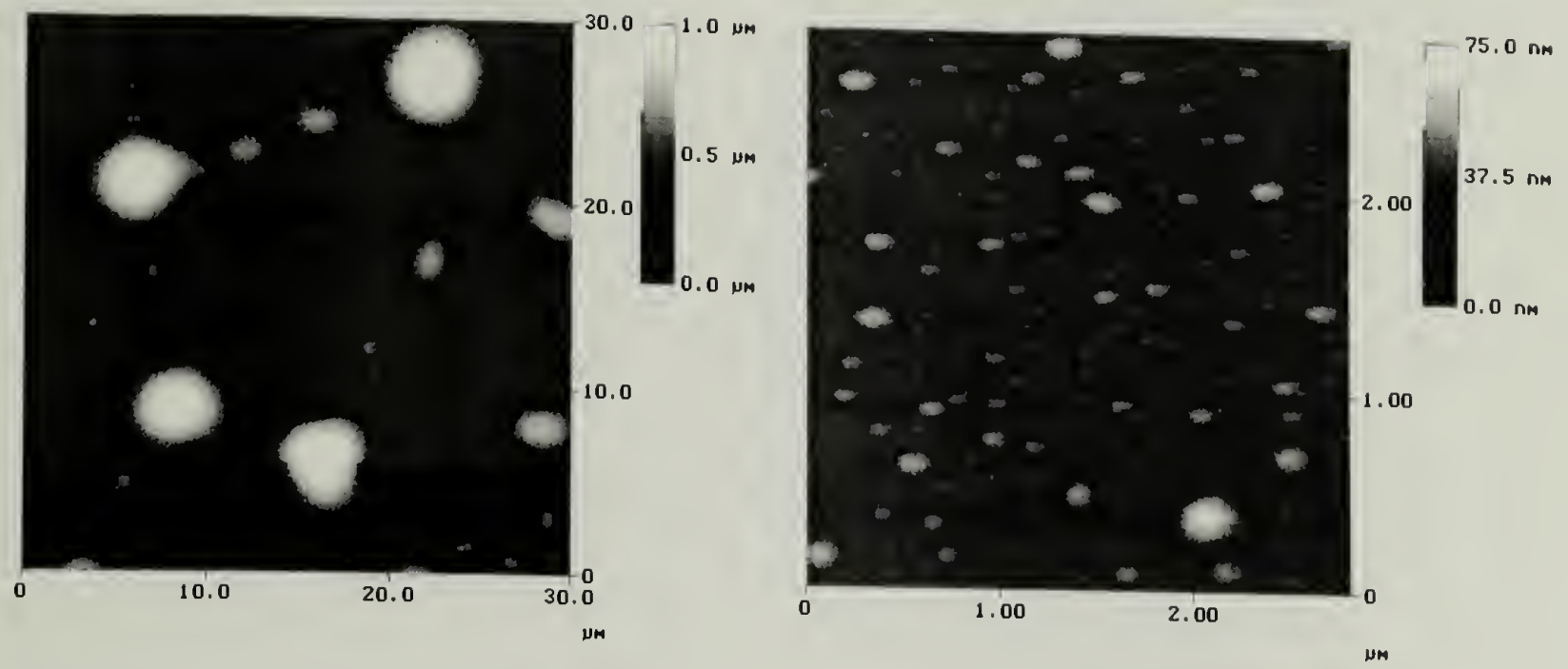

b)

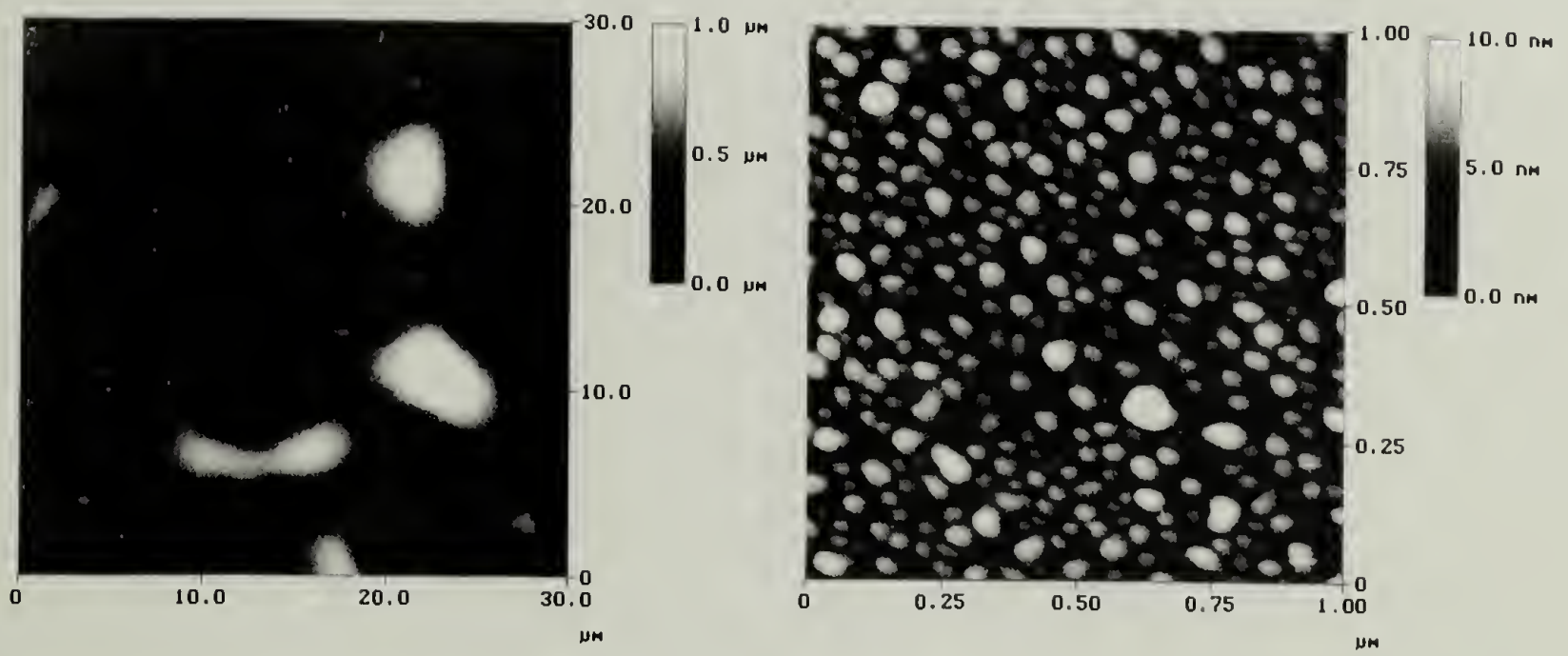

Figure 2.3. AFM height image of PS thin film spin cast onto a) silicon oxide. b) gold. Then annealed for 4 days at 160° C under vacuum. While PS appears to macroscopically dewet both SiOx and Au in large area scans, Au substrate remains partially wet on the nm length scale.

Homopolymer blend films of 95 kMw PS and 96 kMw PMMA (50/50 wt/wt) were spin cast onto homogeneous gold and silicon oxide surfaces at 3500 rpm and heterogeneous surfaces at 3500 and 4500 rpm from a 0.25 wt% toluene solution. To determine the equilibrium wetting properties, these films were then annealed in vacuum for 4 days at 160° C. Figure 2.4 shows the AFM height images of the films cast on homogeneous surfaces. Depending on the substrate chemistry, a different phase morphology is visible on the free surface of each film. While phase separation of the solution into PS-rich and PMMA-rich phases occurred during spinning, no lateral morphology indicative of phase separation is evident on the homogeneous SiOx substrate. This is due to the preference of the PMMA rich phase for the oxide substrate, which it wets uniformly, and the exclusion of the lower surface energy polystyrene to the free surface where it uniformly wets the PMMA underlayer[1]. Thus, a bilayer morphology is formed upon casting, and no domain structure is apparent. The gold substrate, however, presents a much different morphology composed of a matrix of one polymer filled with micron sized domains of the other. The lack of strong preference for either material for the substrate results in the formation of the lateral domain structure, while the domain height can be attributed to preferential solvency of the two phases in toluene. The thinner matrix phase is PS, which remains more highly solvated, while the elevated minor phase is PMMA, which solidifies initially at a greater film thickness [1]. For the gold substrate, in spite of the homopolymer wetting properties found earlier, PS and PMMA domains appear to be covering an equal fraction of the surface area

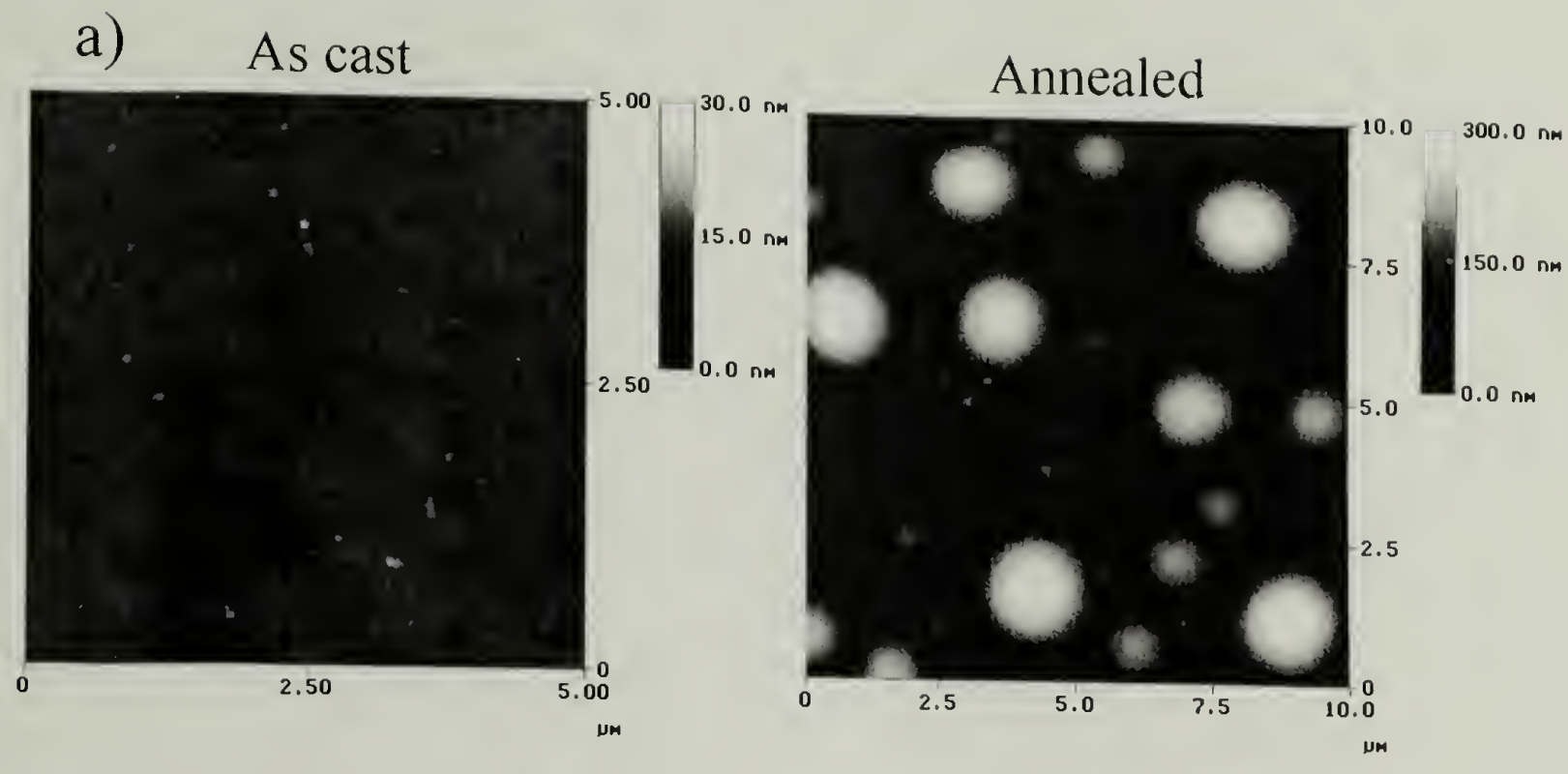

Figure 2.4. AFM height image of PS+PMMA blend thin film spin cast onto a) silicon oxide. b) gold. Left side images are as cast, right side are after a 4 day 160° C anneal.

indicating a non preferential, or neutral surface interaction. The AFM is only showing the free surface morphology however, and the composition at the substrate may be different.

Annealing the films at 160° C for 4 days shows the non-equilibrium nature of the structures formed on spin casting. The bilayer film on the SiOx becomes unstable, as the PS/PMMA interfacial energy is higher than the surface energies of either homopolymer, and results in a dewetting of the PMMA layer by the PS, forming micron sized spherical domains. The laterally phase separated morphology on the gold substrate remains, but the PMMA regions decrease in size. Where the PMMA goes based on the AFM free surface images is unclear, whether directly to the substrate or into the bulk film or even spread over the free surface. Given the lower surface tension of PS however, it's likely that the PMMA domains are being subsumed under the PS matrix, which is why their apparent size seems to decrease. Selective solvent etching will be used to explicitly identify the annealed domain structure later in this chapter.

The morphology of the spin cast blend films on heterogeneous substrates is shown in Figure 2.5. Two different morphologies develop for different spinning speeds, with the morphology of the 4500 rpm sample almost identical to that cast on gold at 3500 rpm. The 3500 rpm sample appears more like a bilayer, however, with the upper layer frozen in the early stages of dewetting the lower. While spinning speed has been shown to vary the morphology of spin cast blend films, the variation is typically seen in the lateral length scale of the phase separated domains, confined by film thickness, and not the overall morphology[1]. Morphology variations, such as a lateral versus a bilayer phase separation, are more likely due to a difference in substrate surface energy. A slight

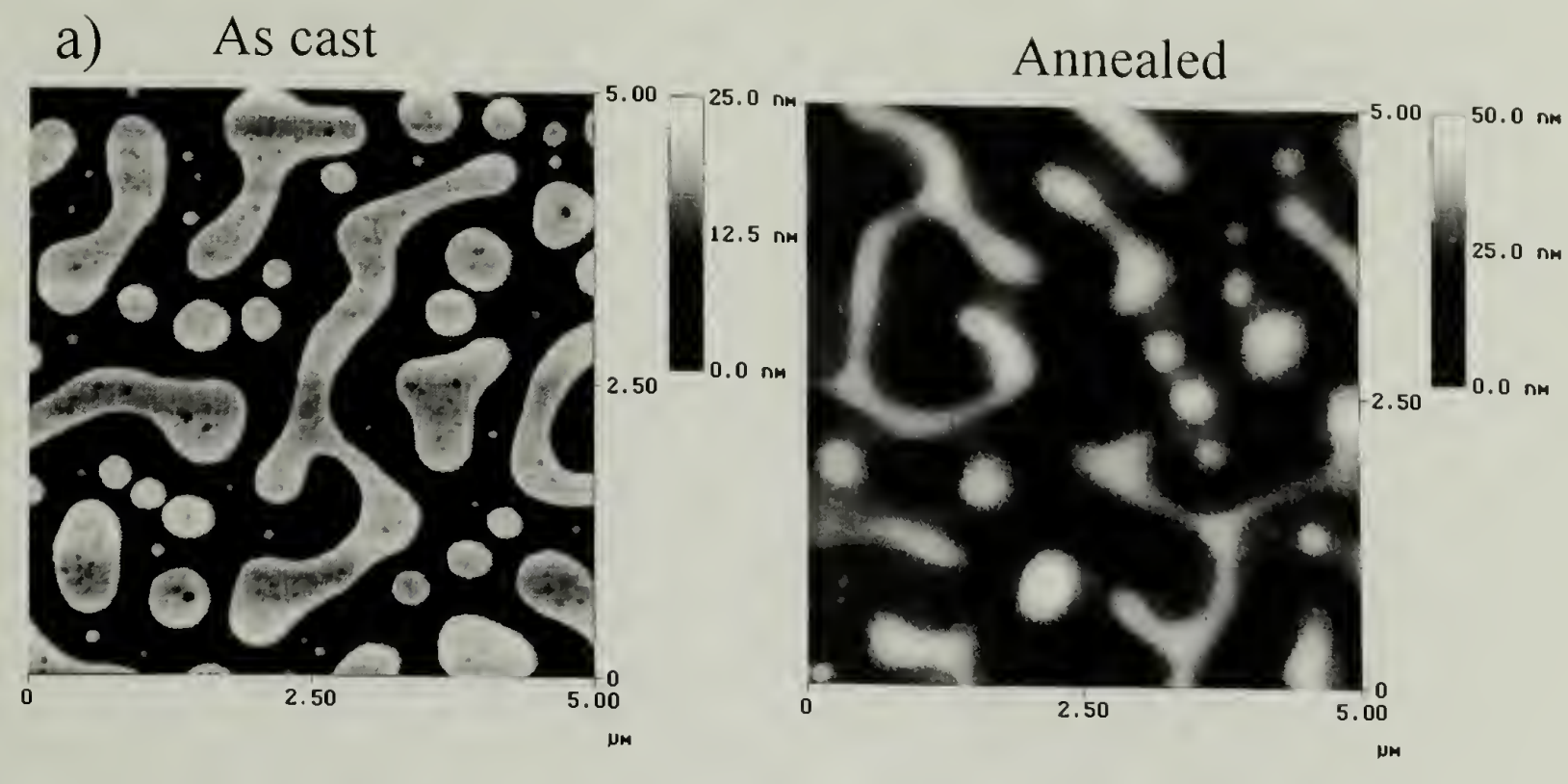

Figure 2.5. AFM height image of PS+PMMA blend thin film spin cast onto heterogeneous substrates at a) 4500 rpm. b) 3500 rpm. Left side images are as cast, right side are after a 4 day 160° C anneal.

change in preparation conditions for the heterogeneous substrates used for the two spin speeds may have produced a more gold-like or more SiOx-like substrate depending on linewidth and metal thickness, despite following the Chapter 1 procedure, and contributed to the morphology change. Upon annealing, the PMMA domains in the 4500 rpm sample decrease in size, again in a manner identical to the film cast on gold, while the structure of the 3500 rpm sample has begun to invert. The higher, dewetted phase has sunk, and the lower hole phase is being forced upwards. This evolution of the morphology, according to a surface energy argument, indicates that the bilayer formed initially on casting may have been of a PS underlayer with a dewet PMMA overlayer. Upon annealing the system tries to invert the morphology to bring the lower surface energy polystyrene to the free surface. This also indicates that the substrate used for 3500 rpm is not more SiOx like, but less, being favorably wet by PS upon casting.

Selective Solvent Etching

Selective solvent etching of the homopolymer blend films on homogeneous and heterogeneous surfaces was performed to confirm the phase morphology identified through spin casting and annealing. For both homogeneous substrates the annealed sample was fractured and each half exposed to a single solvent initially. Figure 2.6 shows the AFM height images of the homopolymer blend film cast on SiOx, annealed, and then solvent etched. The cyclohexane etch removed the large phase separated PS domains that had dewet the underlying PMMA layer, while the acetic acid etch removed the matrix phase, as expected. The AFM height cross section inset in Figure 2.6.b indicates some material is remaining on the substrate in the region below the removed PS

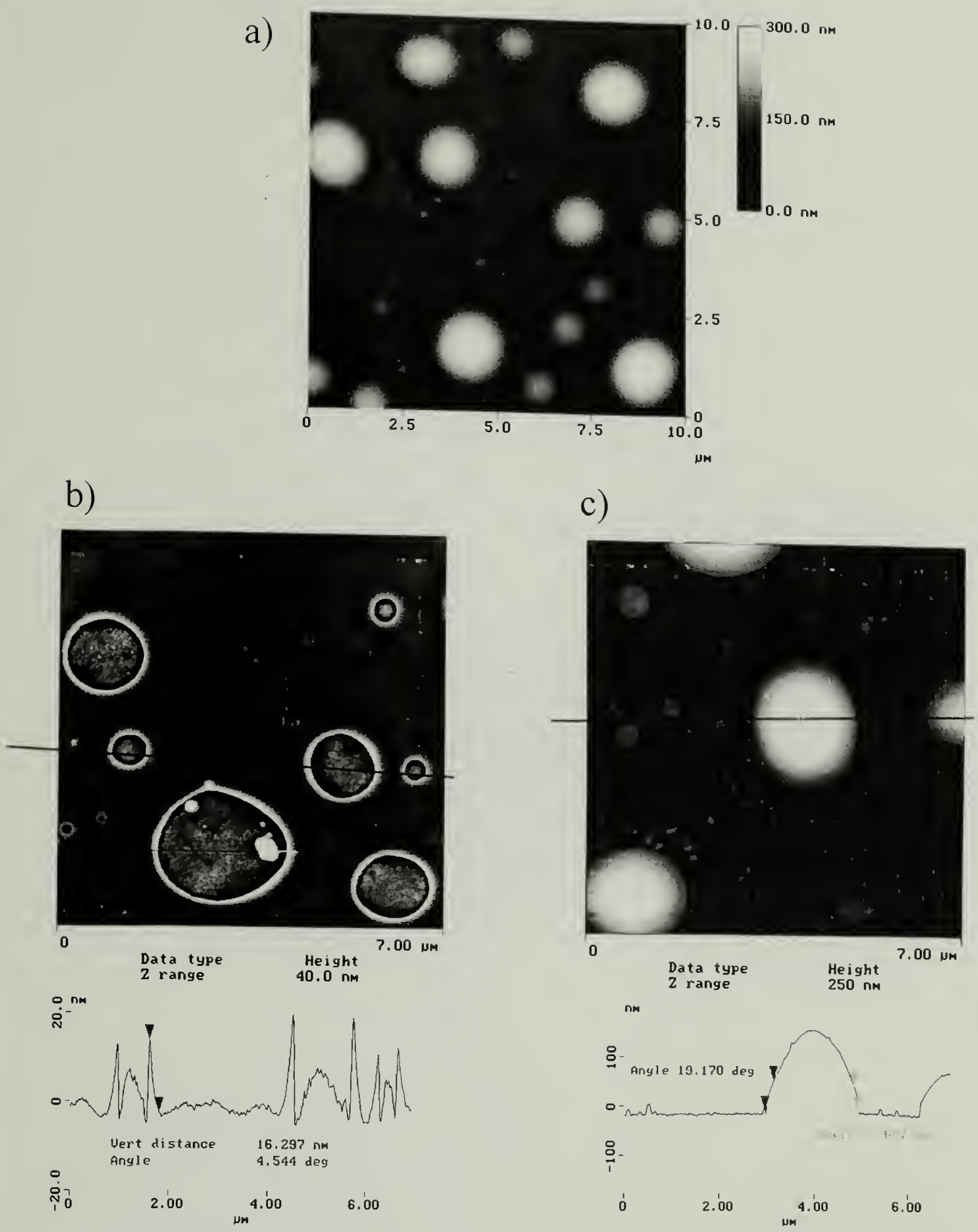

Figure 2.6. AFM height images of PS+PMMA blend thin film spin cast onto SiOx and annealed. a) as cast. b) cyclohexane etch. c) acetic acid etch. Inset are AFM height cross-sections which were produced from the AFM images along the dark line superimposed on the image.

domains, evidently PMMA that remained wet on the substrate. The PS phase did not propagate down to the substrate due to the preferential interaction of the PMMA with the oxide surface.

Images of the solvent etched films on the gold substrate in Figure 2.7 confirmed the assignment of the elevated, minor phase domains as PMMA, and the matrix phase as PS. Given the initial average film thickness of 260 Å, the inset AFM height cross sections indicate that the phase separated domains of both polymer species propagated uninterrupted from the substrate to the free surface. Confirmation of the presence of both species at the substrate supports the conclusion that gold acts as a neutral surface with respect to the macrophase separated domains. Additionally, the height of the PMMA domains on the gold substrate averaged 40 nm, while the PS matrix averaged 15 nm, in accordance with the slightly preferential solvency of toluene for PS which as mentioned, results in a thinner layer upon casting[1].

The heterogeneous substrates were not fractured and selectively etched in both solvents after annealing, rather the 4500 rpm sample was etched in acetic acid while the 3500 rpm sample was etched in cyclohexane. Figure 2.8 shows the AFM height images of the substrates after etching. For the 4500 rpm sample, which had a morphology similar to the blend film cast on gold, acetic acid etching removed the elevated PMMA domains and left the PS matrix. Looking closely at the holes in the PS matrix in Figure 2.8.b where the PMMA was removed from, one can see lines from the metal evaporated on the substrate, showing that the domains propagated throughout the thickness of the

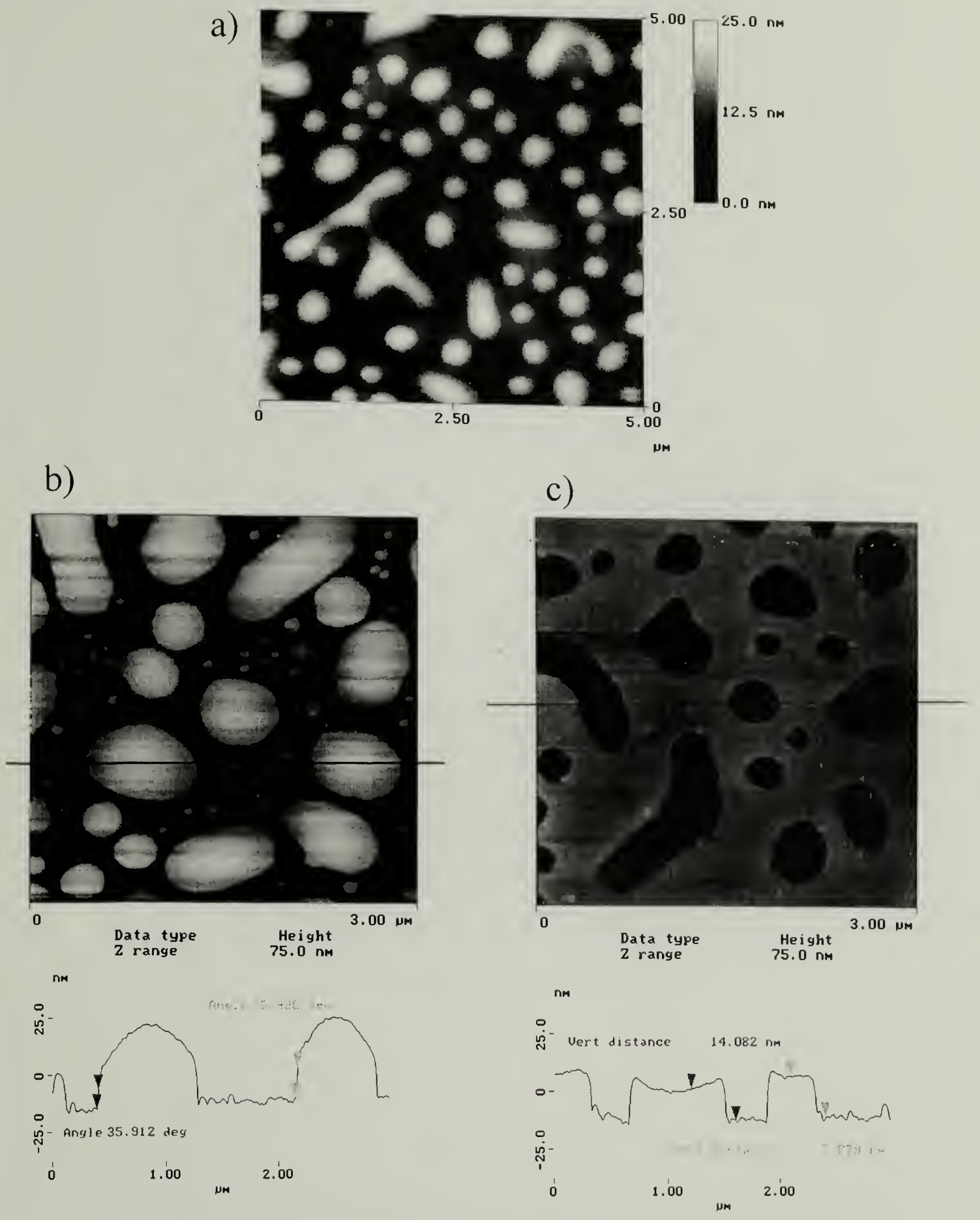

Figure 2.7. AFM height images of PS+PMMA blend thin film spin cast onto gold and annealed. a) as cast. b) cyclohexane etch. c) acetic acid etch. Inset are AFM height cross-sections which were produced from the AFM images along the dark line superimposed on the image.

film. The PS matrix for the image selected covers greater than 50% of the surface area, however, substrate neutrality is still indicated by the presence of both domains at the substrate.

Etching the 3500 rpm sample with cyclohexane to remove the PS reveals a morphology in Figure 2.8.a composed of a PMMA matrix phase. Comparing the shape of this remaining phase to the dewet upper layer in the pre-annealed 3500 rpm sample in Figure 2.5.b, and to the same 'sunken' layer in the annealed 3500 rpm sample in Figure 2.8.a, shows that the initial identification of this layer as the PMMA rich phase was correct. Upon annealing, the PS was forced through the holes in this matrix phase up toward the free surface, and was then removed entirely upon solvent etching. Again, the AFM image of the substrate shows the presence of lines in the hole regions left vacant by the PS removal indicating that the two phases in this sample extended entirely from the substrate to the free surface. In spite of the distinctly different phase morphologies present at the free surface of the two heterogeneous samples, the substrate composition appeared effectively neutral with respect to domain segregation and more gold-like in their surface energetics.

A summary of the phase separated morphology of the blend films cast on the different substrates as determined by solvent etching is presented in Figure 2.9. The schematics are drawn based on the AFM free surface information only, and may not reflect any morphology buried underneath the phase that was not removed by the solvent etch. Image analysis was done on the etched sample images to quantify the fraction of each component present at the free surface. Table 2.3 shows the results. Both the gold and heterogeneous substrates show a majority of PS at the surface, while the SiOx

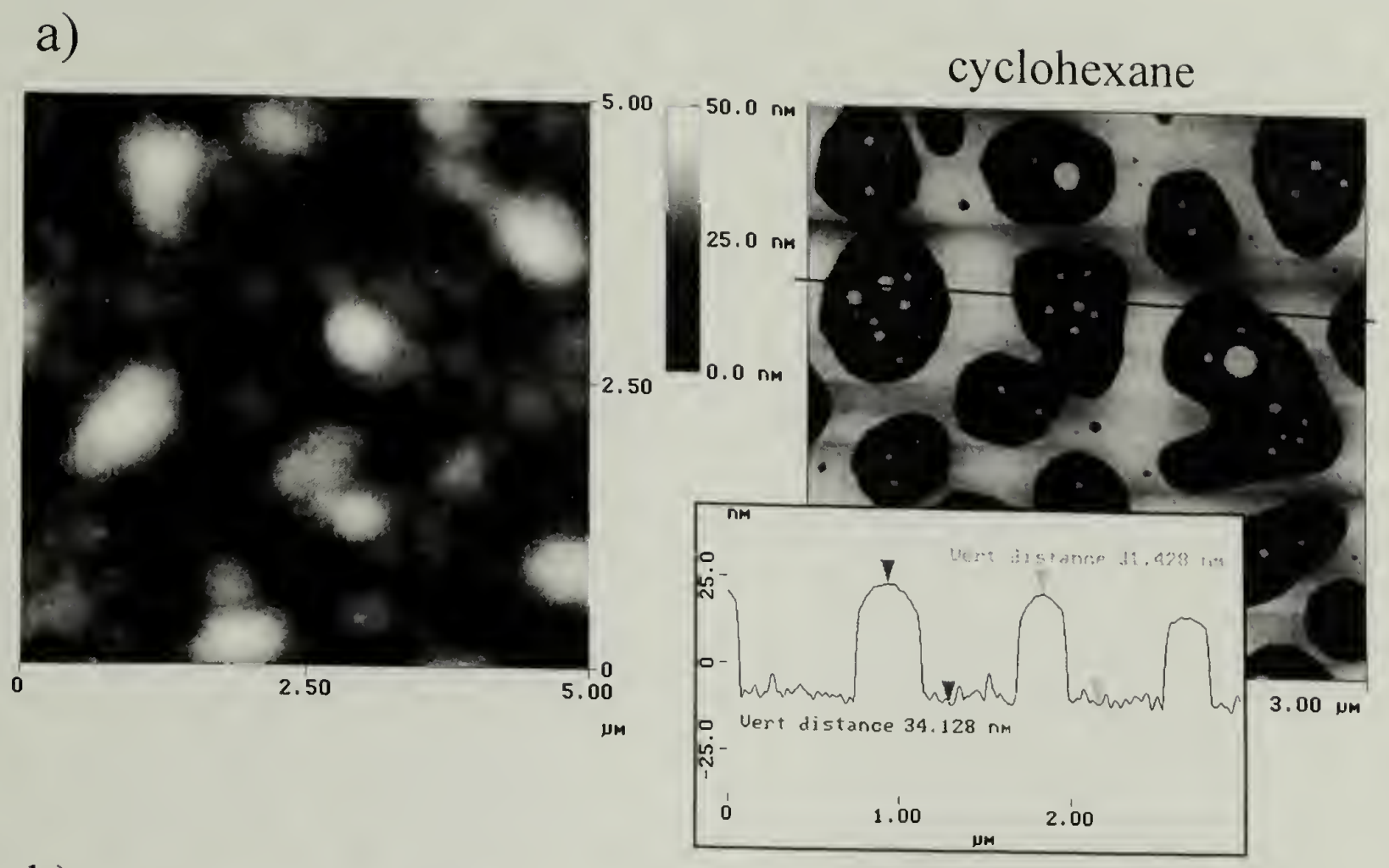

Figure 2.8. AFM height images of PS+PMMA blend thin film spin cast onto heterogeneous surfaces and annealed. a) annealed and cyclohexane etched. b) annealed and acetic acid etched. Inset are AFM height cross-sections which were produced from the AFM images along the dark line superimposed on the image.

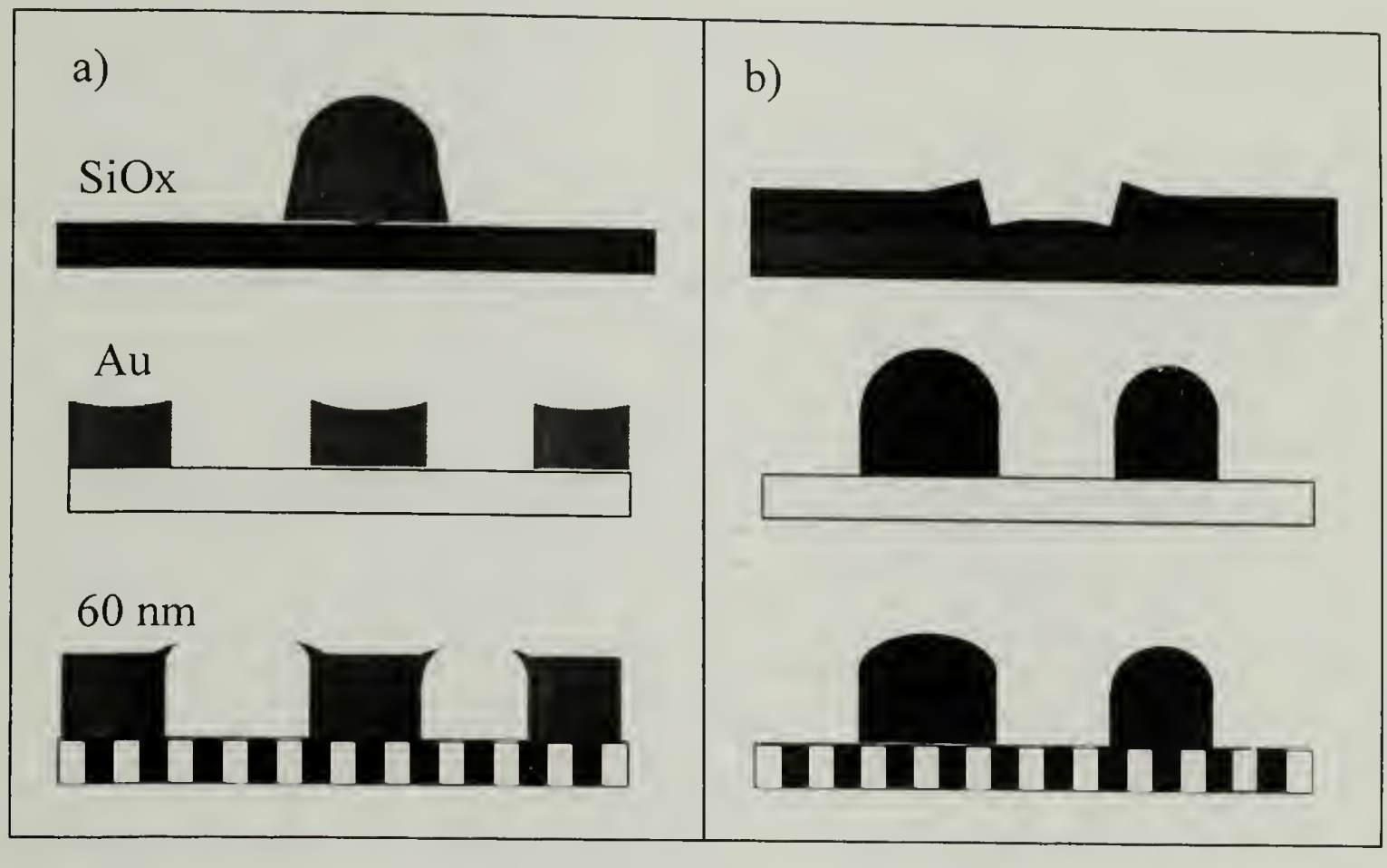

Figure 2.9. Schematic cross-sectional morphology of spin-cast and annealed blend films on different substrates, based on initial solvent-selective etch. a) acetic acid, b) cyclohexane.

substrate shows very little, as the PS phase had dewet into spherical domains. Considering the AFM height data from the cyclohexane etch of the SiOx sample which showed PMMA present at the substrate beneath the etched PS domains, the real fraction of PS present at the substrate is zero, even for the acetic acid etch which left PS domains on the surface. Acetic acid etching was not performed for a long enough period of time to undercut the PS domains, etch the surface stabilized PMMA layer, and remove all of the polymer material above it.

Table 2.3. Fractional surface coverage area of polystyrene upon spin casting and annealing determined from image analysis of solvent etched homopolymer blend films.

AFM Image "sept23.00x"	Substrate	Spin Speed (krpm)	Etch Solvent	Fraction PS After Etch
1	60nm	3.5	cyclohexane	55.9
2	60nm	4.5	acetic acid	68.1
3	SiOx	3.5	cyclohexane	0
4	SiOx	3.5	acetic acid	17
6	Au	3.5	cyclohexane	54.9
7	Au	3.5	acetic acid	72

Complimentary Solvent Etching

Immersing the solvent etched homogeneous substrates in the complimentary solvent allowed for the removal of the remaining phase, and identification of any buried morphologies. Figure 2.10 shows the AFM images taken of the homogeneous substrates after the second etch. Both height images of the SiOx substrate show large round light-shaded patches against a uniform background indicative of material left on the substrate, located beneath the dewet PS domains, despite both solvents having been applied. In Figure 2.10.a the patches are 20 nm thick, almost 10% of the initial film thickness. For this sample, the PS domains were etched first, removing the large blobs, then acetic acid

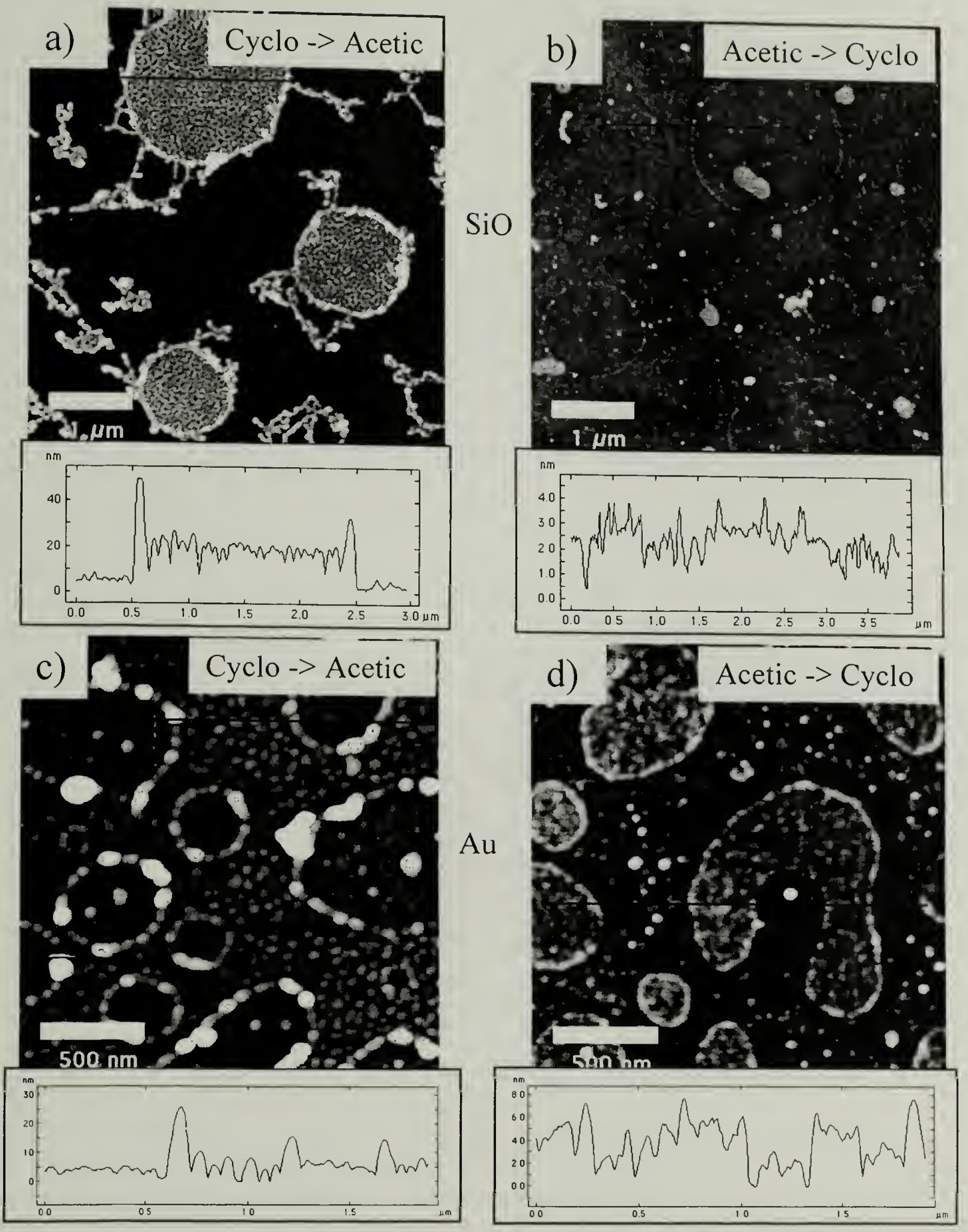

Figure 2.10. AFM height images of SiOx and Au surfaces after a complimentary solvent etch to remove remaining polymer. a) SiOx cyclohexane/acetic acid. b) SiOx acetic acid/cyclohexane. c) Gold cyclohexane/acetic acid. d) Gold acetic acid/cyclohexane. Inset are AFM height cross-sections which were produced from the AFM images along the dark line superimposed on the image.

was applied to remove the matrix PMMA. It was expected that this would remove all of the material on the surface, but the buried interface between the PS and PMMA was not removed, being resistant to etching by both solvents. Thus a blend of some composition resistant to both solvents formed at the interface of the two polymers and remained after complete etching of the surface. The string-like features in the images are likely the remaining interfacial material from between the two polymer phases from the bulk region of the film, which collapsed to the surface after removal of the matrix phase. Figure 2.10.b, etched in the opposite order still shows surface patches, but of much decreased thickness. It is possible that the complimentary cyclohexane etch removed more of the blended phase along with the PS domains, or extracted the PS from the buried interface, leaving only the thin PMMA at the substrate.

The homogeneous gold sample in figure 2.10.c. shows a buried blend phase after the acetic acid complimentary etch morphologically similar to the one left on the SiOx substrate. Thus, in spite of the apparent preference for the PS phase to occupy the surface, a PS+PMMA blend composition formed at the gold substrate below the PS. Looking at the reverse etch process in Figure 2.10.d, we again see a thin surface morphology. However, it is now located beneath the PMMA regions that were initially etched, and it was not removed after the second cyclohexane rinse. This material too must be of blended composition, and thus we see that covering the entire gold surface is a thin layer of blended PS+PMMA that is resistant to selective solvent etching. It is this adsorbed, blended layer which forms on the gold before phase separation during spin casting which effectively renders the substrate neutral and allows for the growth of laterally phase separated domains on the gold surface.

Looking at the heterogeneous surfaces etched in complimentary solvents in figure 2.11.c and d, we again see a thin, selective solvent resistant blended layer remaining on the substrate. In both images, the presence of the blended layer can be confirmed beneath the PS phase only, due to the etch steps performed. The layer is conformal, so that the surface roughness generated by the substrate metallization is visible 'through' it. Selective segregation to either the oxide or gold stripes by the PMMA or PS respectively is not evident on either surface after either etch process. Such a local, specific phase separation would result in the partial removal of the surface phase by the solvent etch, leaving periodic polymer stripes on the substrate surface which is clearly not seen. The spin casting process is too rapid to allow for controlled segregation of the polymer species to the preferred stripes, and therefore the chains see the average surface composition of mixed polar and nonpolar chemistry and adsorb in a blended state accordingly. As in the case of the homogeneous gold substrate, this 'neutral' surface layer allows for the lateral phase separation of the homopolymer blend on spin casting.

A final composite cross-sectional morphology built up from the selective solvent etching process is shown in Figure 2.12. The PS and PMMA phases are indicated by medium gray and dark gray respectively, and the blended interfacial region is denoted by speckled white. The phase dimensions are not drawn to scale. On the homogeneous oxide surface, the PMMA phase wets the substrate entirely, due to favorable interactions, while the PS phase remains dewet on the free surface. A blended interfacial region forms between the two phases which is resistant to selective solvent etching. On the homogeneous gold and heterogeneous substrates, adsorption of both polymer species to the substrate in a non-specific manner produces a selective-solvent resistant blend

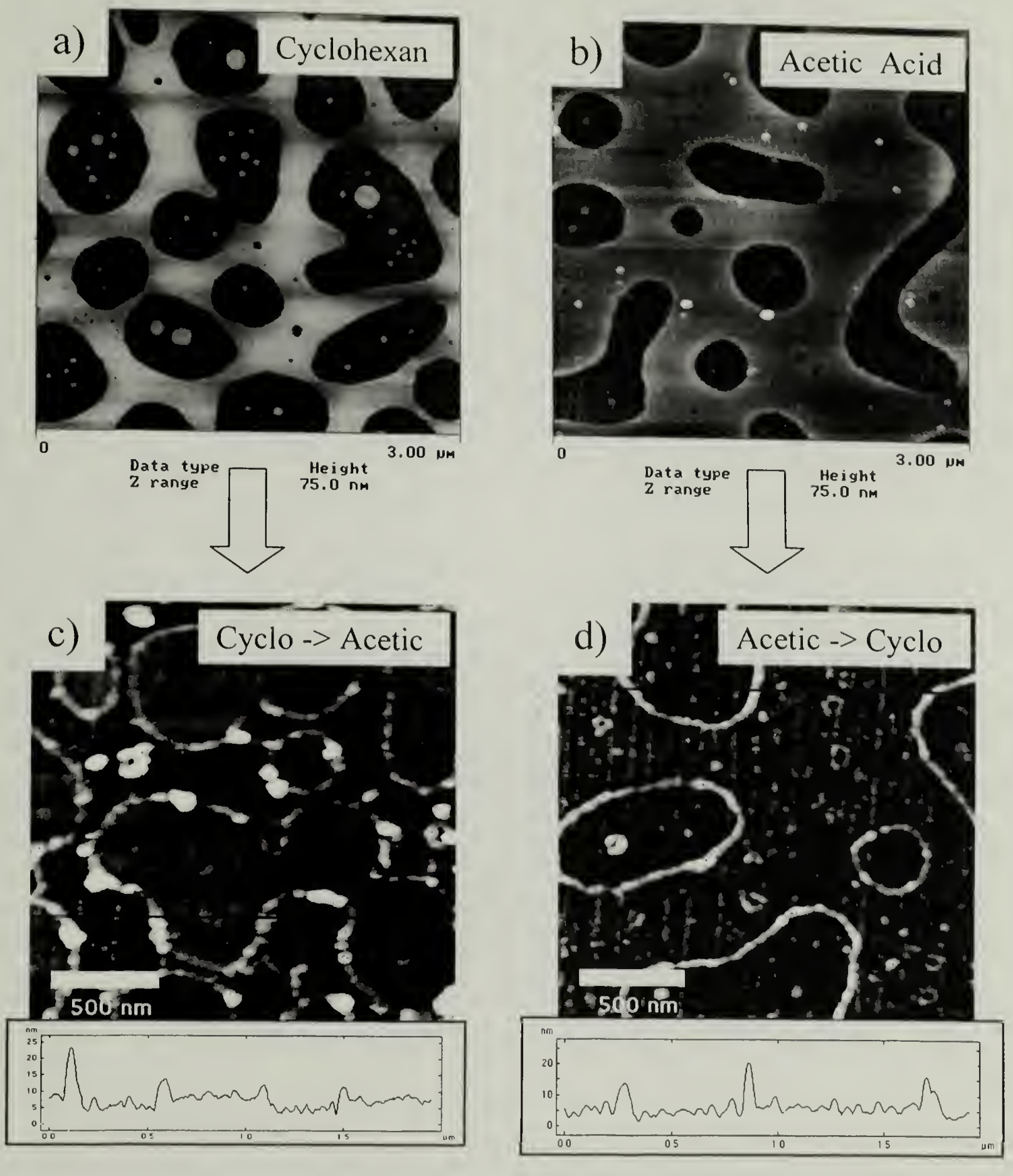

Figure 2.11. AFM height images of heterogeneous surfaces after initial and complimentary solvent etch to remove remaining polymer. a) cyclohexane. b) acetic acid. c) cyclohexane/acetic acid. d) acetic acid/cyclohexane. Inset are AFM height cross-sections which were produced from the AFM images along the dark line superimposed on the image.

composition. The substrates then appear neutral in composition to the phase separating PS and PMMA domains, resulting in a lateral morphology extending from the substrate to the free surface upon spin casting.

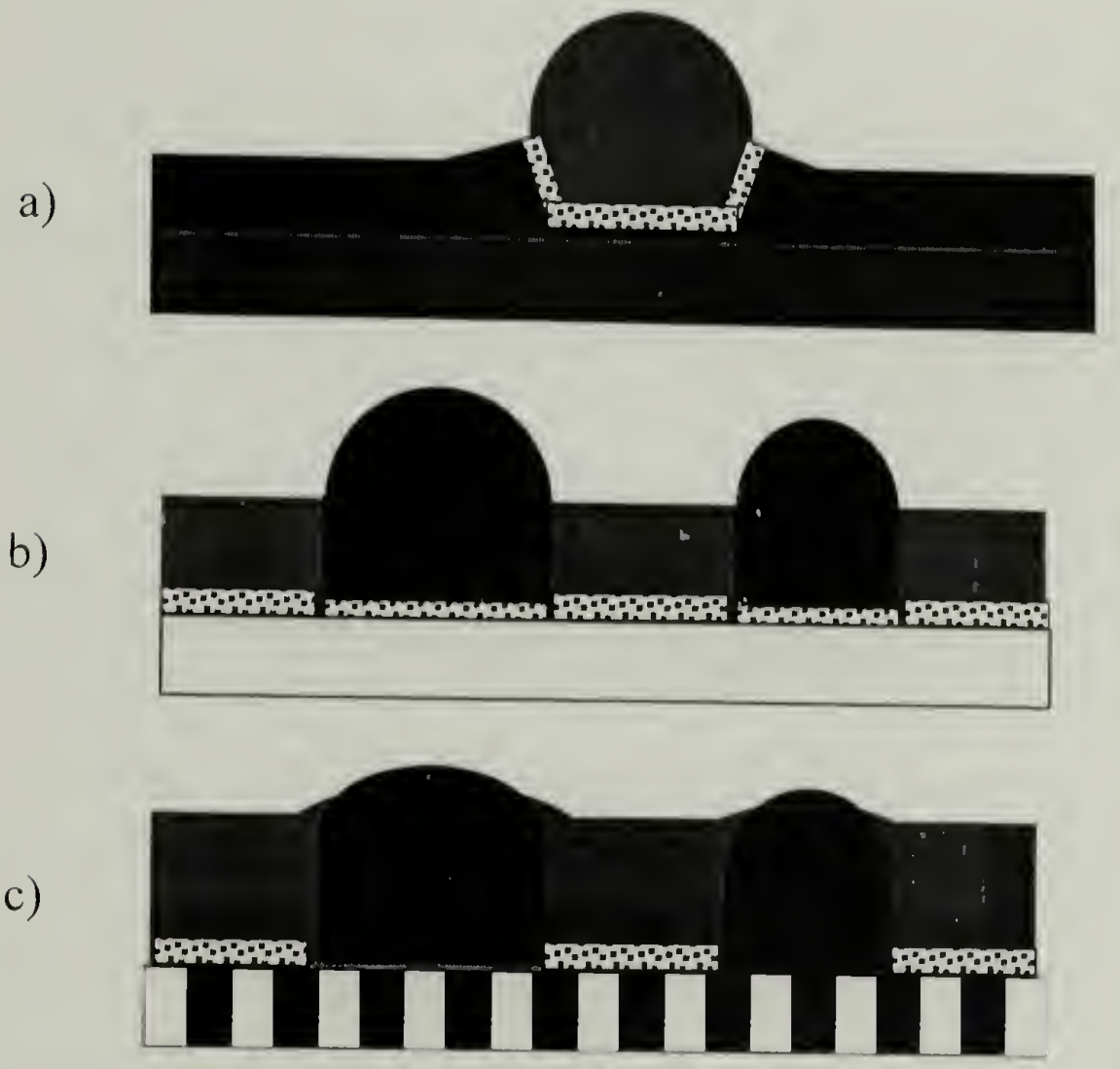

Figure 2.12. Schematic cross-sectional morphology of spin-cast and annealed blend films on different substrates, as reconstructed from all solvent-selective etches. a) SiOx substrate, b) Au substrate, c) 60 nm heterogeneous substrate. PS (light gray), PMMA (dark gray), Blend (dotted).

Solution Casting

Figure 2.13 shows a typical AFM height image of a homopolymer blend solution cast and then cyclohexane etched. The laterally phase separated morphology that develops is similar to that formed on spin casting, and the presence of both polymers at the surface again indicates substrate neutrality. Micron sized PMMA domains are seen in the image, and extend from the substrate up to the full 0.2 μm thickness of the as-cast film. This morphology is typical of all molecular weights used in this study.

In contrast to the spin cast films where solvent etching revealed a conformal homopolymer blend layer underneath the etched domains, the structure of the substrate in the solution cast samples appears much different. Figure 2.14 shows AFM height images of the substrate region of two typical solution cast films, one after a cyclohexane and another after an acetic acid etch. In comparison to Figure 1.6 of a heterogeneous substrate immediately following metal deposition, the substrate after a cyclohexane etch looks remarkably similar. The metal lines are thin, and well resolved, and of 3.5 nm average height. Apparently, the cyclohexane removed all of the PS down to the substrate. No PMMA is evident over the oxide regions, indicating that it was either removed by the cyclohexane, or not present there in the first place. The height image of the acetic acid rinsed region reveals a much different line structure, composed of smooth lines 4-6 nm in thickness, with a larger full width at half maximum than metal lines alone. The amplification in line height indicates not a conformal polymer layer, but a periodic layer of polystyrene homopolymer adsorbed to the gold lines. Upon removing

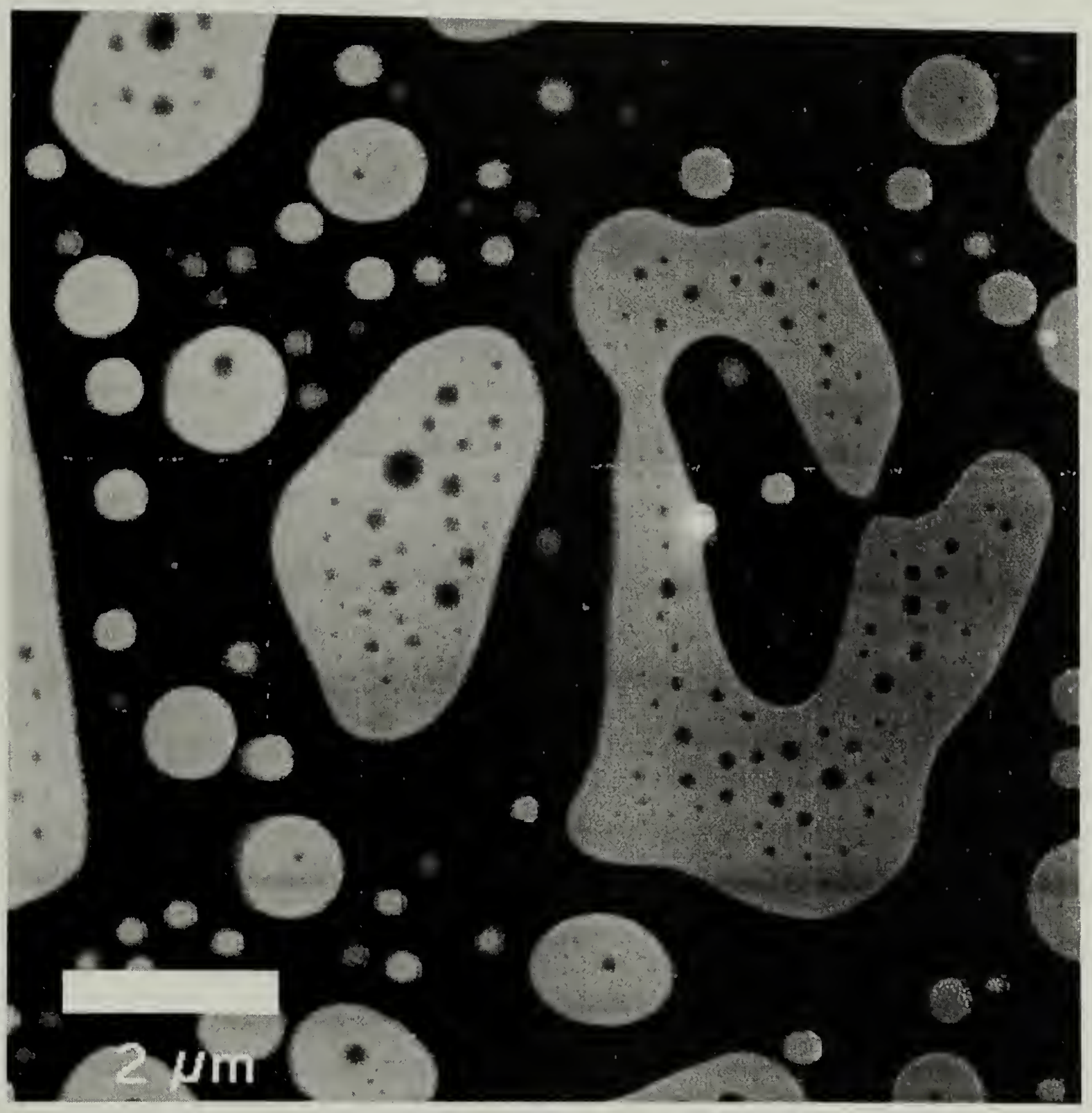

Figure 2.13. AFM height image of 30.3 kMw PS/27 kMw PMMA solution cast blend thin film after cyclohexane etch to remove the PS. Light regions are PMMA.

Cyclohexane

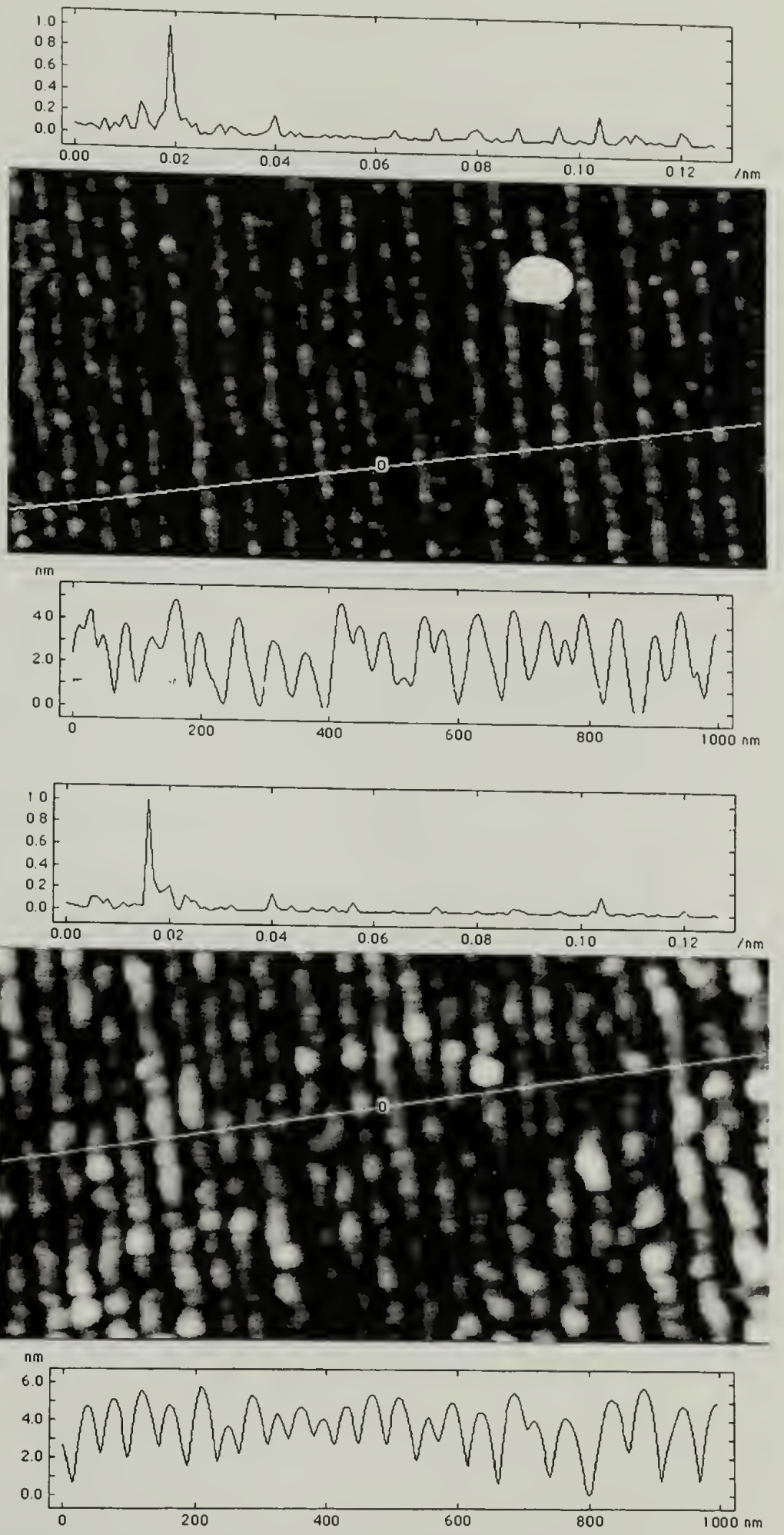

Acetic Acid

Figure 2.14. AFM height images of the nm length scale heterogeneous surface morphology after blend solution casting and selective solvent etching. Upper inset of each image is the fast fourier transform of the line selection labeled on the image to show periodicity of heterogenous surface. Lower inset is the real space cross section of the labeled line selection.

both the PMMA from the macroscopic domain above, and the PMMA adsorbed to the oxide lines between the gold, the morphology of the PS adsorption to the gold lines is revealed.

The preferential adsorption of PS to gold revealed by acetic acid etching is consistent over the entire molecular weight range of solution cast films, as shown in Figure 2.15. The AFM height images show the wide, smooth lines formed by the adsorbed PS. The large blobs greater than 100 nm in size are macroscopic PS domains left on the surface after rinsing the PMMA. As molecular weight is increased, the roughness of the adsorbed polymer lines increase as well, appearing more like a string of overlapping blobs than a uniform line. At the highest molecular weight, 127 k, some overlapping of the collapsed polymer lines is seen as well. This may result from the large radius of gyration of the homopolymer in solution, approximately 10 nm, nearly half the width of the metal lines [4,24]. As these highly extended coils of adsorbed polymer collapse, the higher molecular weight chains may 'spill over' the oxide and merge with neighboring lines. This increase in surface roughness as a function of molecular weight was quantified by AFM image analysis software and plotted in Figure 2.16. Plotted as well is the scaling argument for the film thickness generated by the collapse of an adsorbed polymer chain of increasing molecular weight to an adsorbing strip of constant width, which scales as $N^{1/5}$ [25]. Interestingly, the trend in roughness as a function of molecular weight scales similarly, supporting the argument of selective adsorption of PS to the gold lines from solution.

Selective adsorption of one polymer type from blend solutions to chemically specific surfaces has been demonstrated before, with graft copolymers of polyacrylimide

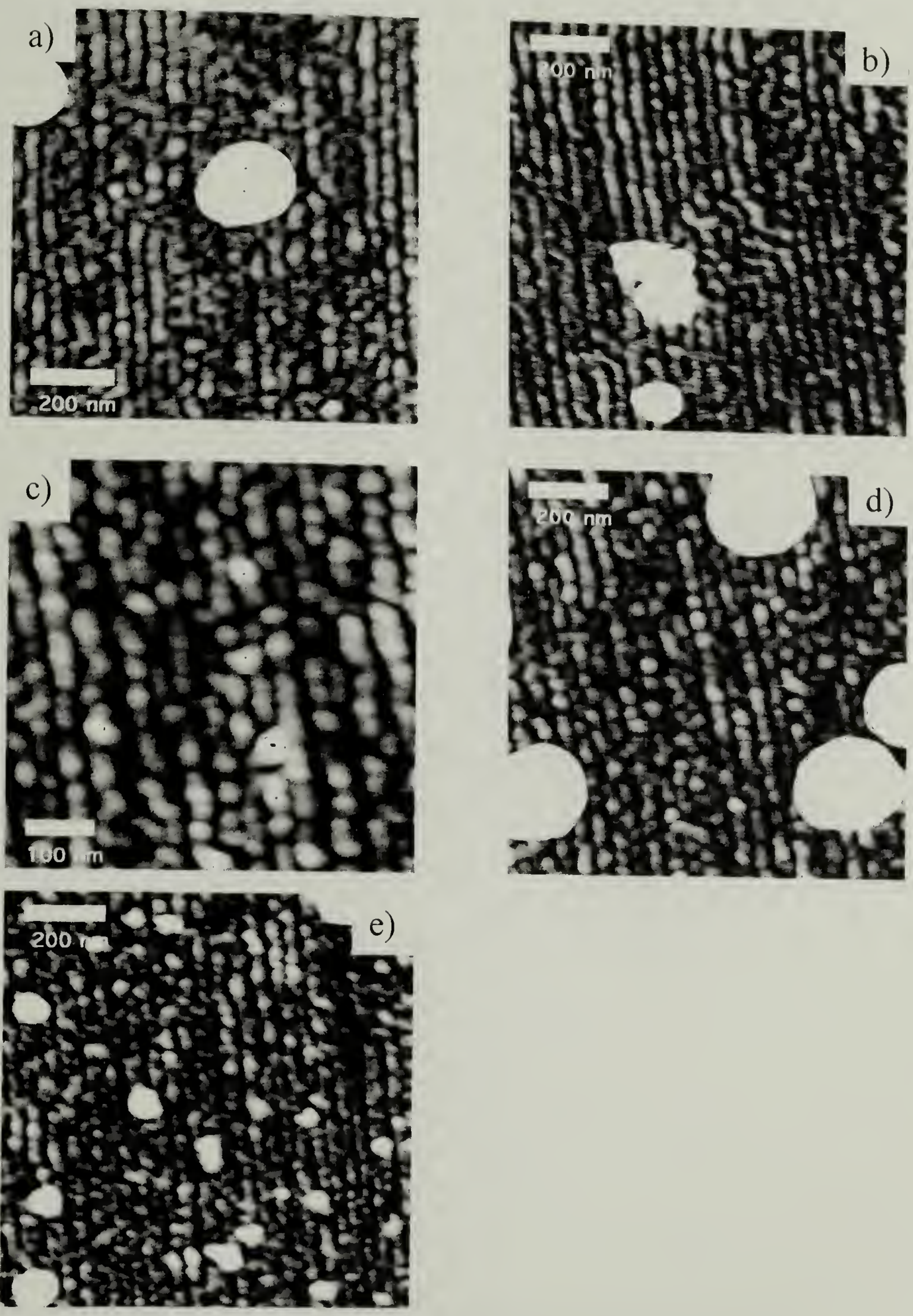

Figure 2.15 AFM height images of the PS remaining on the gold lines of the heterogeneous substrate after solution casting and acetic acid etching. a) 30 k. b) 52 k. c) 66 k. d) 95 k. e) 127 k.

and polyethyleneoxide to titania and silica, respectively [14] and PS to fumed silica in a PS-poly(n-butyl methacrylate)-CCl_4 mixture[15]. Previous experiments however, have not placed two surfaces with distinctly different adsorption properties in such close proximity, with such a small length scale. While PMMA adsorption to the oxide lines is not seen from the cyclohexane etch, it may be inferred from the periodic morphology of the PS layer on gold after the acetic acid etch removed it from the substrate. This periodic surface directed morphology is unique to the solution cast samples, due to the long adsorption time allowed for the polymer to recognize the surface chemistry. Spin casting, the more rapid film preparation technique, allows only non-specific conformal adsorption of a layer of blended composition to the surface due to the significantly shortened casting kinetics. Figure 2.17 contrasts the morphology cross sections generated from selective solvent etching of films prepared by the two casting techniques.

Clearly then, if we wish to use surfaces with nm length scale chemical heterogeneity to impart a specific response in, or direct the ordering of heterogeneous polymer solutions on molecular length scales, casting procedures with longer time scales must be used. Alternatively, if molecular length scale control is not required, rapid casting techniques such as spin casting on chemically heterogeneous surfaces will produce a response in a phase separating blend indicative of surface neutrality. This may indicate parameters for neutral substrate design, whereby the maximum sufficient substrate length scale needed for neutrality is just smaller than the kinetics of the thin film preparation technique allow fluctuations to occur on.

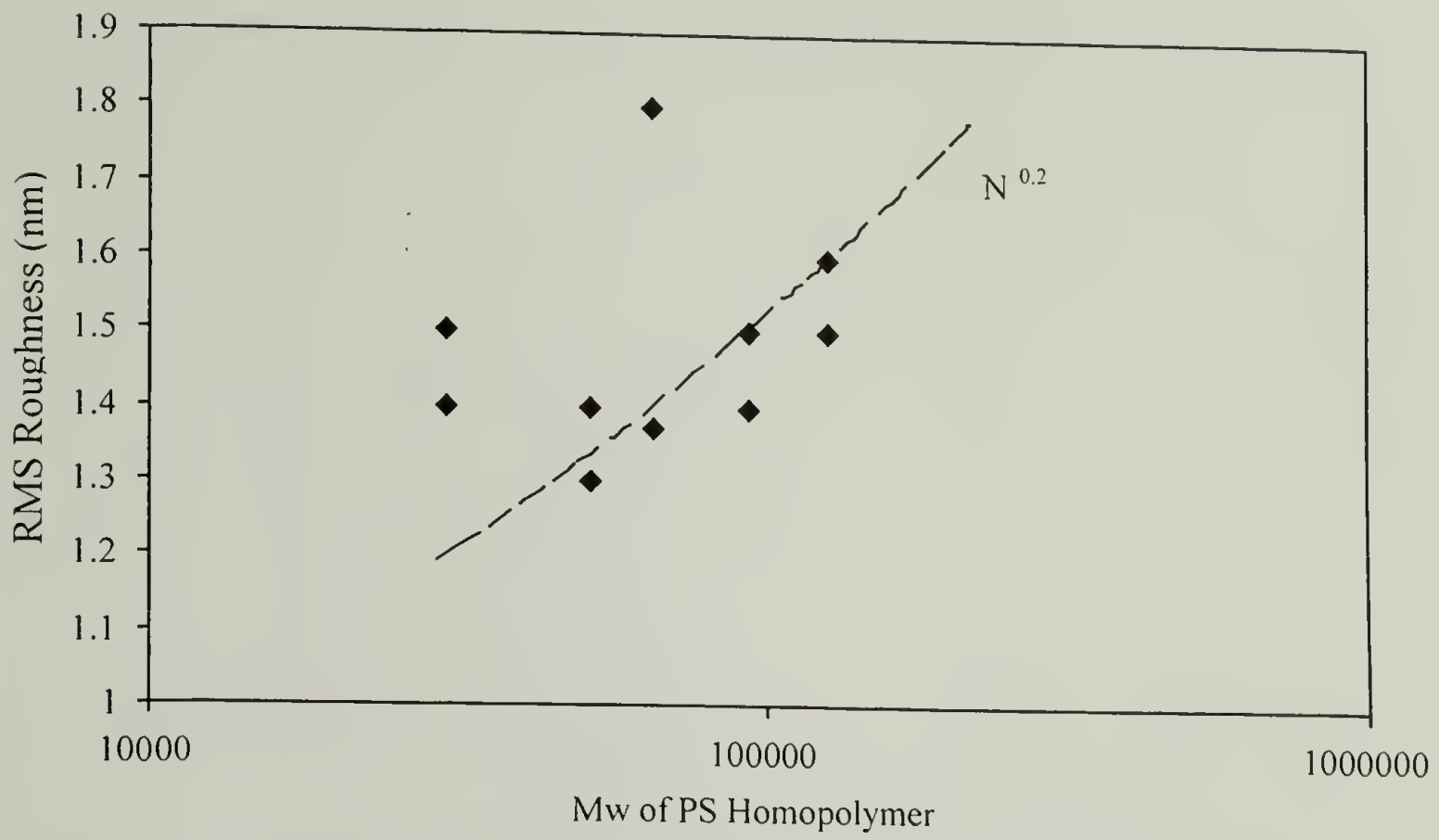

Figure 2.16. RMS roughness of polystyrene remaining on heterogeneous surface after acetic acid etch. Line is scaling law $N^{1/5}$ for thickness of collapsed, adsorbed polymer layer.

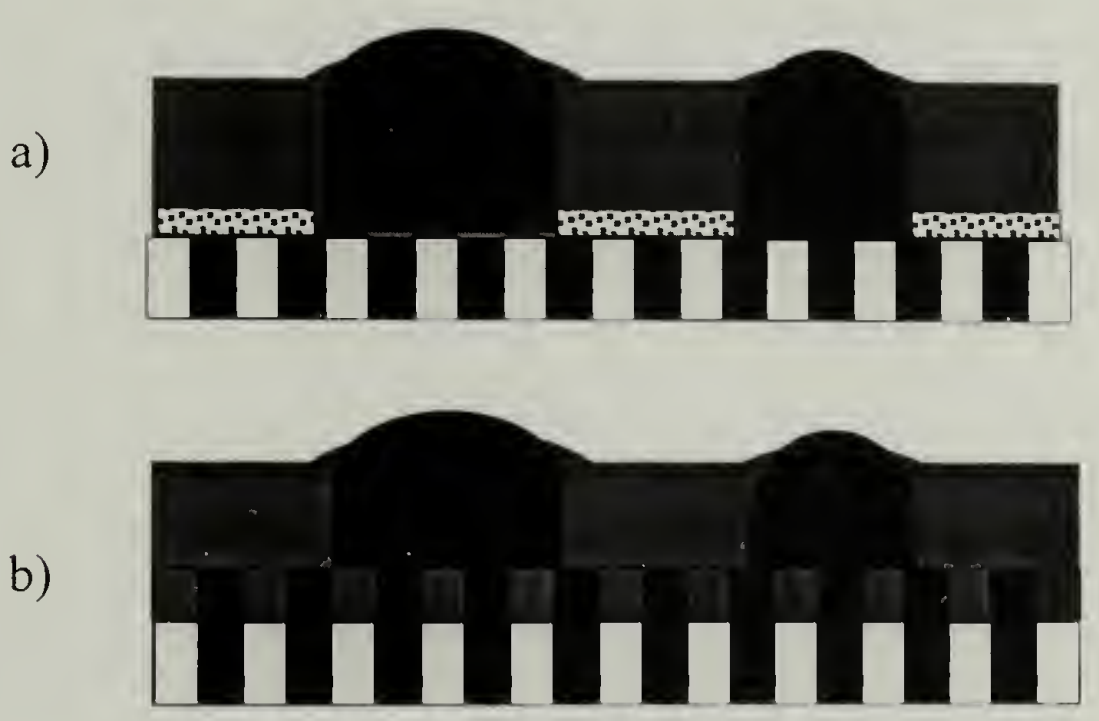

Figure 2.17. Comparison of schematic cross-sectional morphology of a) spin-cast, b) solution cast blend films on heterogeneous substrates, as reconstructed from all solvent-selective etches. PS (light gray), PMMA (dark gray), Blend (dotted).

Conclusion

The thin film preparation techniques of spin casting and solution casting have been used to generate films possessing phase separated morphologies on multiple length scales by casting homopolymer blend solutions onto chemically homogeneous and heterogeneous surfaces. Both solution and spin casting of homopolymer blends produce identical, laterally phase separated morphologies with micron sized domains due to spinodal phase separation, when cast on homogeneous gold and heterogeneous substrates. Both substrates appear 'neutral' to the PS and PMMA rich phases regardless of the casting process, as evidenced by the presence of the phase separated domains of both polymers extending uniformly from the substrate to the free surface. Selective solvent etching, however, revealed distinct differences in the substrate localized morphology depending on surface chemistry and casting conditions. Spin casting is found to produce an ultrathin layer of blended composition adjacent to the substrate on both gold and heterogeneous surfaces due to the rapid and nonspecific adsorption of both polymers to the surface. This blended layer serves as the 'neutral' surface upon which spinodal decomposition takes place, producing the laterally phase separated morphology. Solution casting however, produces an ultrathin layer of phase separated PS and PMMA adsorbed directly to the stripes on the heterogeneous surface. The increased time allowed for diffusion and adsorption during solution casting results in specific adsorption of PS to Au and PMMA to SiOx producing phase separated polymer domains on the nanometer length scale. Selective solvent etching revealed that these domains of adsorbed polymer are only a few nanometers in thickness, and the domain surface roughness increased with

polymer molecular weight. Both results indicate that the origin of these domains is in adsorption, and not in any type of confined spinodal phase separation process. This selectively adsorbed polymer layer then serves as a 'neutral' surface, due to the short length scale over which the composition fluctuates relative to the macroscopic PS and PMMA domains formed upon spinodal decomposition, resulting again in a laterally phase separated morphology on the micron scale. Thus, we find similar morphologies on the micron length scale regardless of substrate composition or casting process, but distinctly different morphologies on the nm length scale depending on both the kinetics of the casting process and the chemistry of the substrate.

References

1. Walheim, S., Böltau , M., Mlynek, J., Krausch, G. & Steiner, U. Structure Formation via Polymer Demixing in Spin-Cast Films. *Macromolecules* **30**, 4995-5003 (1997).

2. Fink, Y., Urbas, A. M., Bawendi, M. G., Joannopoulos, J. D. & Thomas, E. L. Block Copolymers as Photonic Bandgap Materials. *Journal of Lightwave Technology* **17**, 1963-1969 (1999).

3. Chen, W.-L. & Shull, K. R. Hydrophilic Surface Coatings from Acrylic Block Copolymers. *Macromolecules* **32**, 6298-6306 (1999).

4. Brulet, A., Boue, F., Menelle, A. & Cotoon, J. P. Conformation of Polystyrene Chain in Ultrathin Films Obtsined by Spin Coating. *Macromolecules* **33**, 997-2001 (2000).

5. Karim, A. *et al.* Phase-Separation-Induced Surface Patterns in Thin Polymer Blend Films. *Macromolecules* **31**, 857 (1998).

6. Böltau , M., Walheim, S., Mlynek, J., Krausch, G. & Steiner, U. Surface Induced Structure Formation of Polymer Blends on Patterned Substrates. *Nature* **391** (1998).

7. Muller-Buschbaum, P., Vanhoorne, P., Scheumann, V. & Stamm, M. Observation of Nano-Dewetting Structures. *Europhysics Letters* **40**, 655-660 (1997).

8. Steiner, U., Klein, J., Eiser, E., Budkowski, A. & Fetters, L. J. Complete Wetting from Polymer Mixtures. *Science* **258**, 1126-1129 (1992).

9. Reiter, G. Dewetting of Thin Polymer Films. *Physical Review Letters* **68**, 75-78 (1992).

10. Reiter, G. Unstable Thin Polymer Films: Rupture and Dewtting Processes. *Langmuir* **9**, 1344-1351 (1993).

11. Fukunaga, K., Elbs, H. & Krausch, G. Thin Film Phase Separation on a Nanoscopically Patterned Surface. *Langmuir* **16**, 3473-3477 (2000).

12. Kim, G. & Libera, M. Kinetic Constraints on the Development of Surface Microstructure in SBS Thin Films. *Macromolecules* **31**, 2670-2672 (1998).

13. Kim, G. & Libera, M. Morphological Development in Solvent-Cast Polystyrene-Polybutadiene-Polystyrene (SBS) Triblock Copolymer Thin Films. *Macromolecules* **31**, 2569-2577 (1998).

14. Bijsterbosch, H. D., Cohen Stuart, M. A. & Fleer, G. J. Adsorption of Graft Copolymers onto Silica and Titania. *Macromolecules* **31**, 8981-8987 (1998).

15. Lipatov, Y., Chornaya, V. & Todosijchuk, T. Adsorption from Two-Phase Solution of Polymer Blends. *Journal of Colloid and Interface Science* **188**, 32-38 (1996).

16. Green, P. F., Christensen, T. M., Russell, T. P. & Jerome, R. Surface Interaction in Solvent-Cast Polystyrene/Poly(methyl methacrylate) Diblock Copolymers. *Macromolecules* **22**, 2189-2194 (1989).

17. Mochrie, S. G. J., Song, S., Yoon, M., Abernathy, D. L. & Stephenson, G. B. Facetting of Stepped Silicon (113) Surfaces: Self Assembly of Nanoscale Gratings. *Physica B, Condensed Matter* **221**, 105-125 (1996).

18. Yoon, M., Mochrie, S. G. J., Tate, M. W., Gruner, S. M. & Eikenberry, E. F. Periodic Facetting of a Si (113) surface miscut towards (1-10). *Surface Science* **411**, 70-85 (1998).

19. Russell, T. P., Coulon, G., Deline, V. R. & Miller, D. C. Characteristics of the Surface-Induced Orientation for Symmetric Diblock PS/PMMA Copolymers. *Macromolecules* **22**, 4600-4606 (1989).

20. Reiter, G. & Sommer, J.-U. Crystallization of Adsorbed Polymer Monolayers. *Physical Review Letters* **80**, 3771-3774 (1998).

21. Fowkes, F. M. Additivity of Intermolecular Forces at Interfaces. I. Determination of the Contribution to Surface and Interface Tensions of Dispersion Forces in Various Liquids. *Journal of Physical Chemistry* **67**, 2538-2541 (1963).

22. Israelachvili, J. in *Intermolecular and Surface Forces* 176-213 (Academic Press, San Diego, 1992).

23. Cognard, J. & Biochard, C. in *Adhesion* (ed. Allen, K. W.) 169-193 (Elsevier Applied Science, London/NYC, 1984).

24. Fetters, L. J., Lohse, D. J., Richter, D., Witten , T. A. & Zirkel, A. Connection between Polymer Molecular Weight, Density, Chain Dimensions, and Melt Viscoelastic Properties. *Macromolecules* **27**, 4639-4647 (1994).

25. de Gennes, P. G. Adsorption on Stripes. *private communication* (1999).

CHAPTER 3

BLOCK COPOLYMER ULTRA THIN FILMS ON NANOPERIODIC, HETEROGENEOUS SURFACES

Introduction

A homogeneous interfacial interaction places a strong field on thin films which forces the alignment of structures and morphologies parallel to a surface [1-4]. By changing the strength of the interaction, the possibility of locally altering the orientation of the morphology exists [5,6]. Not only is the strength of the interfacial interaction a controlling factor, but also the length scale over which the interaction occurs [7-9]. An equally accessible alternative, therefore, is to use surfaces where the interfacial interaction is laterally heterogeneous, patterned such that the strength of the surface interaction is periodic. Here, we report on the influence of commensurability, between the natural length scales of polymeric systems and the periodic pattern on a chemically heterogeneous substrate, on polymer self-organization.

Recognition by a polymer or response of a polymer to lateral heterogeneities requires the proper selection of the length scales [10-15]. Investigation of phase separating homopolymer blends on patterned substrates by Böltau et. al., revealed that effective replication of a patterned self-assembled monolayer surface by the phase-separated domains occurred only when the period of the surface heterogeneities was commensurate with the coarsened domain sizes[14]. For block copolymers, theory suggests that adsorption to a patterned surface will occur as a self-similar, two-dimensional pattern matching surface film, only when certain conditions are met. Halperin finds that for block copolymer adsorption from solution, the stripe width L must satisfy the limits of

$D<L\leq L^*$, where D is the correlation length of an adsorbed 'blob' of similar chain segments, and $L^*\approx 2N_n\delta^{2/3}a$, where blocks of length N_n segments of size *a* are adsorbed with a surface energy $-k_bT\delta$ per segment[11]. For copolymer melts above the order-disorder transition (ODT), Petera and Muthukumar[12] find an abrupt reorientation of the surface pattern induced segregation of a disordered diblock phase, when the condition $L^* = 2\pi Rg/\sqrt{(2\sqrt{3})}$ is met, with Rg being the radius of gyration of the diblock in the disordered melt. When $L>L^*$ the anisotropic stretching of chains away from the surface to satisfy connectivity constraints results in a parallel orientation of the morphology. Only at $L= L^*$ is a vertical morphology predicted to develop from the surface, which will serve as the precursor for growth of a perpendicular lamellar phase when the system is quenched below the ODT. The commensurability constraint from theory is thus predicted to be more rigid for stretched blocks with $L>L^*$, than for the compressed case, $L<L^*$. It is clear however, that commensurability between the size scale of the polymer and the surface pattern must exist in order to induce recognition of the pattern by the polymer as well as accurate replication.

To determine more conclusively the window of commensurability between copolymer and substrate periods leading to the generation of surface directed morphologies, copolymers on striped surfaces have been investigated by numerical calculations and Monte Carlo simulations[16-20]. These techniques allow for explicit control over boundary conditions, length scales, and system free energy, and have been used to predict the morphology and phase diagram of block copolymer thin films on patterned substrates in confined, thin film geometries. Pereira, through application of the Frenkel-Kontorawa model[16], showed that a striped surface potential could induce a

vertical lamellar morphology in the regime where the block half period $\lambda/2$ is equal to or greater than the stripe width L_s. For incommensurate molecular weights where $\lambda/2>L_s$, thinner films favor commensurate morphologies with perpendicular lamellae composed of compressed chain configurations, where surface energy minimization dominates over entropic chain stretching effects. Thicker films favor incommensurate layers with non pattern-matched films with high energy interfaces. Crossover from commensurate to incommensurate phases as a function of film thickness and surface energy was calculated explicitly based on dimensionless variables, and phase diagrams were constructed to predict morphology. The calculations of Chen and Chakrabarti[17,18] and the simulations of Wang et. al.[19,20] both predict perpendicular lamellar morphologies for the commensurate case, and mixed morphologies for slightly incommensurate molecular weights whereby a commensurate surface bound morphology evolves into an incommensurate phase in thicker films. Chen, however, only examined the phase space where the copolymer period $\lambda \leq$ substrate period, and for ultra thin films of thickness $\leq \lambda$ found a window of commensurability as large as 30% with a defect-rich substrate oriented perpendicular lamellar phase at a degree of commensurability $\delta = 0.667$. Wang performed simulations over the entire commensurability range at a number of film thicknesses to generate the most complete phase diagram. A window of commensurability as large as 50% in compression and 70% in tension was found for ultra thin films of thickness $\lambda/2$, and a more modest 40% and 50% for films of thickness λ. From these studies it is predicted that the window of commensurability should be large enough for a significant range of molecular weights to orient on a single length scale patterned surface. The size of the window over which a perpendicular lamellar

morphology ean extend throughout the entire film thiekness however, may be strongly dependent on both film thickness and surfaee and interfaeial energies.

Here, we will investigate the behavior of bloek eopolymers having different moleeular weights with eharacteristie lamellar periods in the 10s of nm regime on chemieally heterogeneous substrates, in order to determine the effeet of commensurability on a model experimental system. Striped substrates comprising periodieally varying polar (silieon oxide) and non-polar (gold) interaetions have been prepared where the period and stripe width are eomparable to the size of the period of phase-separated bloek copolymer lamellae. The eopolymer poly(styrene-bloek-methyl methacrylate), denoted p(S-b-MMA), will be used beeause of its amphiphilie ehemistry, possessing a polar MMA bloek and a nonpolar PS bloek whieh mimics the substrate chemistry. Ultra thin films will be east from dilute solution and the free surface of the films imaged by atomic foree mieroscopy (AFM) to determine the morphology. The window of commensurability for this experimental system will be explicitly defined, and the defect structures and strain in the lamellar morphology arising from the frustration inherent in the incommensurate phases will be diseussed.

Experimental

Substrates

Heterogeneous substrates were prepared as outlined in Chapter 1. Substrates with a 42 or 52 nm average periodicity and a 3-4 nm average amplitude after metallization were used. Metal linewidths are 25 +/- 2 nm, measured as the full width at half maximum of the peaks generated in an AFM line scan. Some samples were reused after film

characterization, having been rinsed thoroughly in toluene in an ultrasound bath after each experiment to remove the previous polymer layer.

Thin Film Preparation

Symmetric diblock copolymers of p(S-b-MMA) were purchased from Polymer Labs, or synthesized in-house. All of the copolymers were soxhlet extracted in cyclohexane to remove any residual polystyrene homopolymer. Table 3.1 presents the copolymer compositions used, ranging from 53 k (53,000 g/mol) to 535 k, the calculated bulk copolymer period[21], and the degree of commensurability (δ) for each molecular weight. δ is the ratio of the period of the copolymer morphology in the bulk to the period of the heterogeneous striping of the substrate, either 42 nm or 52 nm. Solutions of 0.1 wt% polymer in HPLC grade toluene were prepared.

Table 3.1. Polymers used in thin film casting experiments

Copolymer	Mw (kg/mol)	PDI	Period L (nm)	δ for 42 nm substrate	δ for 52 nm substrate
S/MMA	53		27.38	0.65	0.53
S/MMA	84		36.93	0.88	0.71
S/MMA	107.8	1.1	43.22	1.03	
S/MMA	113	1.1	44.78	1.07	0.86
S/dMMA	121.3	1.12	46.82	1.11	0.90
S/MMA	177		59.95	1.43	1.15
S/MMA	214		67.82	1.61	1.30
S/MMA	300		84.48	2.01	1.62
S/MMA	535		123.04		2.37

Solution casting was performed in a closed glass crystallization dish in the presence of excess solvent, in an effort to control the rate of solvent evaporation and

promote an equilibrium morphology [22]. Substrates were placed within a 600 ml aluminum foil covered glass crystallization dish. Inside the casting container was an additional small dish filled with toluene, to saturate the vapor pressure inside and mediate solvent evaporation from the substrate. A syringe inserted through a small, 0.3 cm^2 hole in the foil covering allowed for wetting of the substrates with polymer solution, as well as controlled evaporation. The substrates were wet entirely, but the solution prevented from spilling over the substrate edge due to surface tension. Solvent evaporated completely over the course of 30 minutes.

Characterization

Thin films were characterized by atomic force microscopy (AFM) on a Digital Instruments Di3100 using tapping mode. The composition and height variations on the film's free surface from the presence of both PS and PMMA lamellae provided a height and phase signal to the AFM tip, from which an image of the morphology was constructed. The bundled AFM software package allowed measurement of the average lamellar period by calculating the Power Spectral Density of each image to determine the dominant surface wavelength. A two-dimensional Fourier transform could be applied to the images as well, and the peak positions measured to determine the same information.

The degree of orientation of the perpendicular lamellae was determined in a manner analogous to the measurement of crystal orientation from Xray scattering data of drawn semicrystalline polymer fibers. The 2D Fourier transform of each AFM image was calculated to produce a reciprocal space scattering pattern. From the scattering data, composed of intensity, I, as a function of scattering vector $\boldsymbol{q}$ and rotation angle ϕ, the average cosine squared can be evaluated using the following equation:

$$< \cos^2 \phi >= \frac{\int_0^{\frac{\pi}{2}} \int_0^{\infty} I(\bar{q},\phi)\sin(\phi)\cos^2(\phi)d\bar{q}\,d\phi}{\int_0^{\frac{\pi}{2}} \int_0^{\infty} I(\bar{q};\phi)\sin(\phi)d\bar{q}d\phi} \qquad (1)$$

The 'orientation' measured by this equation is an average over the angle each scattering center in the material makes with respect to a predefined director at $\phi = 0$. Using Rhinolyzer image analysis software, the scattering data $I(q,\phi)$ were integrated from q to q', since for a given angle ϕ the scattered intensity outside the q range of interest equals zero, yielding $I(\phi)$. $I(\phi)$ was then integrated by summation, calculating $\sin(\phi)$ and $\cos^2(\phi)$ for each $I(\phi)$, completing the $<\cos^2\phi>$ integral. Finally, the orientation function 'f' was evaluated by calculating $(3<\cos^2\phi>-1)/2$, the Hermann's orientation function, which possesses a value of 1 for perfect orientation, and 0 for an isotropic system.

Results and Discussion

Surface Directed Orientation

Figures 3.1 and 3.2 show the AFM phase images of the entire series of films cast on 52 nm substrates from low to high molecular weight. Distinctly different copolymer morphologies are observed as a function of molecular weight, with a clearly defined commensurate regime where surface control over lamellar ordering is expressed. Strong surface directed ordering with few defects is evident for 121 k and 177 k with nearly commensurate δ values of 0.9 and 1.15 respectively. The lower molecular weight 113 k sample with $\delta = 0.86$ and the higher molecular weight 214 k and 177 k samples with $\delta = 1.15$ and $\delta = 1.3$ posses a very defect-rich morphology yet are clearly surface directed. The other molecular weights outside this window possess little or no surface directed

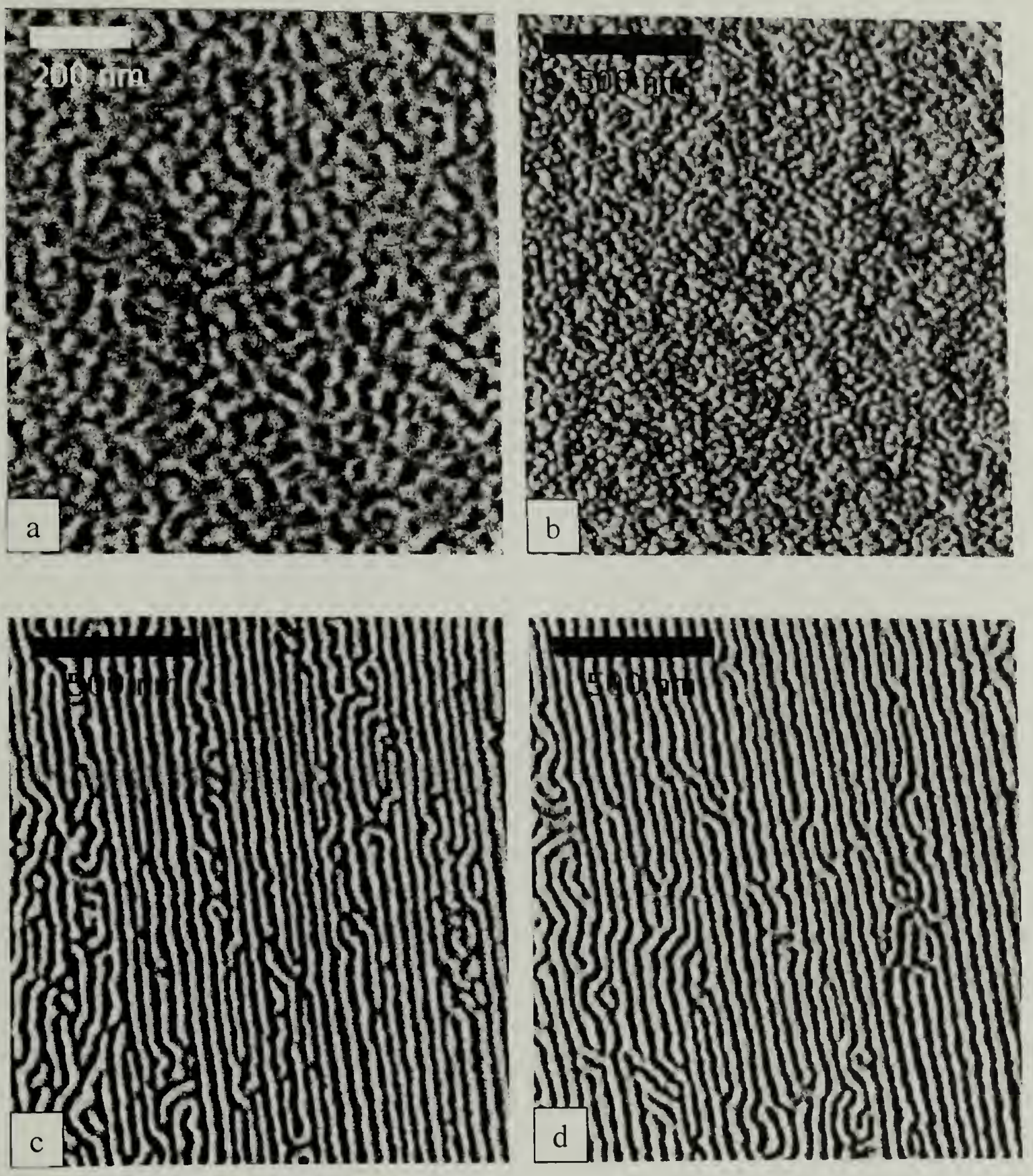

Figure 3.1. AFM tapping mode phase images of the free surface of p(S-b-MMA) films cast from 0.1 wt% toluene solution over 30 minutes onto 52 nm heterogeneous substrates. Images are ordered by molecular weight [degree of commensurability δ] a) 53k [0.53]. b) 84k [0.71]. c) 113k [0.86]. d) 121k [0.90].

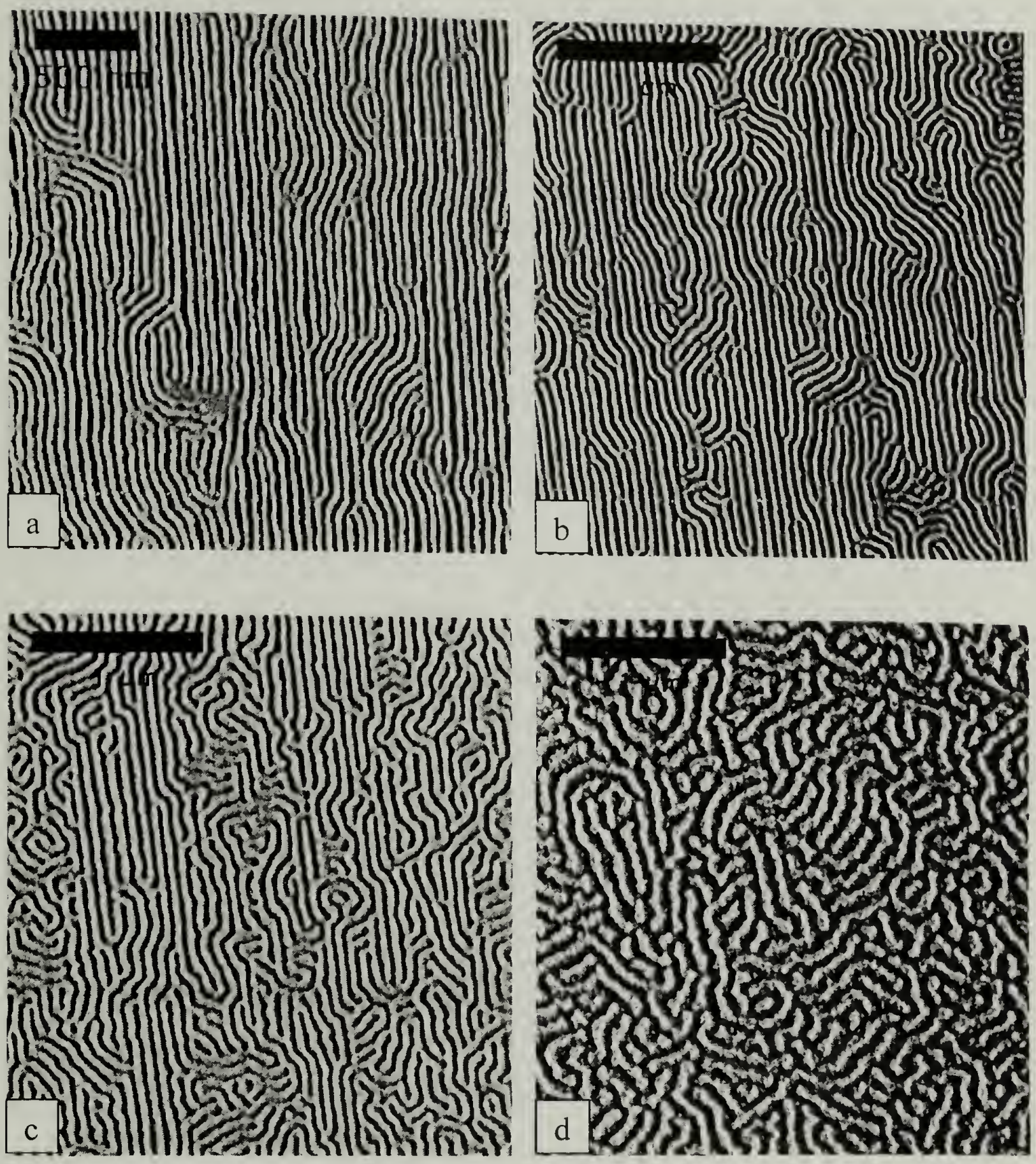

Figure 3.2. AFM tapping mode phase images of the free surface of p(S-b-MMA) films cast from 0.1 wt% toluene solution over 30 minutes onto 52 nm heterogeneous substrates. Images are ordered by molecular weight [degree of commensurability δ] a) 177k [1.15]. b) 214k [1.30]. c) 300k [1.62]. d) 535k [2.37].

ordering. For the lowest molecular weights, 53 k and 84 k, the morphology is unidentifiable, though clearly phase separated according to the color contrast on the AFM phase images which indicates composition fluctuations along the free surface. The highest two molecular weights at 300 k and 535 k possess lamellae oriented perpendicular to the substrate, with the 300 k sample having surface direction over a small fraction of the image area.

All of the morphologies generated on the heterogeneous surfaces are distinctly different than those produced from casting on a homogeneous surface of SiOx or gold. Figure 3.3 shows the morphology of ultrathin films of 113 k copolymer cast upon homogeneous surfaces. For the oxide surface; the lamellar microdomains are oriented parallel to the substrate due to strong interactions between the SiOx and the PMMA. Island and hole formation[23] is indicated by the step from the 0^{th} to the 1^{st} parallel layer of the copolymer lamellae which appears in the lower third of the image. For the gold surface, a mixed morphology is present where both parallel and perpendicular grains of lamellae are present at the free surface of the film. Island and hole formation is not seen, and the film is of uniform thickness. Film thickness measured by AFM for all samples was on the order of 30 nm, less than the natural copolymer period for all molecular weights. While this may contribute to orientation of the morphology normal to the surface due to confinement effects[8,24], it can not explain the lateral uniformity of the morphology present in the commensurate cases, which clearly arises from the heterogeneous substrate.

The degree of surface directed orientation of the perpendicular lamellae for each copolymer can be quantified by determining the orientation function, $f = 3\langle\cos^2\Theta\rangle - 1/2$,

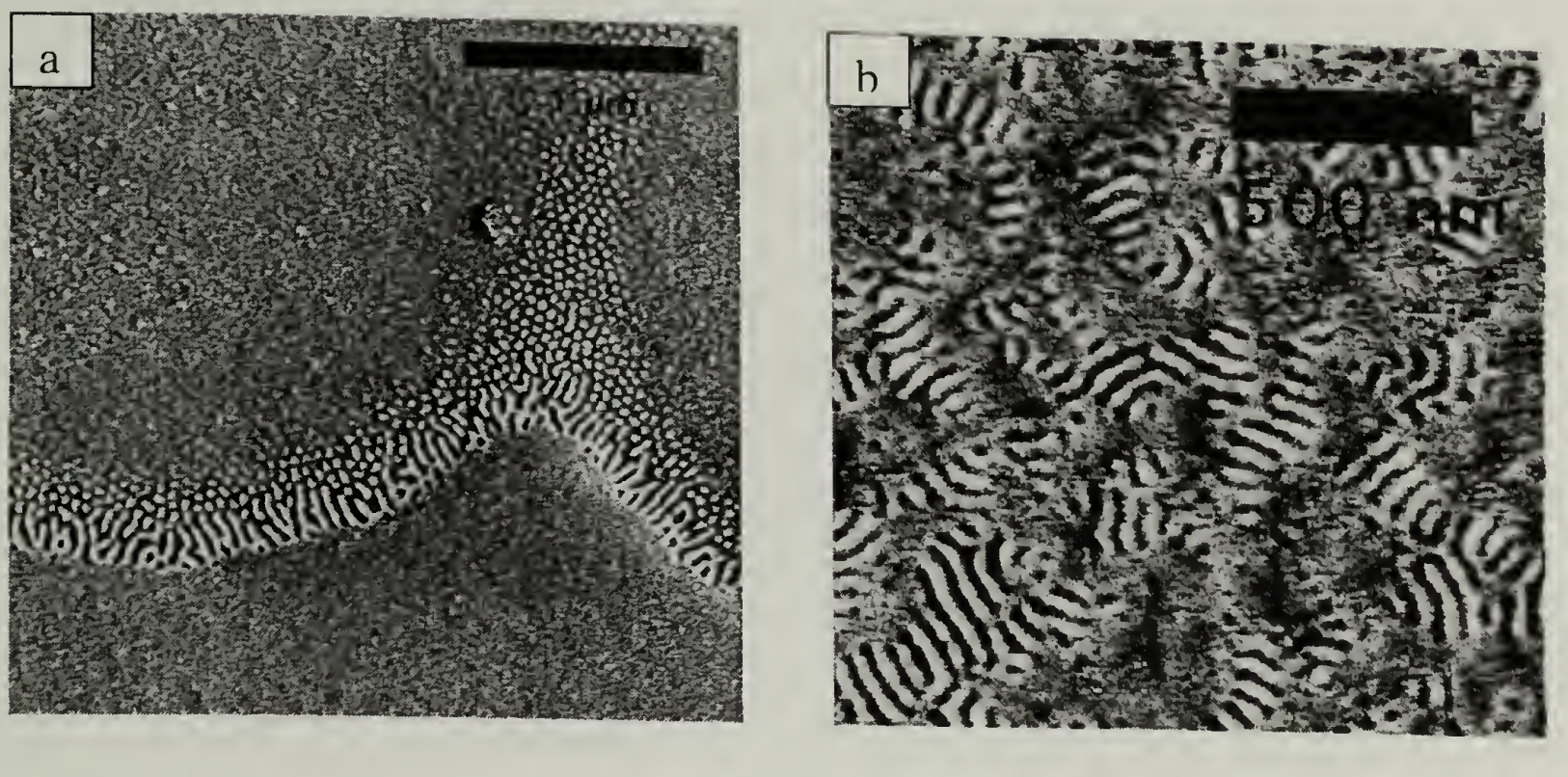

Figure 3.3. AFM phase images of the free surface of p(S-b-MMA) 113 kMw thin films solution cast from 0.1 wt% toluene on a) SiOx. b) Au.

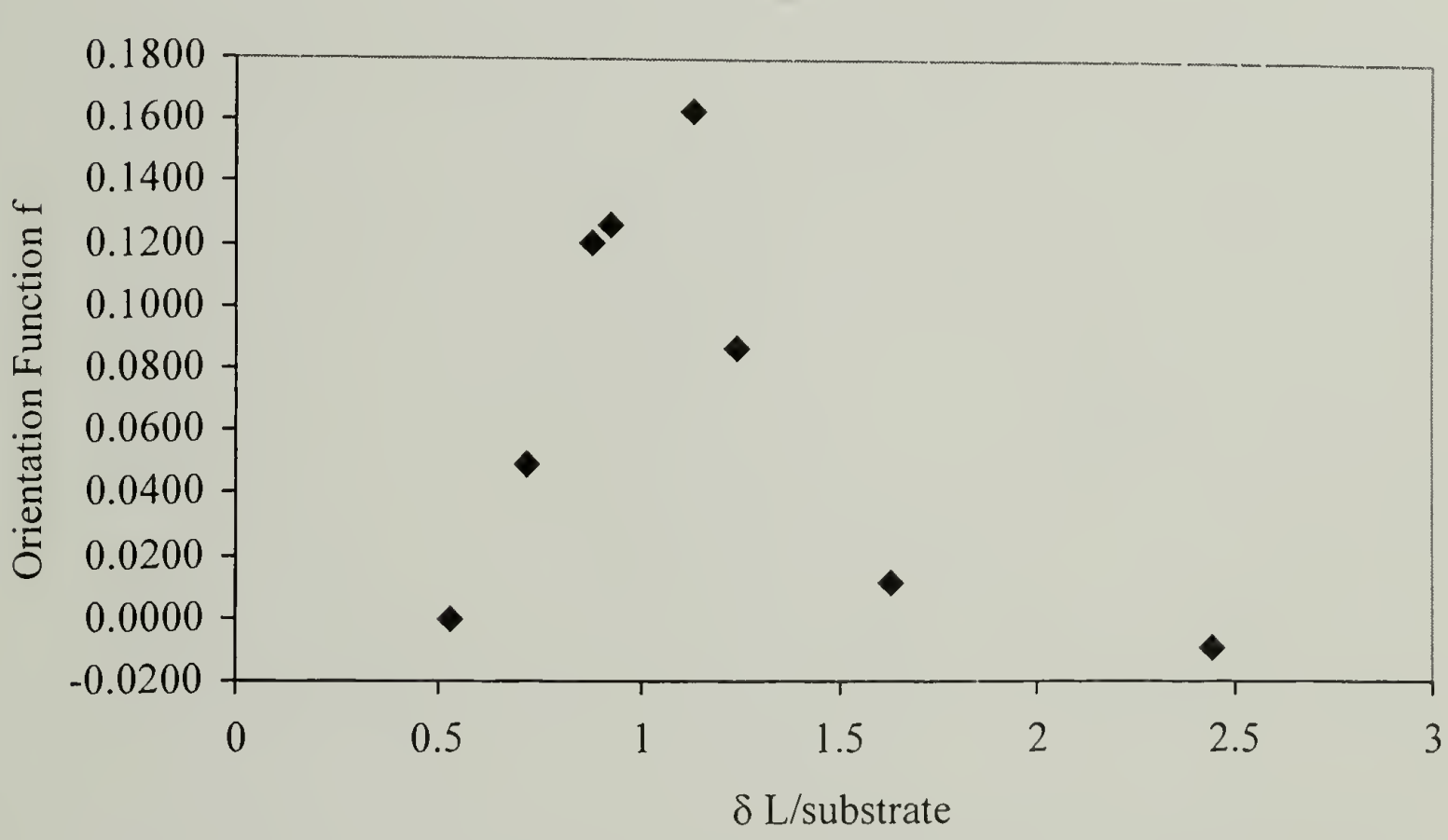

Figure 3.4. Orientation function f as a function of degree of commensurability for solution cast block copolymer thin films on 52 nm heterogeneous substrates.

for each image. f is calculated from the image analysis of the AFM data as outlined above, and plotted in Figure 3.4 as a function of the degree of commensurability. The peak in the data centered around $\delta = 1$, where the degree of surface directed ordering of the lamellae is highest, is the window of commensurability for this system. Incommensurate cases with too low or high a copolymer period, possess no strong surface direction and maintain a value of $f \approx 0$. The width of the window of commensurability, taken as the full width at half maximum of the Gaussian curve fit to the data is +/- .25 δ, indicating a 25% mismatch between copolymer period and substrate period is the maximum allowed for a reasonable replication of the substrate pattern by the polymer. This value is significantly smaller than that predicted by the studies of Chen and Wang, for films of thickness $< \lambda$. The much shorter copolymer chain lengths needed to model copolymers for their calculations and simulations may have resulted in an underestimate of the entropic penalty for stretching the chains onto an incommensurate patterned substrate, and allowed substrate replicating morphologies at higher values of δ.

If commensurability of length scales between the copolymer and the substrate is truly driving the orientation of the morphology seen on the 52 nm substrates, then decreasing the substrate period should shift the window to lower molecular weights, bringing surface directed ordering to unoriented copolymers, and removing orientation from others. Figures 3.5 and 3.6 show the AFM phase images of a series of copolymers cast on a 42 nm substrate. In Figure 3.5.b we see that what was previously an unoriented morphology for the 84 k copolymer is now a defect-rich oriented phase. With $\delta = 0.88$ on a 42 nm substrate, the 84 k copolymer has become slightly more commensurate than before, allowing the morphology to follow the substrate pattern and become oriented.

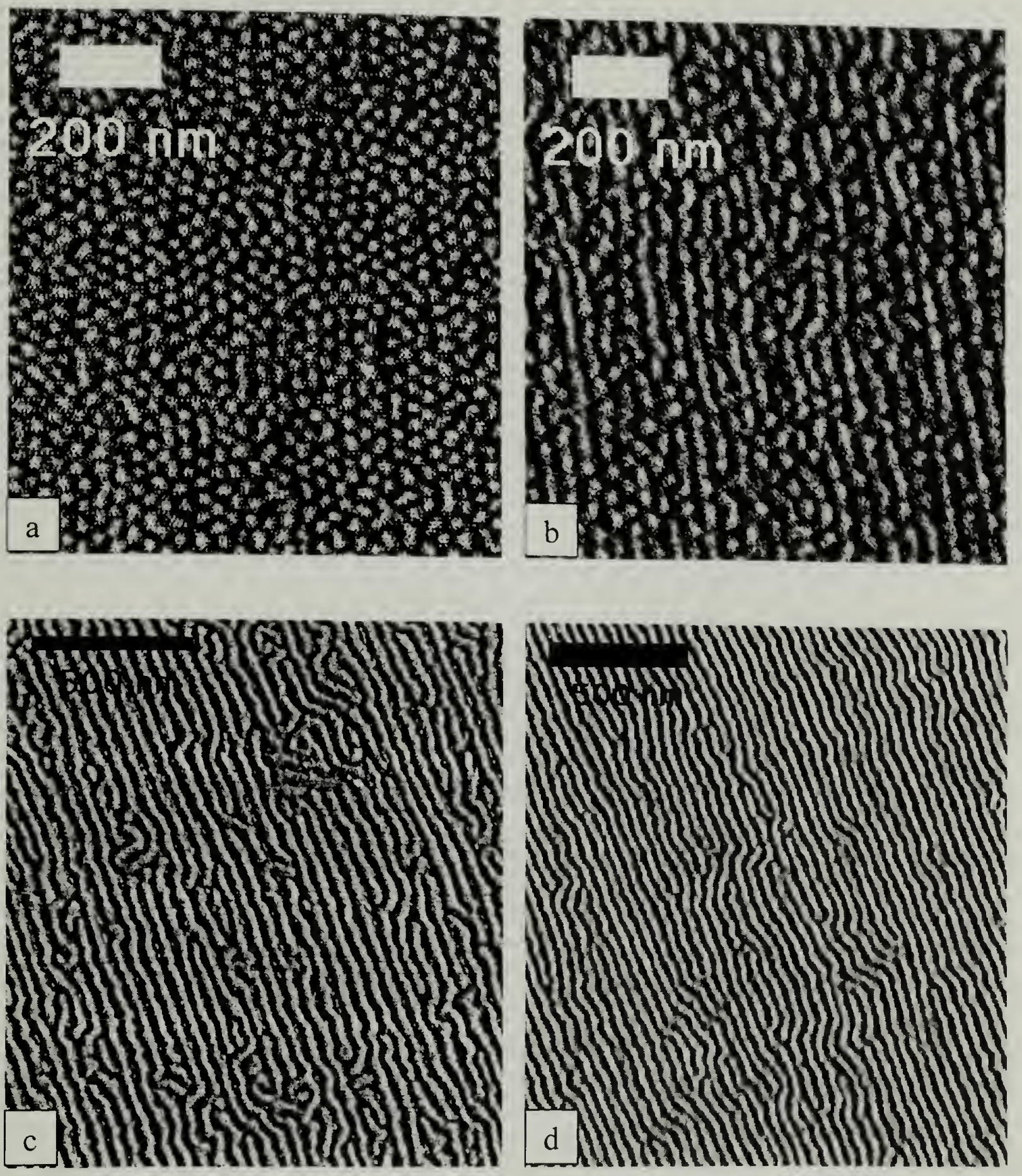

Figure 3.5. AFM tapping mode phase images of the free surface of p(S-b-MMA) films cast from 0.1 wt% toluene solution over 30 minutes onto 42 nm heterogeneous substrates. Images are ordered by molecular weight [degree of commensurability δ] a) 53k [0.65]. b) 84k [0.88]. c) 113k [1.03]. d) 121k [1.07].

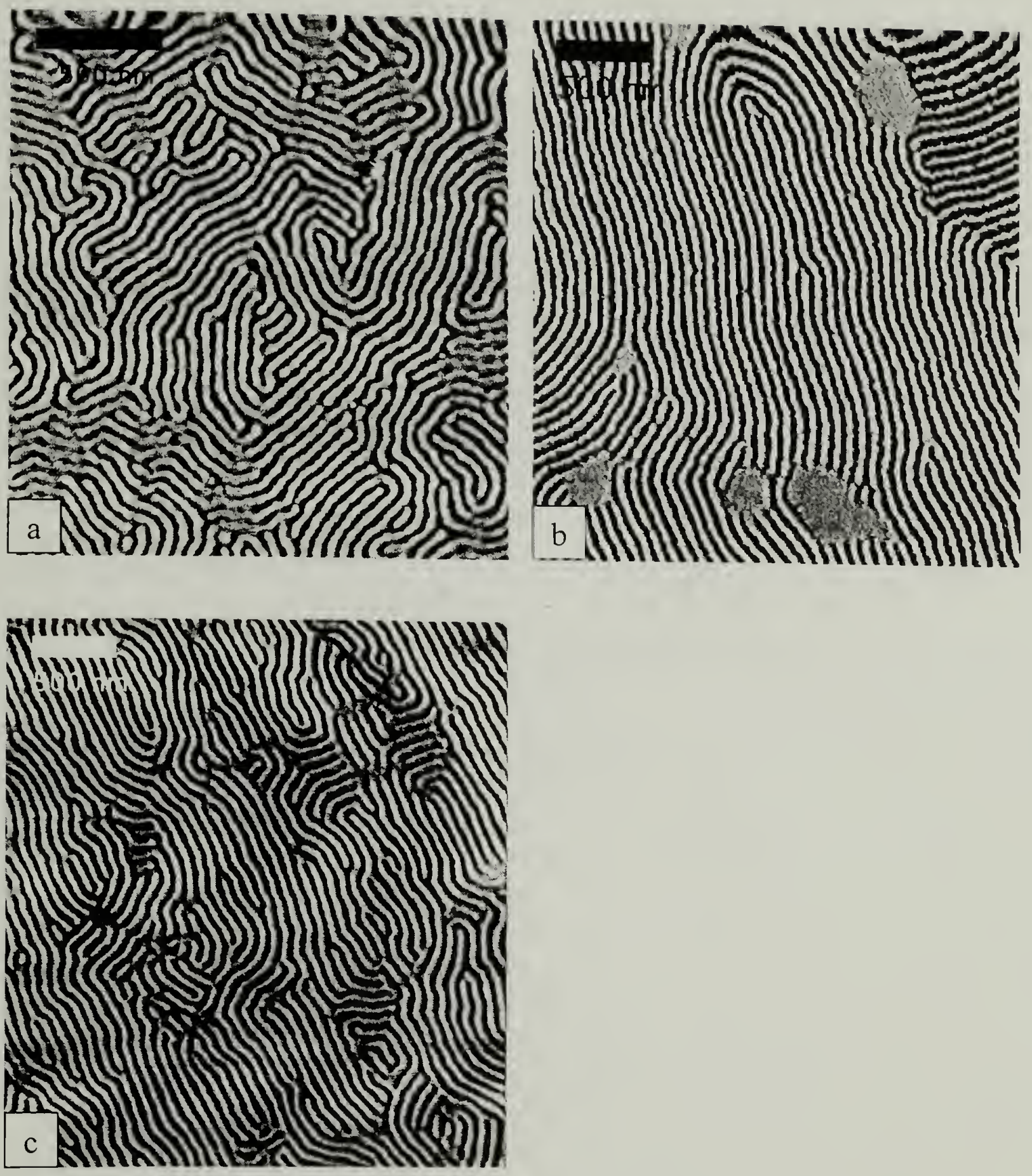

Figure 3.6. AFM tapping mode phase images of the free surface of p(S-b-MMA) films cast from 0.1 wt% toluene solution over 30 minutes onto 42 nm heterogeneous substrates. Images are ordered by molecular weight [degree of /commensurability δ] a) 121k [1.11]. b) 214k [1.61]. c) 300k [2.01]

For the higher molecular weights however, the opposite has happened. Molecular weights of 121 k and higher organize into perpendicular lamellar morphologies without any surface direction.

Figure 3.7 plots the value of the orientation function f for the copolymers on the 42 nm substrates as a function of the degree of commensurability δ. The window of commensurability is present, but it appears narrower than the 52 nm substrate window. The data point spread precludes a useful curve fit to the data, however the lack of orientation in the 121 k sample bounds the window to roughly 10% in compression. The defect rich ordering in the 84 k sample, with δ = .88, puts the window lower bound at 10-15% as well. Such a molecular weight dependence on the width and asymmetry of the commensurability window has not been investigated by any theoretical or numerical analysis. Some asymmetry is evident in the phase diagram of Wang. et. al.[20], however it is weighted in the opposite manner, with a larger window in tension than compression. Annealing was performed on the solution cast films to determine whether the cast morphologies are the equilibrium morphology or a kinetically trapped phase. Samples were placed in a vacuum oven and annealed at 160° C for 3 days. AFM images showed no change on any samples, with exception of the 53 k and 84 k copolymers cast on 42 nm substrates. Figure 3.8 shows the AFM images of the two films before and after annealing. The defect-rich, discontinuous perpendicular lamellar morphology of the 84 k sample has coarsened into a much more highly ordered and surface-oriented lamellar phase. The 53 k sample has coarsened as well, but the improvement in ordering is

minimal, with only a few lamellae oriented by the substrate pattern. The degree of improvement in ordering was quantified by image analysis and incorporated into the plot in Figure 3.7 as the open square symbols.

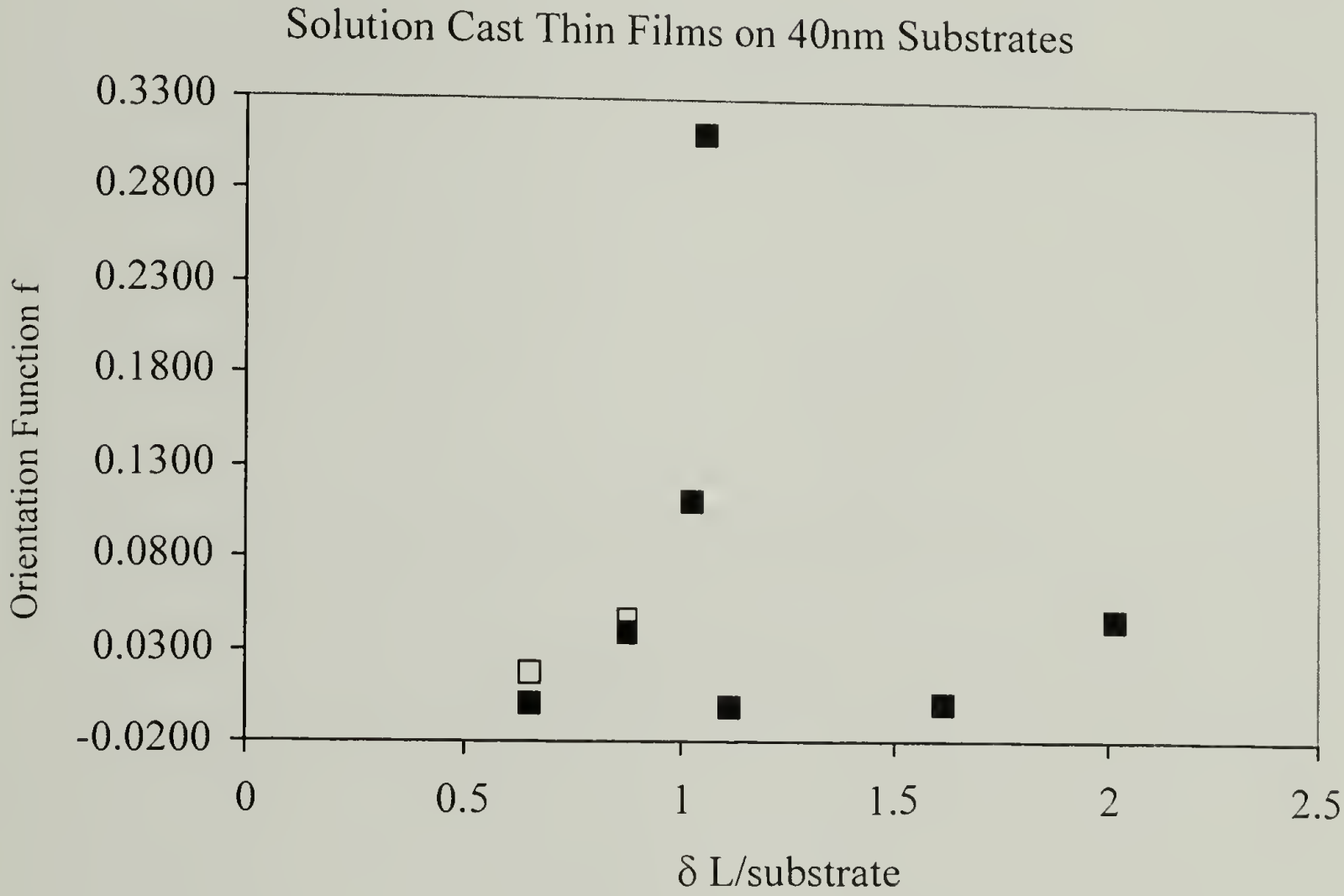

Figure 3.7. Orientation function f as a function of degree of comensurability for solution cast block copolymer thin films on 42 nm heterogeneous substrates. Open squares indicate change in orientation function value after annealing.

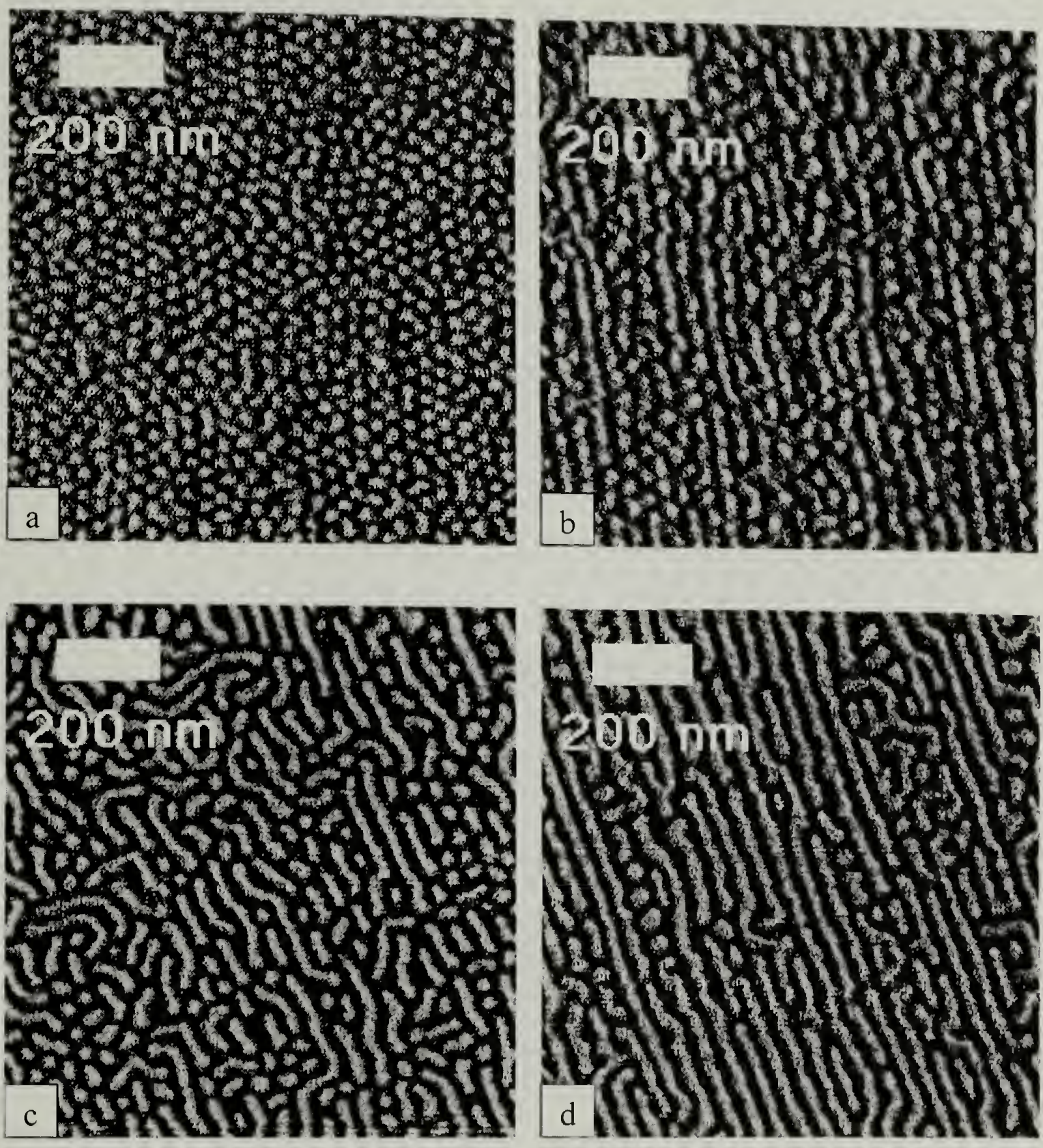

Figure 3.8. AFM tapping mode phase images of the free surface of p(S-b-MMA) films cast from 0.1 wt% toluene solution over 30 minutes onto 42 nm heterogeneous substrates. a) 53k as cast b) 84k as cast c) 53k annealed d) 84k annealed.

Strain

Analysis of the AFM images of the substrate oriented commensurate morphologies in Figures 3.1, 3.2, 3.5, and 3.6 reveals a change in the copolymer lamellar period as a function of molecular weight. While this is to expected of the bulk lamellar morphology of a copolymer which scales like $N^{0.65}$ for a p(S-b-MMA) copolymer[21], for these ultrathin films possessing a strong surface direction one might expect the lamellar period to be coupled to the substrate period and therefore constant as a function of molecular weight due to 'confinement' by the substrate chemistry. Preferential segregation of PMMA to the oxide and PS to the gold stripes occurs at the substrate on a single length scale, 42 or 52 nm, despite the copolymer molecular weight, and thus for the surface oriented phases one would expect a copolymer period of only 42 or 52 nm. This is clearly not the case however, and in Figure 3.9 the measured free surface copolymer period for all samples is plotted as a function of molecular weight. The solid line on the graph is the bulk copolymer period scaling law derived empirically for P(S-b-MMA) by Anastasiadis et. al.[21]. What is observed is a molecular weight dependence that is neither constant nor bulk like. For the lower molecular weights a copolymer period larger than the bulk is measured, and for higher molecular weights a smaller copolymer period is measured. Thus for the surface directed phases in the commensurate regime, for $\delta < 1$ the copolymer period is positively strained, but not to an extent large enough to map the lamellar morphology onto the substrate period. For the copolymers with $\delta > 1$, the opposite is true, and the morphology must compress to follow the substrate pattern. As the strain in the morphology is not sufficient for a 1:1 mapping, defects must be periodically generated in the perpendicular lamellar morphology to allow

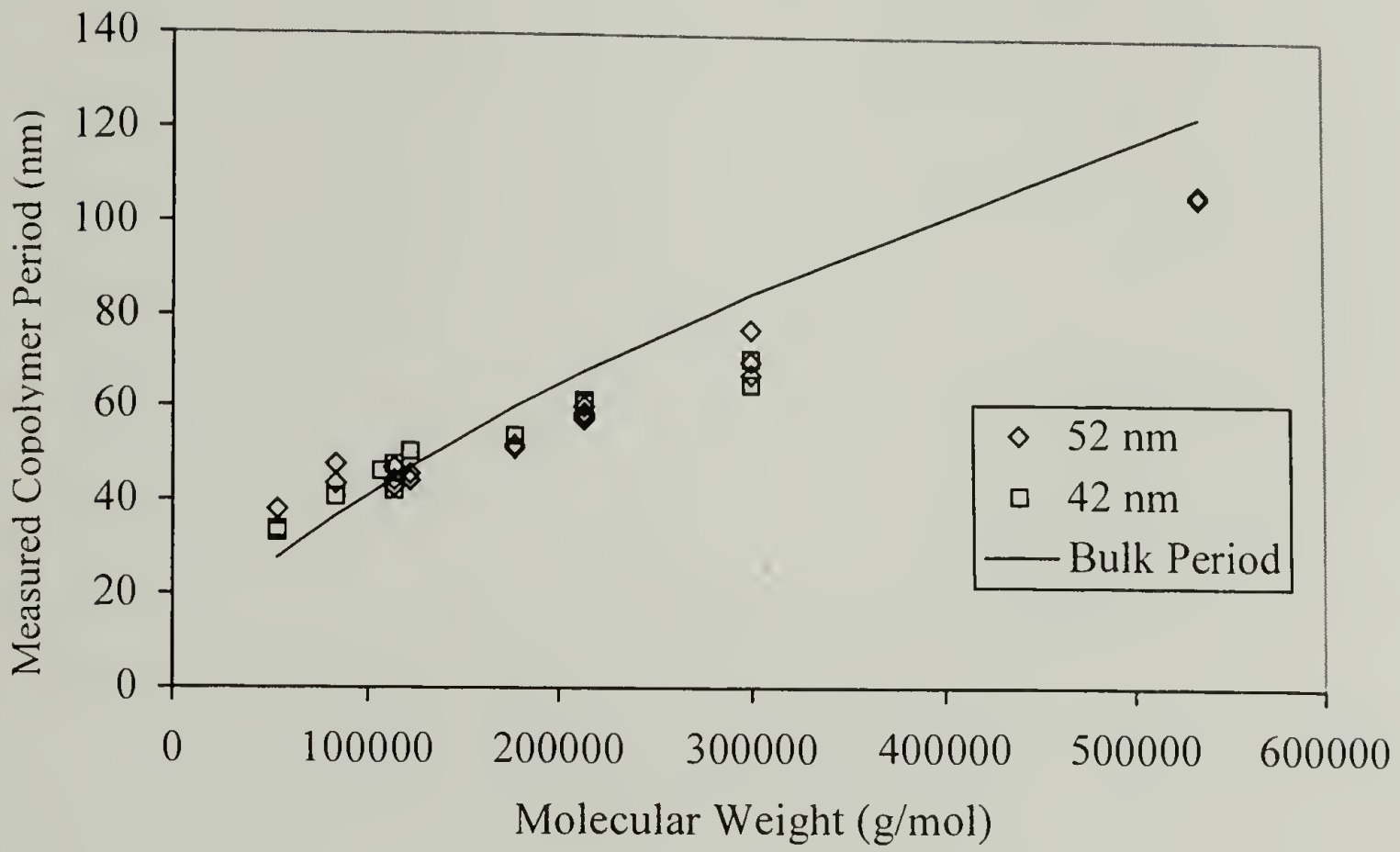

Figure 3.9. Block copolymer period as a function of molecular weight. Diamonds indicate films on 52 nm substrates, squares for 42 nm substrates. Line is based on calculation of bulk copolymer period.

for recovery of registration between the polymer and the substrate. As δ varies farther from 1, the defect density in the surface directed phase increases until ultimately no surface direction is possible because of the large degree of incommensurability between copolymer and substrate.

Figure 3.10 plots the data in terms of strain in the copolymer period as a function of the degree of commensurability. There is a distinct linear dependence in the measured strain as a function of δ running through zero strain at $\delta = 1$. Lower molecular weight samples must stretch, while higher molecular weight samples must compress to map the lamellar morphology onto the substrate pattern. For values of $\delta > 1.5$ the strain becomes independent of molecular weight and the data level off. For these high molecular weight copolymers the substrate chemistry alternates on a length scale too small for the lamellae to follow and an unoriented perpendicular morphology forms, driven by confinement. The unoriented copolymers are free to adopt a more bulk-like copolymer period, producing the crossover in the data. Any strain remaining is due to the confinement of the morphology to a thickness $<< \lambda$, not the substrate pattern which is completely ignored.

The amount of strain seen in the oriented lamellar morphologies is large, as high as 40% in tension for the lower molecular weights and 20% in compression for the higher samples, but is not unreasonable considering previous experimental studies on strain in confined lamellar morphologies. Lambooy et. al. observed strain in p(S-b-MMA) copolymer lamellae confined between two preferential SiOx surfaces[7]. When the separation distance between the surfaces was not an integer number of layers, the lamellae were found to stretch or compress as necessary to fill space. The maximum

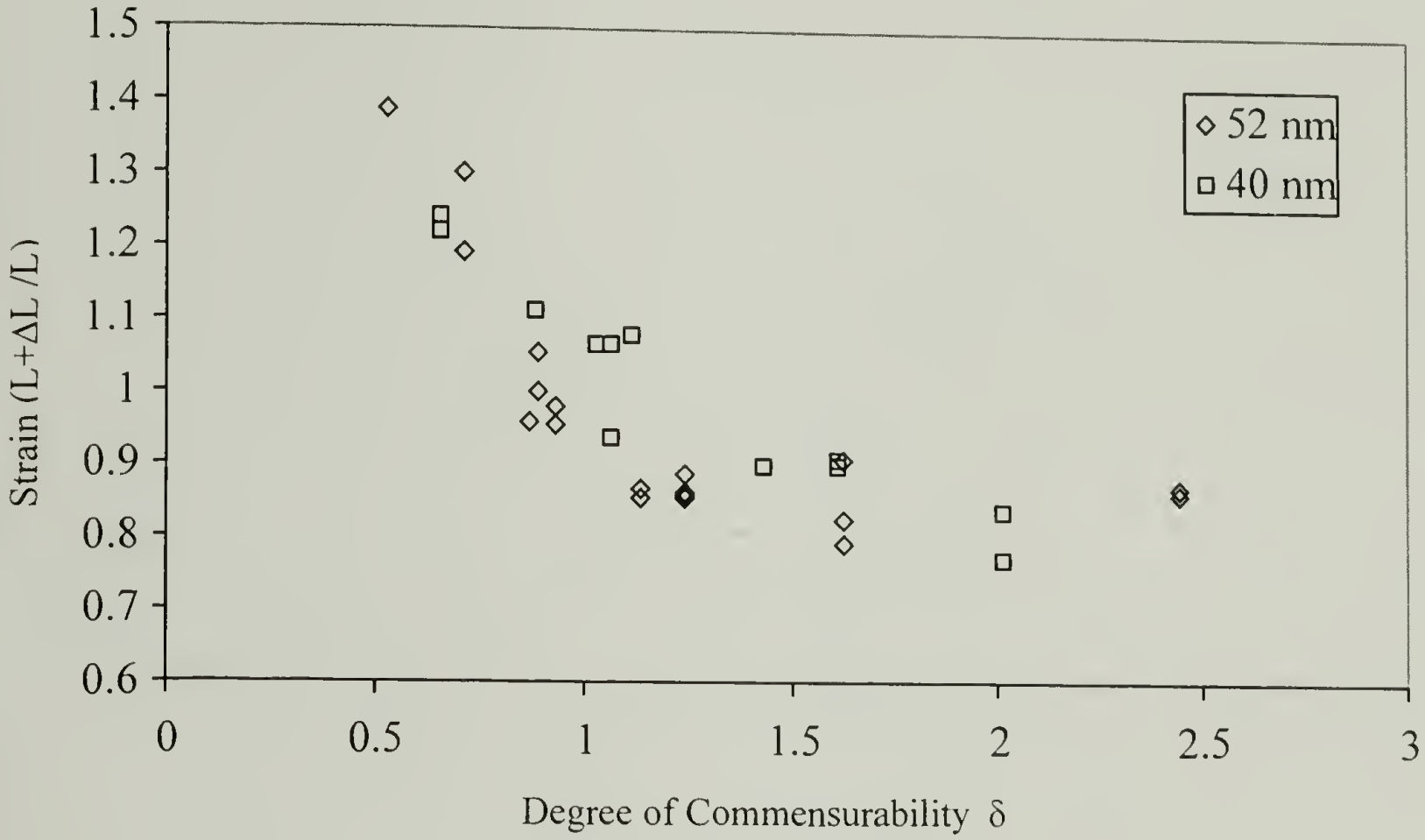

Figure 3.10. Strain in lamellar period at free surface as a function of the degree of commensurability, δ.

strain allowed to a given lamellar layer was estimated at $L_o/2n$, where L_o was the bulk copolymer period and n the number of confined lamellae in the system, making the maximum strain allowed for a single confined lamellar repeat layer 50%. Increasing the separation between confining surfaces to a distance greater than 1.5 L_o would result in the insertion of a new lamellar layer, with both layers possessing a compressive strain of 25% per layer. Despite the many lamellar layers generated on heterogeneous surfaces, each layer is locally confined by the substrate chemistry and therefore strains as large as 40% are not unreasonable for this experimental system.

Defects

The defects present in the commensurate lamellar morphologies which disrupt the long range ordering are due to both mismatch between the copolymer period and the substrate period where $\delta \neq 1$, and the imperfections in the substrate. As δ deviates farther from 1, the defect concentration in the lamellar ordering increases. In the range of $.75 < \delta < 1$ where the lamellar layers are in tension, several defect modes are implemented to alleviate local strain and restore registry of the lamellar morphology with the underlying substrate. Figure 3.11 presents the dominant defect structures observed. The lowest energy defect mode is stretching and compression, whereby the lamellar period strains locally to map onto the substrate pattern. If strain is not sufficient, individual lamellae are found to undulate along their length, effectively increasing the surface area covered without requiring excessive linear strain normal to the lamellar director. This mode sacrifices surface contact energy at the expense of the more costly entropic stretching energy. When the mismatch becomes too great for either of these modes, insertion of new lamellar planes is found, similar to a dislocation in crystalline materials. Ultimately,

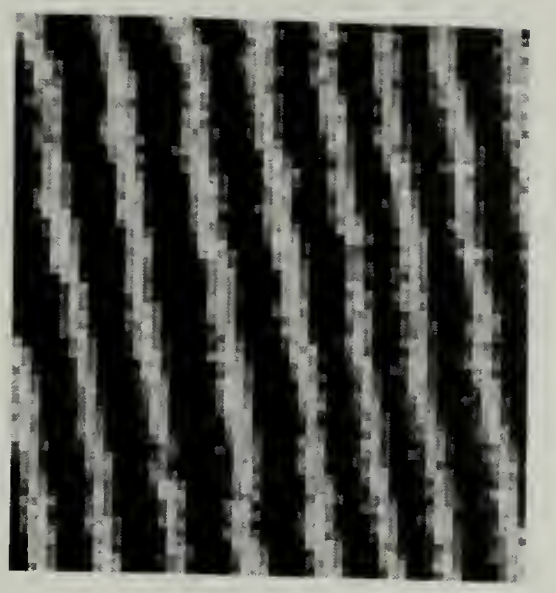

Stretching/Compression

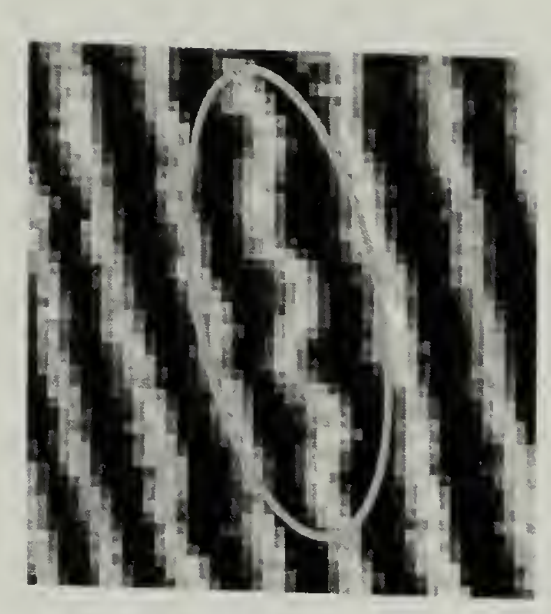

Undulations

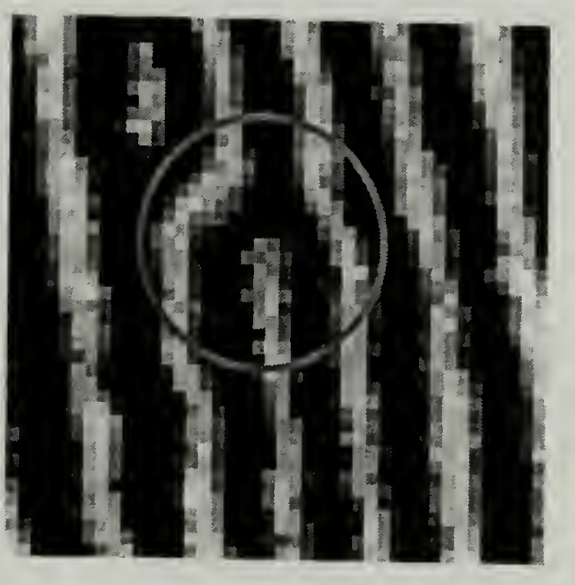

Dislocations

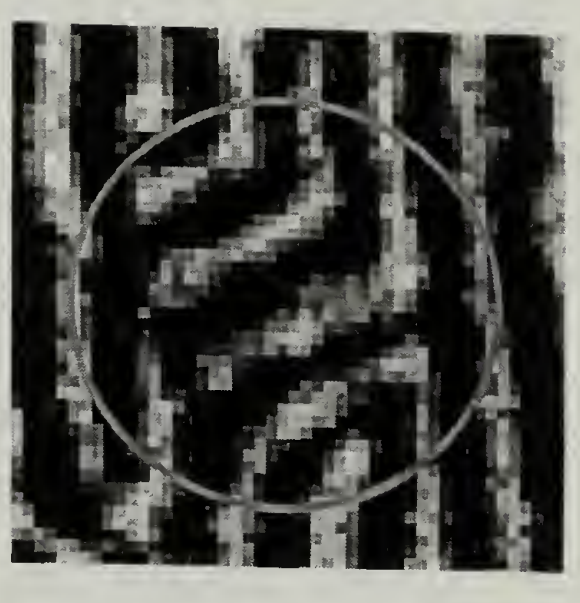

Domain reorientation

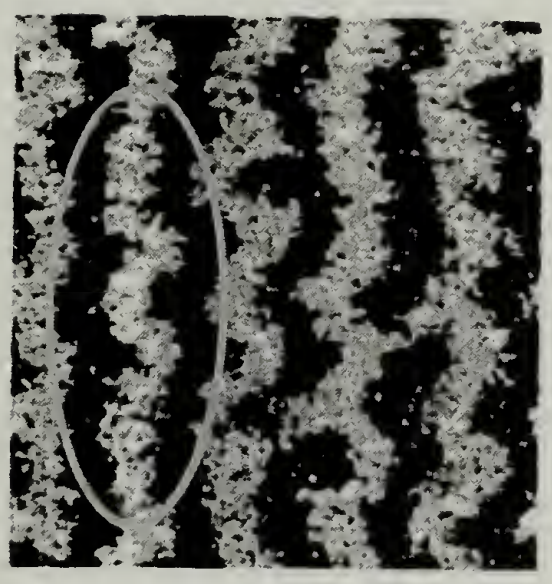

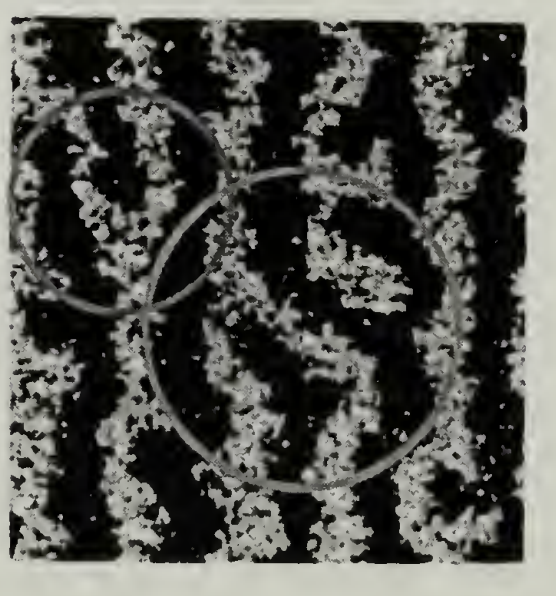

Figure 3.11. AFM height images of common defect structures observed in the lamellar morphology of solution cast block copolymer thin films on heterogeneous surfaces. Upper four images are experimental data, lower two are images derived from simulations from reference[18].

a local domain reorientation can occur, sacrificing the most interfacial energy to reduce strain energy. In the range of $1 < \delta < 1.4$, while lamellar orientation persists in some regions, in others the surface direction is completely ignored. The defect modes of stretching/compression and undulations are not observed, and while dislocations are evident in the morphology, the reoriented grain defect structure dominates.

Of the primary defect structures seen experimentally, all are observed in the images of Chen and Chakrabarty generated from their numerical calculations[18]. The bottom of Figure 3.11 shows images taken from their work, with the observed defect structures highlighted. As only the regime of $\delta < 1$ was studied in their work, the crossover to reorientation defect dominated morphologies was not seen. The data of Wang et. al.[19] do show a distinct change in the nature of their slightly incommensurate morphologies in going from tension to compression, however. An increase in the observed "$|||^{T}$" phase, or "transposed perpendicular lamellae", which is an example of a reoriented grain defect, is observed for their simulated morphologies with $\delta > 1$.

New Polymer System

As proof of concept, poly(styrene-block-2-vinlypyrridine), denoted p(S-b-2VP), was solution cast onto homogeneous gold, SiOx, and a 42 nm heterogeneous substrate. Like p(S-b-MMA), styrene is the nonpolar block and vinyl pyridine is the polar block. The same casting procedure and solution concentration was used. For p(S-b-MMA), a 100 k copolymer was roughly commensurate, therefore a 100 k p(S-b-2VP) was chosen. Figure 3.12 shows the AFM images of the free surface morphology of the films cast on the three substrates. On both homogeneous substrates the morphology is identical, forming perpendicular cylinders in thicker regions, and mixed parallel and perpendicular

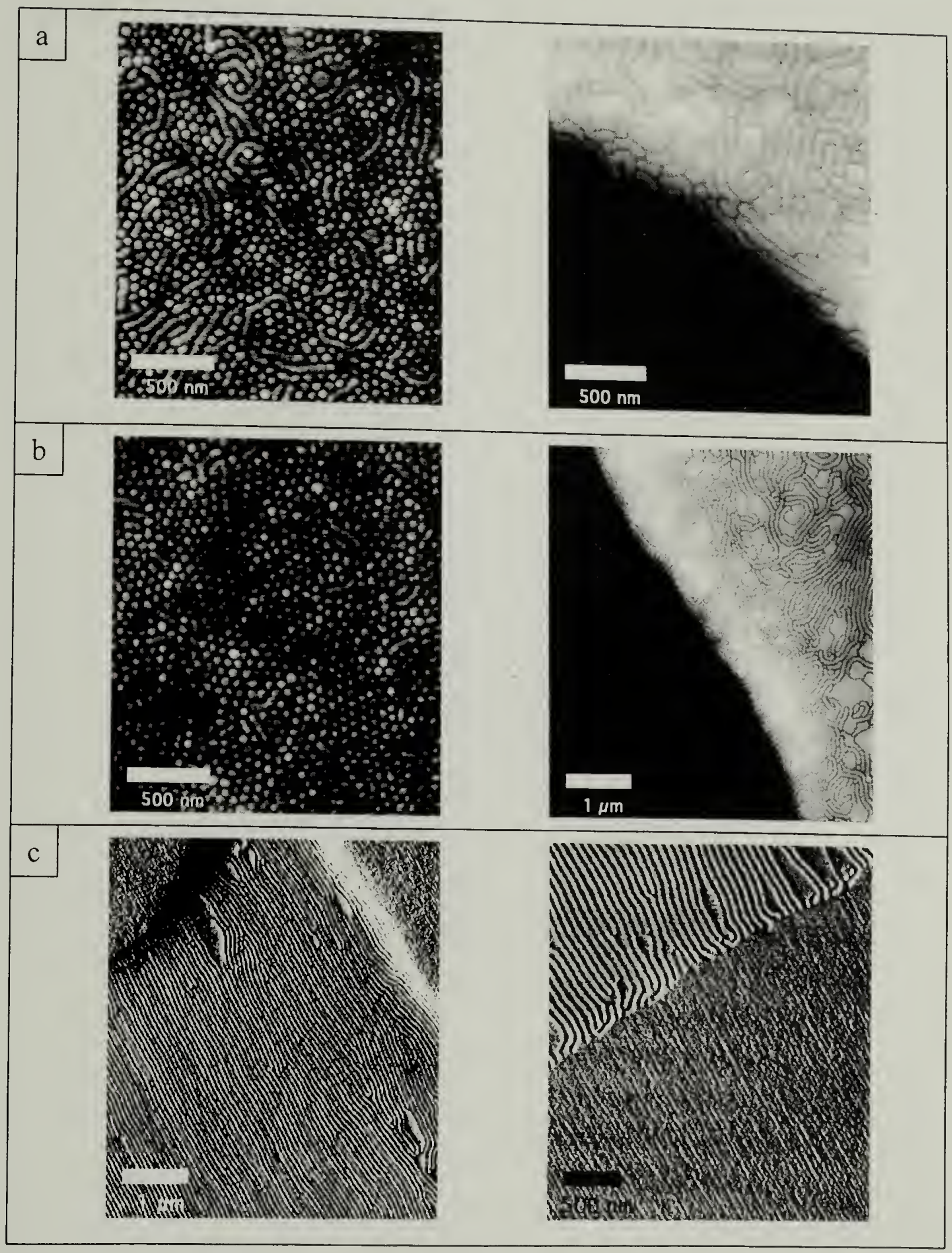

Figure 3.12. AFM images of 100k p(S-b-2VP) thin films solution cast from 0.1 wt% toluene onto various substrates. a) SiOx (height images) b) Au (height images) c) 42 nm heterogeneous substrate (phase images).

lamellae in thinner regions. Such a complex morphology forms due to a competition between confinement, preferential solvency of the PS in toluene, and the lower surface energy of 2VP. On the heterogeneous substrate however, large domains of perpendicular lamellae oriented by the substrate pattern are evident. The oriented regions span many microns, and are reasonably defect free. What is most striking about the oriented morphology is difference in length scale that is apparent between the polymer and the substrate. Despite having the same molecular weight as the p(S-b-MMA) copolymer, the p(S-b-2VP) is in the strong segregation limit, and the period of the lamellar morphology is much larger, 70 nm as measured by the AFM. Therefore this polymer accepts nearly defect-free surface direction at $\delta \approx 1.75$, far outside the window of commensurability for p(S-b-MMA) on a 42 nm substrate. However, in changing the polymer chemistry we have changed the strength of surface interactions, and this may account for a resized window of commensurability for the new polymer system.

Conclusion

These studies have shown that laterally periodic, chemically heterogeneous surfaces with nanometer periodicity can serve as templates to control the orientation and long range ordering of block copolymer lamellae. The strength of surface control over lamellar ordering and orientation is found to be strongly dependent on the degree of commensurability between polymer and substrate patterning, where up to a 25% mismatch between complementing length scales still allows strong substrate control. When the match between copolymer and substrate period is slightly incommensurate, with $0.75 < \delta < 1.25$, the copolymer lamellae are found to strain uniformly in an effort to map the preferred bulk copolymer period onto the substrate length scale. The strain is not

sufficient for a 1:1 mapping, so defects are generated in the thin film which disrupt the lateral long range orientation of the lamellae, but relieve the local strain at the expense of unfavorable surface contacts, and bring the copolymer back into registry with the substrate pattern. The defect structures are observed to vary with δ as well, with extension, compression, undulations, dislocations and reorientation of the lamellae occurring in tension, but reoriented lamellar grains dominating in compression. Finally, surface control over lamellar ordering has been extended to a different polymer system, indicating a variety of materials and substrate chemistry should be acceptable for generating oriented films. The window of commensurability for new systems, however, will be dependent on the strength of surface and interfacial interactions, how strongly segregated the copolymer is, and the film thickness.

These studies were supported by the National Science Foundation Materials Science and Research Center at the University of Massachusetts at Amherst, the Department of Energy, Office of Basic Energy Sciences, and the Center for Environmentally Appropriate Materials at the University of Massachusetts at Amherst. The authors wish to thank Christopher Stafford for assistance with GPC characterization, and block copolymer synthesis.

References

1. Kikuchi, M. & Binder, K. Microphase Separation in Thin Films of the Symmetric Diblock-Copolymer Melt. *Journal of Chemical Physics* 101, 3367-3377 (1994).

2. Pickett, G. T., Witten, T. A. & Nagel, S. R. Equilibrium Surface Orientation of Lamellae. *Macromolecules* 26, 3194-3199 (1993).

3. Puri, S., Binder, K. & Frisch, H. L. Surface effects on spinodal decomposition in binary mixtures: The case with long ranged surface fields. *Physical Review E* 56, 6991-7000 (1997).

4. Pickett, G. T. & Balazs, A. C. Equilibrium Orientation of Confined Diblock Copolymer Films. *Macromolecules* 30, 3097-3103 (1997).

5. Kellogg, G. J. *et al.* Observed Surface Energy Effects in Confined Diblock Copolymers. *Physical Revier Letters* 76, 2503-2506 (1996).

6. Mansky, P., Liu, Y., Huang, E., Russell, T. P. & Hawker, C. Controlling Polymer-Surface Interactions with Random Copolymer Brushes. *Science* 275, 1458 (1997).

7. Lambooy, P. *et al.* Observed Frustration in Confined Block Copolymers. *Physical Review Letters* 72, 2899-2902 (1994).

8. Walton, D. G., Kellogg, G. J., Mayes, A. M., Lambooy, P. & Russell, T. P. A free Energy Model for Confined Diblock Copolymers. *Macromolecules* 27, 6225-6228 (1994).

9. Koneripalli, N., Singh, N., Levicky, R., Gallagher, P. D. & Satija, S. K. Confined Block Copolymer Thin Films. *Macromolecules* 28, 2897-2904 (1995).

10. Balazs, A. C., Huang, K., McElwain, P. & Brady, J. E. Polymer Adsorption on Laterally Heterogeneous Surfaces: A Monte Carlo Computer Model. *Macromolecules* 24, 714-717 (1991).

11. Halperin, A., Sommer, J. U. & Daoud, M. Copolymers at Striped Surfaces: Coupling Effects. *Europhysics Letters* 29, 297-302 (1995).

12. Petera, D. & Muthukumar, M. Self-Consistent Field Theory of Diblock Copolyer Melts at Patterned Surfaces. *Journal of Chemical Physics* 109, 5101-5107 (1998).

13. Pereira, G. G. & Williams, D. R. M. Diblock Copolymer Thin Films on Heterogeneous Striped Surfaces: Commensurate, Incommensurate, and Inverted Lamellae. *Physical Review Letters* 80, 2849-2852 (1998).

14. Böltau , M., Walheim, S., Mlynek, J., Krausch, G. & Steiner, U. Surface Induced Structure Formation of Polymer Blends on Patterned Substrates. *Nature* 391 (1998).

15. Karim, A. *et al.* Phase Separation of Ultrathin Polymer-Blend Films on Patterned Substrates. *Physical Review E* 57, R6273-R6276 (1998).

16. Pereira, G. G. & Williams, D. R. M. Equilibrium Properties of Diblock Copolymer Thin Films on a Heterogeneous, Striped Surface. *Macromolecules* 31, 5904-5915 (1998).

17. Chakrabarti, A. & Chen, H. Block Copolymer Films on Patterned Surfaces. *Journal of polymer Science, B* 36, 3127-3136 (1998).

18. Chen, H. & Chakrabarti, A. Morphology of Thin Block Copolymer Films on Chemically Patterned Substrates. *Journal of Chemical Physics* 108, 6897-6905 (1998).

19. Wang, Q., Yan, Q., Nealey, P. F. & de Pablo, J. J. Monte Carlo Simulations of Diblock Copolymer Thin Films Confined between Chemically Heterogeneous Hard Surfaces. *Macromolecules* 33, 4512-4525 (2000).

20. Wang, Q., Nath, S. K., Graham, M. D., Nealey, P. F. & de Pablo, J. J. Symmetric Diblock Copolymer Thin Films Confined between Homogeneous and Patterned Surfaces: Simulations and Theory. *Journal of Chemical Physics* 112, 9996-10010 (2000).

21. Anastasiadis, S. H., Russell, T. P., Satija, S. K. & Majkrzak, C. F. The Morphology of Symmetric Diblock Copolymers as Revealed by Neutron Reflectivity. *Journal of Chemical Physics* 92, 5677-5691 (1990).

22. Kim, G. & Libera, M. Morphological Development in Solvent-Cast Polystyrene-Polybutadiene-Polystyrene (SBS) Triblock Copolymer Thin Films. *Macromolecules* 31, 2569-2577 (1998).

23. Coulon, G., Daillant, J., Collin, B., Benattar, J. J. & Gallot, Y. Time Evolution of the Free Surface of Ultrathin Copolymer Films. *Macromolecules* 26, 1582-1589 (1993).

24. Fasolka, M. J., Harris, D. J., Mayes, A. M., Yoon, M. & Mochrie, S. G. J. Observed Substrate Topography-Mediated Lateral Patterning of Diblock Copolymer Films. *Physical Review Letters* 79, 3018-3021 (1997).

CHAPTER 4

PROPAGATION OF NANOPATTERNED SUBSTRATE TEMPLATED ORDERING OF BLOCK COPOLYMERS IN THICK FILMS

Introduction

The use of block copolymers as templates for the fabrication of novel nanostructured materials has flourished due to the ease with which such templates can be prepared, and functionalized[1-3], and to the variety of distinct nanostructures that can be generated from copolymer morphologies. Incorporation of these new materials into devices, however, is significantly hindered by the lack of local control over the self-assembly process that is the foundation of copolymer-based nanostructure synthesis. Microscopic grain sizes[4], grain boundaries, and various defect structures[5] both reduce the overall yield of the target nanostructure, and prohibit real-space characterization and serial addressing for testing and device incorporation. As a consequence, block copolymer morphologies at surfaces have been investigated with increasingly complex schemes in an effort to understand the effect of interfacial energy and confinement on orientation. Such knowledge will enable the realization of defect free, oriented nanoscopic structures over large areas for use in future devices.

A basis for the control over morphology and orientation has already been established in block copolymer thin films. Interfacial interactions impart an orientation of a lamellar morphology parallel to a surface, even above the ordering temperature[6,7]. The confinement of morphologies by film thickness showed that the balance of enthalpy and entropy could be used to reorient the morphology in an ultrathin film[8-11], produce a controlled roughness via island and hole formation at a thin film's free surface[12], or

induce tension and compression in a copolymer morphology under one dimensional confinement[13]. This understanding has enabled the design of experiments with more stringent control[14] in an effort to produce a desired morphology and orientation, and recent studies have established a strong precedent for surface or interface templated growth. Chemically[15] and topographically[16] patterned surfaces, and static[17] and moving interfaces or phase boundaries[18] have all been used to generate controlled oriented nanostructures over large areas. Theoretical approaches[19-23] and simulations[24,25] have also indicated that, with the appropriate surface boundary conditions and processing procedures, lateral control over nanostructures may propagate microns away from a surface providing true three dimensional control over self assembled nanostructures[26]. Here we show experimental results of such control over the lamellar morphology of a diblock copolymer, and discuss the experimental limits over which such control can be achieved.

Previously, it was shown[15], that when solution cast on a chemically heterogeneous, flat surface comprised of 30 nm alternating stripes of nonpolar gold (Au) and polar silicon oxide (SiOx), a symmetric block copolymer of poly(styrene-block-methyl methacrylate), denoted p(S-b-MMA), ordered with the lamellar microdomains oriented normal to the surface and along the stripe direction. While confinement of the thin films contributed to the perpendicular orientation of the lamellar microdomains, the strong coupling between the polar PMMA and SiOx and the nonpolar PS and Au produced an additional orientation of the domains parallel to the Au/SiOx stripes. The interactions between the blocks of the copolymer and the surface stripes were strong

enough to orient the morphology when as much as a 25% mismatch between the copolymer period and the substrate stripe period was present.

Here, experimental results are presented on thick copolymer films prepared on chemically heterogeneous surfaces, where confinement effects due to film thickness are removed. These experiments address the issue of whether the substrate chemical heterogeneities alone are sufficient to orient the block copolymer morphology normal to the surface and in the stripe direction, and if so, how far into the bulk of the film such an oriented morphology will propagate. Additionally, the commensurability of length scales between the copolymer period and the substrate pattern is examined, and the results are then compared to the case of ultra thin confined films. Finally, the role of ordering kinetics and its influence on the propagation of a surface directed morphology into the bulk region of the films are discussed.

Experimental

Polymers

Symmetric diblock copolymers of p(S-b-MMA) were purchased from Polymer Labs, or synthesized in-house. All of the copolymers were soxhlet extracted in cyclohexane to remove any residual polystyrene homopolymer. Table 4.1 presents the copolymer compositions used, ranging from 53 k (53,000 g/mol) to 214 k, the calculated bulk copolymer period[27], and degree of commensurability (δ) for each molecular weight. δ is the ratio of the period of the copolymer morphology in the bulk to the period of the heterogeneous striping of the substrate, 42 nm. Solutions of 5 wt% polymer in HPLC grade toluene were prepared.

Table 4.1. Summary of the p(S-b-MMA) copolymers used in experiments. One sample possessed a deuterated methyl methacrylate block (dMMA). [a]The copolymer period was calculated from an empirical formula derived by Anastasiadis et. al. [27] δ is the 'degree of commensurability', a ratio of the copolymer bulk period to the average substrate stripe periodicity of 42 nm.

Copolymer	Mw (kg/mol)	Period [a] L (nm)	δ for 42 nm substrate
S/MMA	53	27.38	0.65
S/MMA	73	33.71	0.80
S/MMA	84	36.93	0.88
S/MMA	107.8	43.22	1.03
S/MMA	113	44.78	1.07
S/dMMA	121.3	46.82	1.11
S/MMA	177	59.95	1.43
S/MMA	214	67.82	1.61

Heterogeneous Surfaces

Chemically heterogeneous substrates were prepared by glancing angle metal evaporation on facetted Si substrates. Si (113) substrates miscut 1.1° toward the (-1-10) pole were resistively heated and cleaned under UHV conditions by cycling the surface temperature between 1000 and 1523° C. Surfaces were then annealed for 100 sec at 1180° C to produce facets of 42 nm average periodicity, with an 8 nm standard deviation, and less than 1 nm amplitude. These surfaces were then mounted in a thermal evaporator with a 4° angle between the metal source normal and the surface parallel, so that the evaporated metal atoms were incident only on the facing edge of the facets. 1.5 nm of chromium was evaporated initially as an adhesion layer, followed by 2.5 nm of gold (Au), producing a striped, chemically heterogeneous surface with 4.5 nm roughness. The exact processing conditions are described in detail in Chapter 1. A simple calculation shows that this roughness is not significant enough to perturb the chain conformation and

morphology of a block copolymer[28], and hence the surface is effectively a flat, striped surface with alternating polar oxide and nonpolar gold lines of slightly asymmetric widths. The gold lines are narrower, of order 20 nm, but an exact width is not measurable due to radius of curvature limitations of the AFM tip. New substrates were prepared for each polymer film cast, as the destructive characterization techniques prevented substrate re-use.

Film Preparation

Solution casting was done in a closed glass crystallization dish in the presence of excess solvent, in an effort to control the rate of solvent evaporation and promote an equilibrium morphology[5]. Small 0.25 cm^2 heterogeneous substrates were placed within a 600 ml aluminum foil covered glass crystallization dish. Inside the casting container was an additional small dish filled with toluene, to saturate the vapor pressure inside and mediate solvent evaporation from the substrate. A syringe inserted through a small, 0.3 cm^2 hole in the foil covering allowed for wetting of the substrates with polymer solution as well as controlled evaporation. The small substrates were wet entirely with a 5μl droplet, such that the surface was completely wet but the solution did not spill over the substrate edge. The solvent evaporated completely over the course of 30 minutes, producing a transparent film of nonuniform thickness. The roughness of a given film's free surface scaled with polymer molecular weight, an indication of some non-equilibrium kinetic control over the film's free-surface morphology upon solvent evaporation [29,30].

Characterization

Characterization of the solution cast polymer films was done by field emission scanning electron microscopy (FESEM) on a JEOL 6320. Cast films were first annealed at 190° C for 2 days to promote relaxation of the polymer film and improve adhesion, which proved necessary to prevent film cracking and delamination from the substrate during cryofracture. Samples were then scored with a diamond scribe either parallel or perpendicular to the surface striping on the backside, and held submerged in liquid nitrogen for 45 seconds with knife-edged pliers aligned with the scribe line. Gripping pressure on the pliers would cause the substrate to cleave along the scribe line producing two facing cross-sections. Sections were mounted edge-up on an aluminum FESEM mount with carbon tape. To enhance the topography of the fracture surface CF_4 reactive ion etching (RIE) was used. The inherent directionality and etch contrast between PS and PMMA in CF_4 RIE allowed for the development of a material dependent topography on the fracture surfaces after a brief, low power etch[1,31,32]. Finally, a 20 nm plasma deposited gold coating was applied to the sample, and the FESEM produced crisp images of PS lamellar microdomains in relief from the cross-sections.

Results and Discussion

FESEM images of films solution cast from three molecular weights of p(S-b-MMA) on homogeneous Au and SiOx surfaces are shown in Figure 4.1. The substrates can be distinguished by the appearance of the polymer/substrate interface. The presence of the bright 50 nm thick line at the polymer/Au/Si interface results from the uniform metallization of the substrate by the Au. The dark gap appearing at the polymer/Si interface of the homogeneous Si substrate is caused by electron beam damage. PMMA is

rapidly degraded in the electron beam, which results in an adhesive failure at the interface and a pulling of the film away from the surface. This delamination was not seen at the polymer/Au interface due to the presence of a more robust PS wetting layer. The lamellar morphology, however, is seen to be oriented parallel to the substrate regardless of surface chemistry. For all molecular weights over 84 k, a similar morphology is observed. However, for the 84 k sample the lamellar morphology was visible only at the substrate/polymer interface, not in the bulk, as shown in Figure 4.1.a. For all of the lower molecular weight copolymers, the cryofracture/RIE imaging technique was unsuccessful due to the broadness of interface between the PS and PMMA microdomains and resulting lack of RIE etch specificity.

The distance over which the surface directed parallel orientation propagates into the bulk for samples cast on homogeneous substrates is found strongly dependant on molecular weight, as evident in the images of Figure 4.1. The largest propagation length is seen in the lower molecular weight 84 k sample, averaging 0.5 μm or roughly 12 periods, while the highest molecular weight samples show only one or two lamellar layers parallel to the interface before losing orientation. Additionally, the apparent grain size both parallel and perpendicular to the lamellar stacking direction decreases with increasing molecular weight in a similar fashion. In all cases the distance over which the surface directed morphology propagates away from the surface is less then or equal to the apparent bulk grain size. Therefore, it is clear that the generation of a surface directed morphology upon solution casting is a kinetically limited process. The chain mobility is significantly reduced for the higher molecular weight samples preventing coarsening of the grains, and shorter correlation lengths are produced.

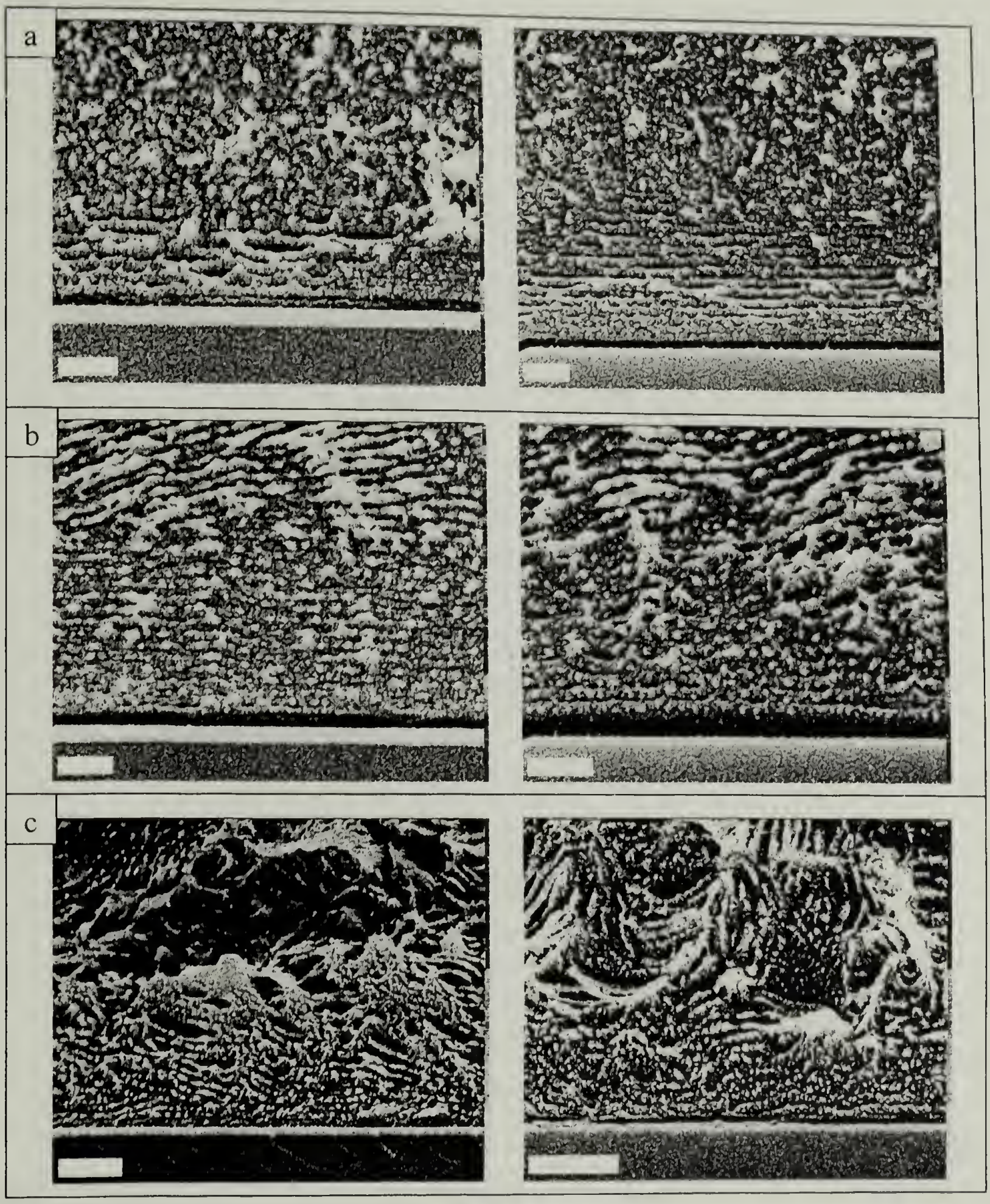

Figure 4.1. FESEM cross-sectional images of a) 84 k, 0.2 μm scale bar. b) 107 k, 0.2 μm scale bar. c) 214 k, 0.5 μm scale bar. On Au (left) and SiOx (right) homogeneous substrates.

The FESEM images of the entire molecular weight range from 53 k to 214 k p(S-b-MMA) solution cast on 42 nm Au/SiOx heterogeneous surfaces are shown in Figure 4.2 through Figure 4.5. The substrates were fractured perpendicular to the surface striping. As molecular weight is increased, the orientation of the lamellar morphology is seen to change from parallel to perpendicular and back to parallel to the surface, with exception of the lowest molecular weight samples with unidentifiable morphologies. For the 107 k copolymer shown in Figure 4.3.b, the calculated period is nearly commensurate with the surface pattern with a δ of 1.03. The surface directed perpendicular lamellar ordering is almost perfect, with few defects seen. The morphology propagates approximately 0.5 μm into the bulk, similar to the propagation length of the parallel morphology on a homogeneous surface. These results suggest that segregation of the copolymer chains to the interface and templating by the striped surface occur prior to the onset of phase separation. With the PMMA block adsorbed to the oxide and PS onto the gold, the copolymer chains lay parallel to the surface and in registry with the stripes. The segregation at the interface then drives the lamellar morphology normal to the substrate into the bulk. For the incommensurate molecular weights, surface segregation does not occur in a controlled, periodic fashion. The entropy penalty required of the surface chains to strain to the substrate dictated length scale outweighs the resulting favorable enthalpic interaction. The system is forced to choose between a parallel lamellar morphology with unfavorable polymer/surface contacts, or an unoriented perpendicular morphology with both unfavorable polymer/surface contacts and increased interfacial area due to grain boundaries. As the former results in a lower free energy state, a

preference develops at the substrate for a single component, either PS or PMMA, and a parallel morphology is driven into the bulk. The surface directed ordering, whether initially parallel or perpendicular to the substrate, propagates only far enough into the bulk to meet the phase separated grains formed there. There is no evidence that either orientation has a stronger influence on the propagation distance, indicating a kinetic factor limiting the development of surface directed morphologies.

The sensitivity of surface directed orientation to the commensurability of surface and polymer length scales in thick films is clearly seen in Figure 4.4.a for the 113 k sample. In this case $\delta = 1.07$, and a perpendicular lamellar ordering rich with defects is seen. The primary defect mode is shown on the far right of the image. The light striping due to the metallization of the perpendicular PS lamellae appears to increase abruptly in periodicity. This is due to a reorientation of the lamellae such that they remain perpendicular to the surface but are no longer aligned with the substrate pattern. This 'reoriented grain' defect structure was also found in the ultrathin films from Chapter 3 as well[15], and dominated the morphology for incommensurate systems with a lamellar period higher than the substrate pattern length scale, $\delta > 1$, as is the case here. Reoriented perpendicular lamellar grain defects are also seen in the calculations of Chen and Chakrabarti[22,23] and the simulations of Wang et. al.[24,25]. In the former work, defects were apparent for $L_{surface} = 3/4\ L_{copolymer}$ ($\delta = 0.667$) at film thickness $D = 15$, while for the latter '$|||^T$' were seen originating at the substrate for $L_{surface} = 1/3\text{-}2/3\ L_{copolymer}$ ($\delta = 1.5$ - 3).

a

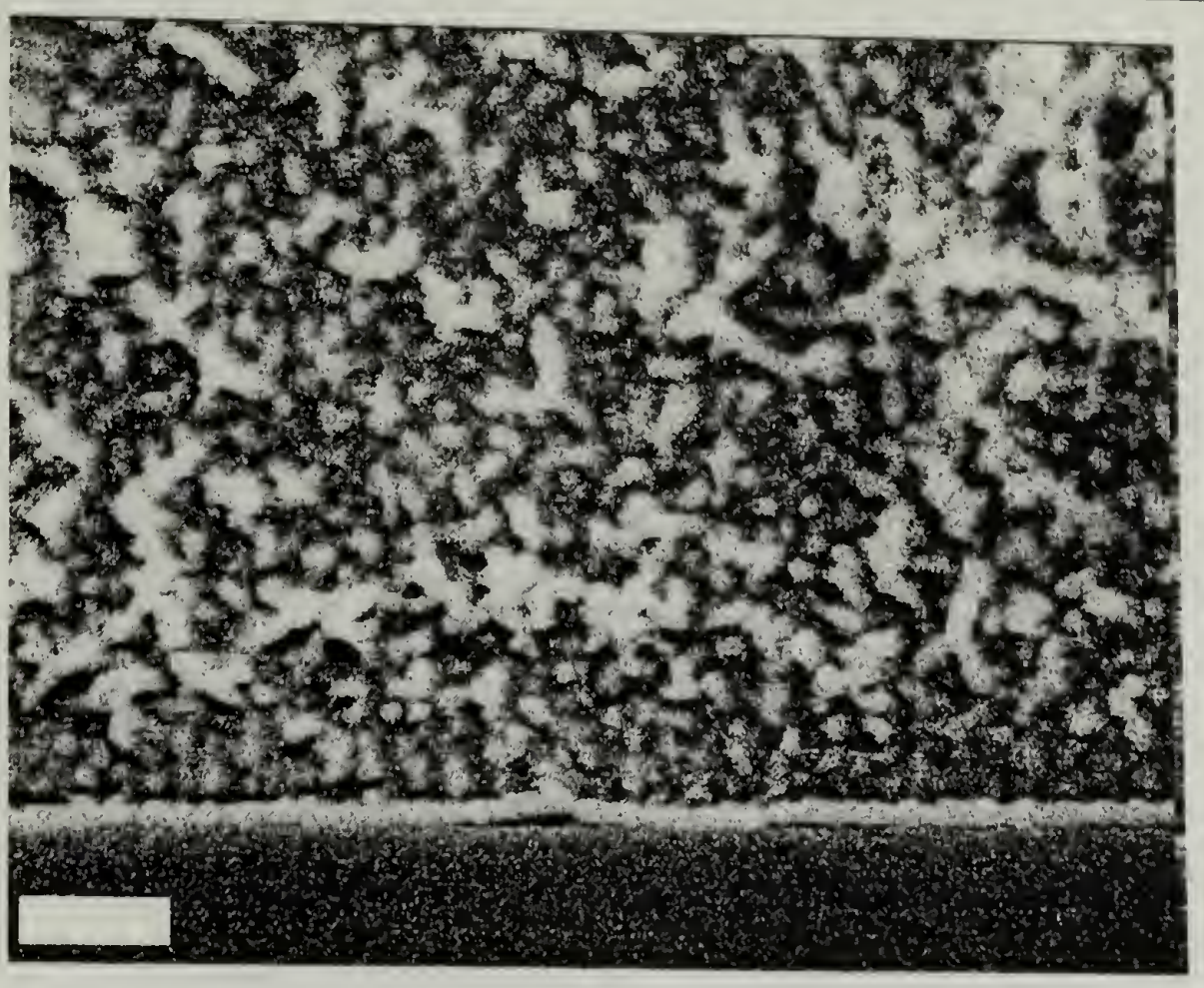

b

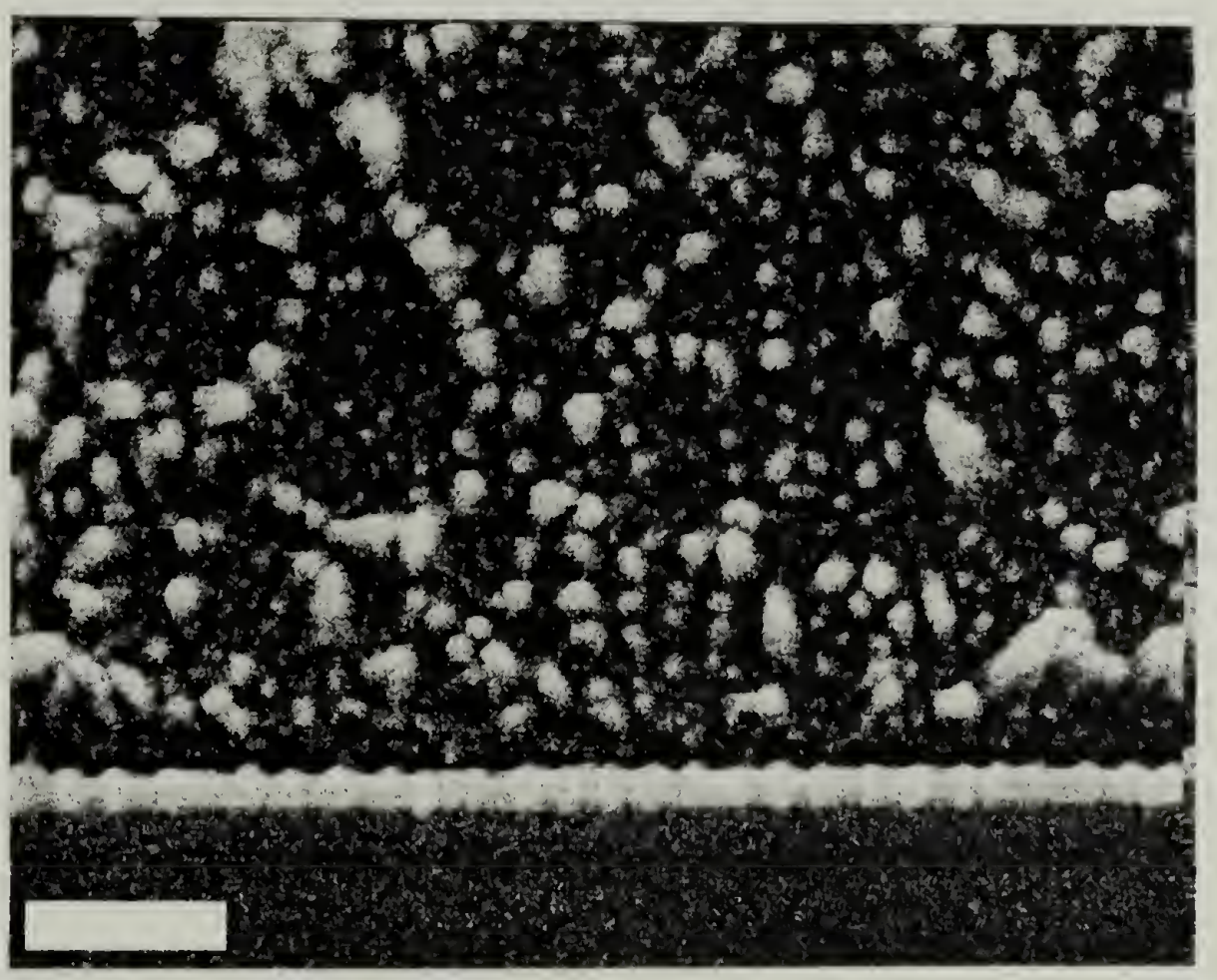

Figure 4.2. FESEM cross-sectional images of a) 53 k [δ= 0.65]. b) 73 k [δ = 0.80], on 42 nm heterogeneous surface. Scale bar is 0.2 μm.

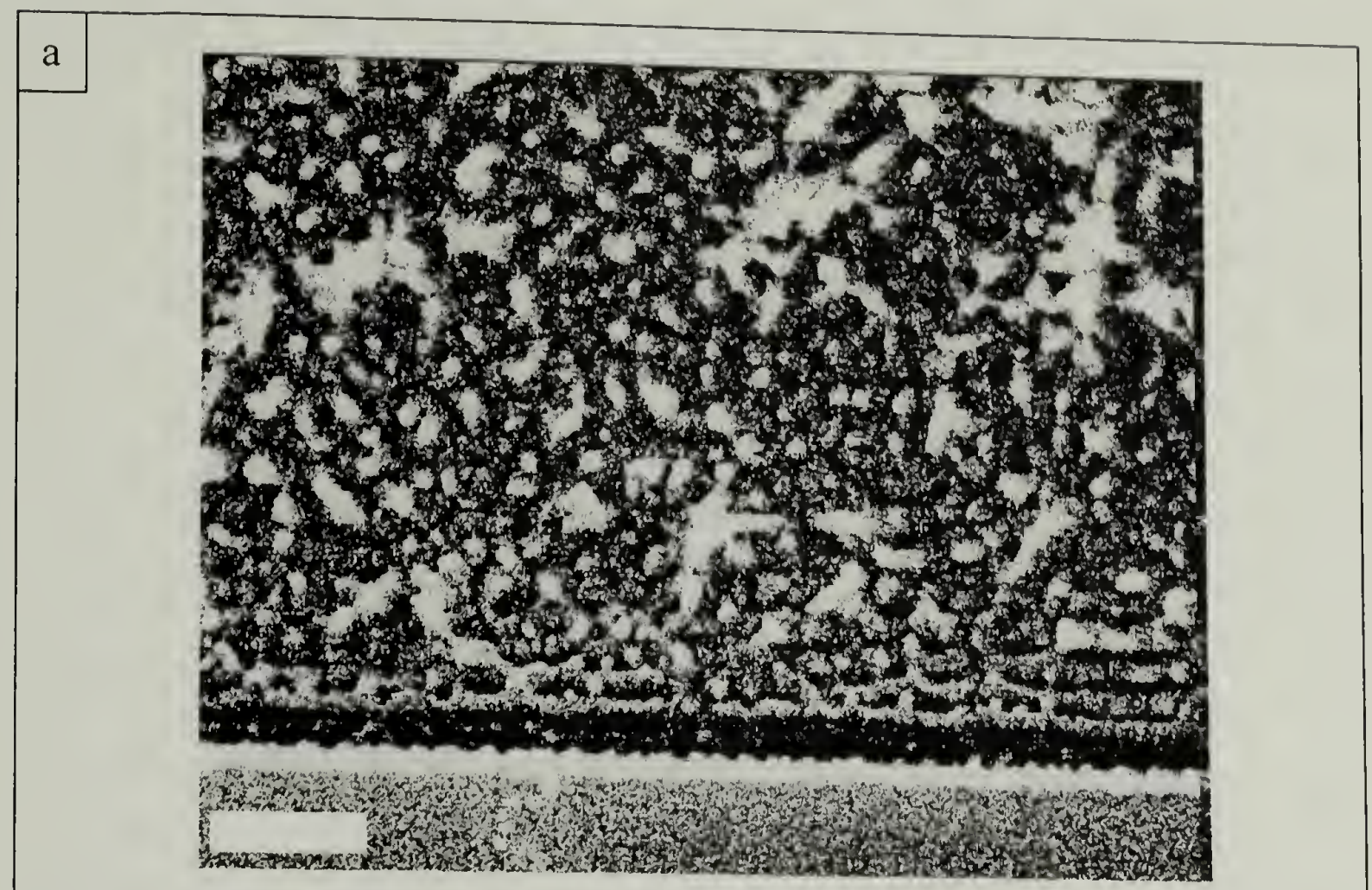

Figure 4.3. FESEM cross-sectional images of a) 84 k [δ= 0. 88]. b) 107 k [δ= 1.03], on 42 nm heterogeneous surface. Scale bar is a) 0.2 μm. b) 0.5 μm.

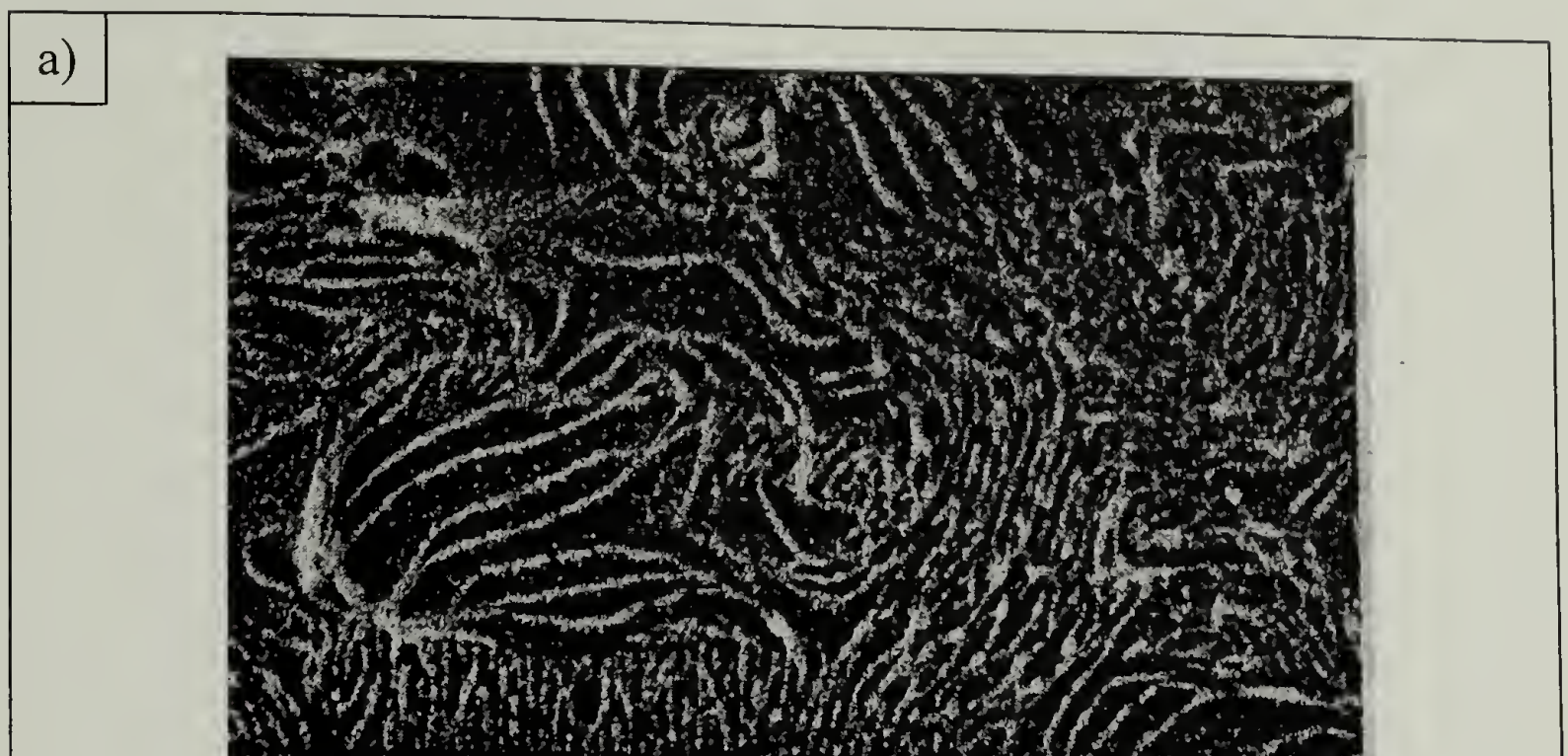

Figure 4.4. FESEM cross-sectional images of a) 113 k [δ= 1.07]. b) 121 k [δ= 1.11], on 42 nm heterogeneous surface. Scale bar is 0.5 μm.

Figure 4.5. FESEM cross-sectional images of a) 177 k [δ= 1.43]. b) 214 k [δ= 1.61], on 42 nm heterogeneous surface. Scale bar is 0.5 μm.

A further increase in molecular weight to 121 k ($\delta = 1.11$, Figure 4.4.b) results in a parallel orientation of the lamellae, with no evidence of surface directed perpendicular ordering. All of the higher molecular weight copolymer films possess a parallel orientation at the substrate as well. As parallel ordering is seen for the lower molecular weight 84 k sample, with $\delta = 0.88$, it is clear that for thick films, a 10% mismatch between copolymer period and surface pattern is sufficient to disrupt a surface directed perpendicular lamellar phase. This window of commensurability is much narrower than that seen for ultrathin films, where samples with $0.75 < \delta < 1.25$ possess a lamellar morphology oriented normal to the substrate and aligned with the stripes. For the ultrathin films however, confinement plays a dominant role in driving a perpendicular lamellar orientation, even in the more incommensurate samples[33]. Thus the patterned substrate chemistry need only direct the reoriented ultrathin film morphology in the slightly incommensurate samples, producing an apparently wider window of commensurability. In preparing thicker films, confinement effects have been eliminated and substrate patterning alone is responsible for reorienting the copolymer morphology at the interface.

In no case is a uniformly unoriented perpendicular lamellar morphology observed at the substrate/polymer interface, which would indicate a 'neutrality' of the substrate chemistry with respect to its interaction with the copolymer chains[32]. Effective neutrality of the substrate may arise from the periodic alternation of substrate chemistry on a length scale much smaller than the copolymer period can follow, such as from an end-grafted random copolymer brush, or our heterogeneous surfaces for the case of $\delta >> 1$. The parallel orientation of the higher molecular weight incommensurate copolymers

in this work however, indicates that the heterogeneous substrates are not explicitly neutral toward the higher molecular weight copolymers in spite of the rapidly alternating chemistry. While limitations of the FESEM characterization technique prohibit explicit identification of a wetting layer at the substrate, the lack of delamination from election beam degradation of the higher molecular weight parallel morphologies indicates a PS wetting layer similar to that on the homogeneous gold surface in Figure 2.

Confirmation of our description of the lamellar morphologies for 107 k and 113 k copolymers can be obtained by cryofracturing the substrates parallel to the striping. If the lamellar ordering at the surface were truly perpendicular to the substrate and aligned with the stripes, then the parallel fracture surface would be devoid of any structure at the interface, yet in the bulk show lamellar grains. Figure 4.6 shows a fracture cross section parallel to the stripe pattern for 107 k and 113 k. For the 107 k sample, no structure is evident at the interface. In the bulk however, microns from the surface, different lamellar orientations are seen. For the 113 k sample, evidence of perpendicular lamellae both parallel and perpendicular to the fracture plane (stripe direction) are seen. This particular image was chosen to exemplify the mixed perpendicular morphology that can develop due to reoriented grain defects. Increasing or decreasing molecular weight past the 10% commensurability window yields a parallel lamellar morphology in this fracture direction as well.

a

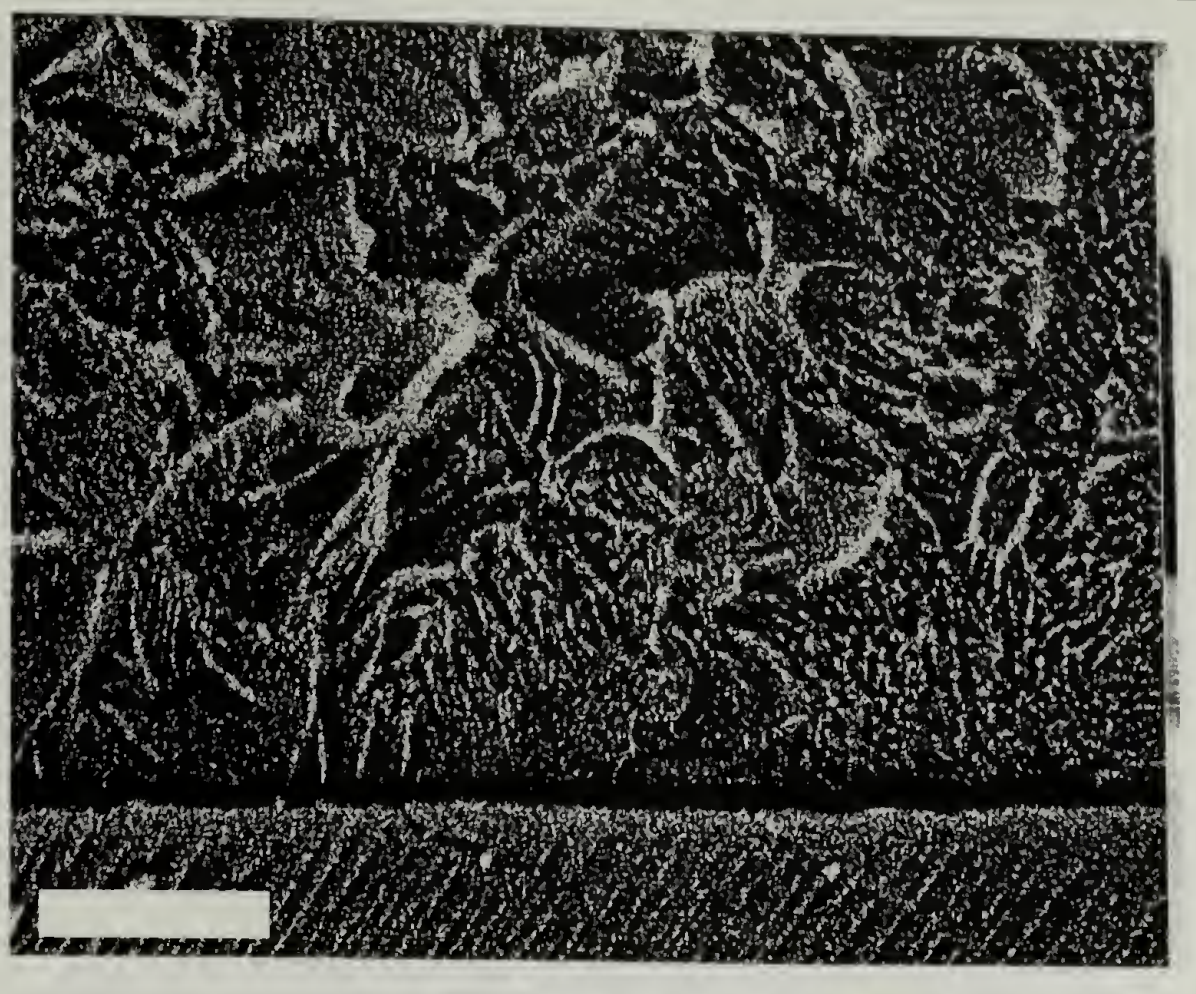

b

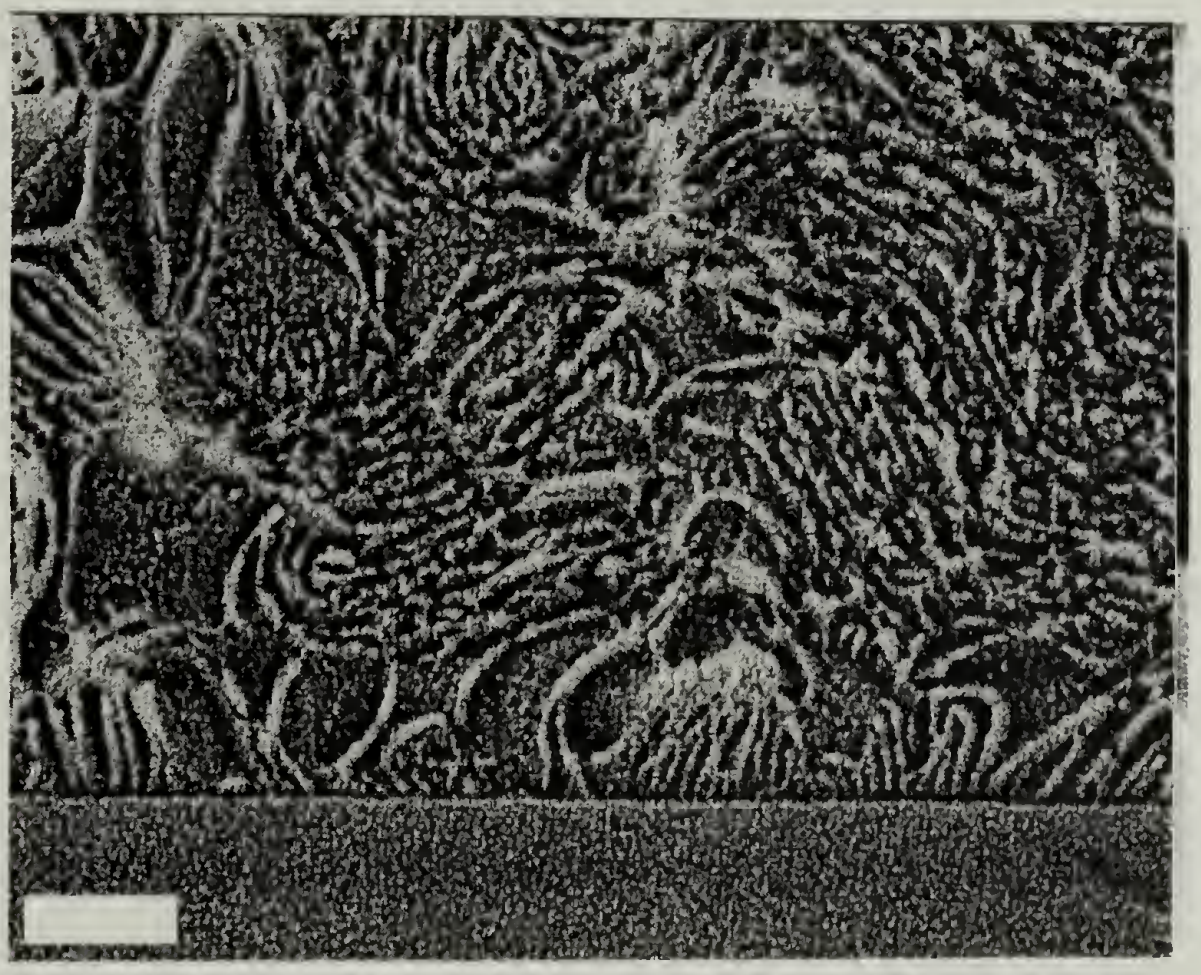

Figure 4.6. FESEM cross-sectional images of a) 107 k, 1 μm scale bar. b) 113 k, 1 μm scale bar, on 42 nm heterogeneous surfaces. Substrate fractured parallel to surface heterogeneities.

Conclusion

We have shown that by patterning a substrate with the appropriate chemistry and length scale, it can be used as a template to direct the ordering and orientation of block copolymer lamellar morphologies into the film bulk. Striped surfaces of nonpolar gold and polar silicon oxide with 42 nm periodicity guide the growth and ordering of p(S-b-MMA). For films greater than 5 μm thickness, commensurability is found to be a key factor in generating surface directed morphologies. Copolymer films with a bulk lamellar period nearly equivalent to that of the substrate follow the substrate pattern upon solution casting and orient perpendicular to the interface. When the mismatch is greater than only 10%, the lamellar microdomains orient parallel to the surface. In all cases, kinetics limit the distance to which the structure propagates into the bulk. An increase in molecular weight results in a reduction in mobility, grain size, and the distance over which surface directed morphologies propagate into the bulk.

These studies were supported by the National Science Foundation Materials Research Center at the University of Massachusetts at Amherst, The Department of Energy, Office of Basic Energy Sciences, and NETI. The authors thank Christopher Stafford for assistance with synthesis and characterization of block copolymers, Larry Lurio and Harold Gibson at Argonne National Labs and Mirang Yoon for assistance in facetted silicon preparation, and Louis Raboin for FESEM expertise.

References

1. Harrison, C., Park, M., Chaikin, P. M., Register, R. A. & Adamson, D. H. Lithography with a Mask of Block Copolymer Microstructures. *Journal of Vacuum Science and Technology B* **16**, 544-552 (1998).

2. Chan, V. Z.-H. *et al.* Ordered Bicontinuous Nanoporous and Nanorelief Ceramic Films from Sefl Assembling Polymer Precursors. *Science* **286**, 1716-1719 (1999).

3. Lammertink, R. G. H. *et al.* Nanostructured Thin Films of Organic-Organometallic Block Copolymers: One-Step Lithography with Poly(ferrocenylsilanes). *Advanced Materials* **12**, 98-102 (2000).

4. Garetz, B. A. *et al.* Orientation Correlations in Lamellar Block Copolymers. *Macromolecules* **29**, 4675-4679 (1996).

5. Kim, G. & Libera, M. Morphological Development in Solvent-Cast Polystyrene-Polybutadiene-Polystyrene (SBS) Triblock Copolymer Thin Films. *Macromolecules* **31**, 2569-2577 (1998).

6. Russell, T. P., Coulon, G., Deline, V. R. & Miller, D. C. Characteristics of the Surface-Induced Orientation for Symmetric Diblock PS/PMMA Copolymers. *Macromolecules* **22**, 4600-4606 (1989).

7. Mansky, P. *et al.* Interfacial Segregation in Disordered Block Copolymers: Effect of Tunable Surface Potentials. *Physical Review Letters* **79**, 237-240 (1997).

8. Walton, D. G., Kellogg, G. J., Mayes, A. M., Lambooy, P. & Russell, T. P. A free Energy Model for Confined Diblock Copolymers. *Macromolecules* **27**, 6225-6228 (1994).

9. Henkee, C. S., Thomas, E. L. & Fetters, L. J. Effect of Surface Constraints on the Ordering of Block Copolymer Domains. *Journal of Materials Science* **23**, 1685-1694 (1988).

10. Koneripalli, N. *et al.* Confinement-Induced Morphological Changes in Diblock Copolymer Films. *Langmuir* **12**, 6681-6690 (1996).

11. Fasolka, M. J., Banerjee, P., Mayes, A. M., Pickett, G. & Balazs, A. C. Morphology of Ultrathin Supported Diblock Copolymer Films: Theory and Experiemnt. *Macromolecules* **33**, 5702-5712 (2000).

12. Coulon, G., Daillant, J., Collin, B., Benattar, J. J. & Gallot, Y. Time Evolution of the Free Surface of Ultrathin Copolymer Films. *Macromolecules* **26**, 1582-1589 (1993).

13. Lambooy, P. *et al.* Observed Frustration in Confined Block Copolymers. *Physical Review Letters* **72**, 2899-2902 (1994).

14. Heier, J., Kramer, E. J., Walheim, S. & Krausch, G. Thin Diblock Copolymer Films on Chemically Heterogeneous Surfaces. *Macromolecules* **30**, 6610-6614 (1997).

15. Rockford, L. *et al.* Polymers on Nanoperiodic, Heterogeneous Surfaces. *Physical Review Letters* **82**, 2602-2605 (1999).

16. Fasolka, M. J., Harris, D. J., Mayes, A. M., Yoon, M. & Mochrie, S. G. J. Observed Substrate Topography-Mediated Lateral Patterning of Diblock Copolymer Films. *Physical Review Letters* **79**, 3018-3021 (1997).

17. Reiter, G. *et al.* Nanometer-Scale Surface Patterns with Long-Range Order Created by Crystallization of Diblock Copolymers. *Physical Review Letters* **83**, 3844-3847 (1999).

18. De Rosa, C., Cheolmin, P., Thomas, E. L. & Lotz, B. Microdomain Patterns from Directional Eutectic Solidification and Epitaxy. *Nature* **405**, 433-437 (2000).

19. Pereira, G. G. & Williams, D. R. M. Diblock Copolymer Films on Striped Surfaces: Commensurate, Incommensurate and Inverted Lamellae. (1997).

20. Petera, D. & Muthukumar, M. Effect of Patterned Surface on Diblock-Copolymer Melts and Polymer Blends Near the Critical Point. *Journal of Chemical Physics* **107**, 9640 (1997).

21. Halperin, A., Sommer, J. U. & Daoud, M. Copolymers at Striped Surfaces: Coupling Effects. *Europhysics Letters* **29**, 297-302 (1995).

22. Chen, H. & Chakrabarti, A. Morphology of Thin Block Copolymer Films on Chemically Patterned Substrates. *Journal of Chemical Physics* **108**, 6897-6905 (1998).

23. Chakrabarti, A. & Chen, H. Block Copolymer Films on Patterned Surfaces. *Journal of polymer Science, B* **36**, 3127-3136 (1998).

24. Wang, Q., Nath, S. K., Graham, M. D., Nealey, P. F. & de Pablo, J. J. Symmetric Diblock Copolymer Thin Films Confined between Homogeneous and Patterned Surfaces: Simulations and Theory. *Journal of Chemical Physics* **112**, 9996-10010 (2000).

25. Wang, Q., Yan, Q., Nealey, P. F. & de Pablo, J. J. Monte Carlo Simulations of Diblock Copolymer Thin Films Confined between Chemically Heterogeneous Hard Surfaces. *Macromolecules* **33**, 4512-4525 (2000).

26. Petera, D. & Muthukumar, M. Self-Consistent Field Theory of Diblock Copolyer Melts at Patterned Surfaces. *Journal of Chemical Physics* **109**, 5101-5107 (1998).

27. Anastasiadis, S. H., Russell, T. P., Satija, S. K. & Majkrzak, C. F. The Morphology of Symmetric Diblock Copolymers as Revealed by Neutron Reflectivity. *Journal of Chemical Physics* **92**, 5677-5691 (1990).

28. Pickett, G. T., Witten, T. A. & Nagel, S. R. Equilibrium Surface Orientation of Lamellae. *Macromolecules* **26**, 3194-3199 (1993).

29. Kim, G. & Libera, M. Kinetic Constraints on the Development of Surface Microstructure in SBS Thin Films. *Macromolecules* **31**, 2670-2672 (1998).

30. Green, P. F., Christensen, T. M., Russell, T. P. & Jerome, R. Surface Interaction in Solvent-Cast Polystyrene/Poly(methyl methacrylate) Diblock Copolymers. *Macromolecules* **22**, 2189-2194 (1989).

31. Harada, K. Plasma Etching Durability of Poly(methyl Methacrylate). *Journal of Applied Polymer Science* **26**, 1961-1973 (1981).

32. Huang, E. Perpendicular Orientation of Microphase Separated Morphologies near Neutral Surfaces. *review article section* (1998).

33. Pickett, G. T. & Balazs, A. C. Equilibrium Orientation of Confined Diblock Copolymer Films. *Macromolecules* **30**, 3097-3103 (1997).

CHAPTER 5

SUGGESTIONS FOR FUTURE WORK

Introduction

This study of polymer phase separation and morphology on chemically heterogeneous surfaces with molecular length scales, has borne interesting results and answered important questions about commensurability of length scales, molecular pattern matching, and the kinetics of forming ordered morphologies. Because of the experimental difficulty in preparing the chemically heterogeneous surfaces however, more detailed investigation of certain aspects of this thesis proved impossible. With this chapter I make some brief comments on possibilities for future work that can be achieved through a refinement of the substrate preparation process.

Facetted Surfaces

In Chapter 1, the preparation of facetted heterogeneous surfaces was outlined and discussed. One difficulty encountered was the kinetics of step formation on the facetted surfaces which results in a large initial distribution in both groove period and amplitude, yet a small average groove period. Figure 1.3 plots the peak position, or groove periodicity, for two substrates with a 1.3° miscut annealed at two temperatures, along with the half width at half maximum (HWHM) of the scattering from the measured peaks, as a function of anneal time. The data were collected from Xray scattering performed in-situ from Song. et al.[1] The data show that as the substrates are annealed for a longer time, average groove period increases, and the distribution decreases. This result was borne out as well in the data of table 1.3 taken from ex-situ AFM measurements on substrates prepared for this thesis. Consequently, in order to generate the shorter groove

periods needed for copolymer study, brief anneal times were used and a large distribution around the average groove period was tolerated. It is fortunate that the groove period distribution was not so large that it precluded any surface directed orientation of copolymers that were commensurate with the average groove period. Ideally, facetting conditions that could generate a much more uniform groove distribution on the nanometer length scale would be desired.

Two experiments should be considered to make improvements in substrate preparation. The first of course is to prepare substrates with virtually zero groove period distribution to determine more exactly the breadth of the window of commensurability. It is possible that fluctuations about the average periodicity allowed for increased surface direction in the slightly incommensurate copolymers prepared in ultrathin films. For example, groove periods in the range between 30 and 70 nm were not unusual on the 52 nm substrates, and locally some ordering in the vicinity of these defects could have occurred in the higher and lower molecular weight incommensurate copolymers. This ordering may have contributed to some broadening of the commensurability window, and an overestimate of its breadth. The second experiment is to generate substrates with the same average periodicity, yet different, increasing distributions about the average, and study the ordering of a single molecular weight copolymer on it. In this manner, the strength of the effect of substrate period fluctuations on ordering and defect generation attributable to substrate imperfections could be measured. Additionally, a deeper understanding of the tolerances allowed in commensurate systems may be gained, so that one could answer the question of 'how perfect' a substrate need to be to generate a 'near perfect' response in polymer morphology.

The substrates prepared with a gradient in facet period suffered significantly from the kinetics of facet formation. As shown in figures 1.9 and 1.10, the local distribution in groove period was larger than any gradient that developed in substrate periodicity. If we wish to study the effects of commensurability in a combinatorial manner, such that the ordering of a copolymer with a single period can be investigated on a controlled, varying substrate, the procedure for generating a surface gradient should be determined. Such a controlled gradient in surface roughness or chemistry could also benefit studies of wetting phenomena, surface neutrality, and commensurability effects in systems other than block copolymers. Despite the extended, half hour anneal of the final gradient substrate prepared, the average period distribution was still too large. Anneal times on the order of a day would perhaps be necessary to minimize the groove period distribution and generate a functional gradient. However, along with a thermal gradient generated along the trapezoidal surface, gradients in strain due to differences in local thermal expansion are produced. The coarsening process of the facet structure is directed by strain associated with the edges of the facets[2], and it is possible that despite an extended annealing time, the additional surface strain may overwhelm the ordering process and generate a gradient surface with a large distribution. It is even possible that a strong surface strain could produce a surface with a large distribution and no gradient at all. Further experimentation would be required to resolve this issue. If the use of uniform and gradient facetted surfaces in a variety of future experiments could be justified, then perhaps a thesis project focusing purely on refining and controlling the facetting process would be considered. At this time however, given the advances in ordering and orienting of block copolymer morphology over large areas, such thin films may be useful as

patterning templates long before the questions surrounding the kinetics of silicon step formation can be answered.

Strength of Surface Interactions

While the preferential wetting of poly(methyl methacrylate) (PMMA) and dewetting of polystyrene (PS) on silicon oxide (SiOx) has been established with a variety of previous experiments, the preferential wetting of gold by PS has not been as thoroughly investigated. A number of experiments were performed in this thesis in an attempt to confirm the preferential wetting of non polar gold by non polar PS, but the results were inconsistent. Thin film dewetting experiments performed in Chapter 2 designed to confirm this preference in fact showed that PMMA remained wet while PS dewet both SiOx and gold substrates after thin film annealing. Spin casting of homopolymer blend solutions from toluene in Chapter 2 showed the typical bilayer morphology of PMMA wetting SiOx in Figure 2.4, but lateral phase separation of the blend on both a gold and heterogeneous surface indicating surface neutrality, not a strong preference for PS. In Chapter 4, however, fracture cross sections of block copolymer films solution cast on homogeneous gold surfaces did not show the same beam damage as films cast on SiOx surfaces, indicating but not confirming the presence of a PS wetting layer at the gold substrate. Only the preferential adsorption of PS to the gold stripes after solution casting in Chapter 2, Figure 2.14 and 2.15, showed any indication of a preferential interaction between PS and Gold. These results suggest that a strong preference of PS for Au does not exist, rather gold is only slightly preferential to PS when a choice is given to both PS and PMMA to occupy the same surface area.

However, the exact nature and strength of this interaction has not been established. These results also indicate that mutually favorable/unfavorable interactions between two polymer species and a heterogeneous substrate may in fact not be necessary to establish patterning based on surface recognition. For these experiments we may consider the SiOx stripe strongly preferential, and the Au stripe effectively neutral, and we still find strongly surface directed patterning. The occupation of the SiOx stripes by the PMMA forces the PS into the gold regions, which is acceptable due to the weak interaction there.

These results therefore establish a precedent whereby an entire surface need not be strongly directing, and therefore easier to prepare, for all polymers to be studied upon it. As long as a surface is patterned with the appropriate length scale and surface interactions for one of the two polymer species, the desired surface pattern replication will be established. Experimental confirmation of this could be easily performed on the same experimental system, if the appropriate steps were taken to functionalize the heterogeneous substrates. For example, silane coupling of the appropriate small molecule to the oxide stripes of a SiOx/gold surface could alter the chemistry, making the oxide regions highly nonpolar, and hence preferential for PS instead of PMMA. Thus preferential segregation of PS to the non polar stripes and the resulting squeezing-out of PMMA to the neutral Au stripes should produce the same surface directed ordering with the opposite surface preferential interaction. The facile functionalization of a gold surface with a thiol-substituted small molecule could also allow for further variation in surface functionalization so that a wide range of new polymer systems and different strengths of interactions can be studied.

Structure of Defects

Defects in the lamellar morphology of solution cast films of block copolymer on heterogenenous surfaces are apparent in all oriented films. As mentioned in Chapter 3, the defects are present because of the mismatch between the natural copolymer period and the substrate period, and the strong confinement of the copolymer at the substrate interface which forces the copolymer to strain to match the substrate period to minimize interfacial and strain energy. The data show a clear trend in both the concentration of defects as well as the dominant defect morphology as a function of δ, the degree of commensurability. As one would expect, the farther the value of δ from 1, the larger the defect concentration. What is interesting is the change in the morphology of the defects as a function of δ. For films in tension, lamellar stretching and compression, undulations, dislocations, and small grain reorientations are present, while for films in compression, large reoriented grain defects dominate. Although the calculations of Chen and Chakrabarti have predicted similar defect structures[3,4], a more thorough investigation of the structure of defects as a function of δ is lacking. Using electron-beam lithography, a patterned, chemically heterogeneous surface could be prepared with a number of micron sized patches with different periodicities. Such a surface would be ideal for studying defects due to the controlled length scale and small patch area, which would prevent multiple defect structures from overlapping. A carefully prepared gradient facetted surface would serve the same purpose nicely.

Window of Commensurability

The experimental results collected here, as well as the calculations and simulations performed by other groups, have gone a long way to explain the existence of a window of commensurability. However, because of the limited parameter space explored in the theoretical studies, only this experimental work has placed a quantitative limit to the breadth of the window in thin and thick films. Experimentally, however, we are limited to the system we choose to investigate and therefore the limits found here are quantitative only for that system. While there is qualitative agreement between experimental and theoretical predictions, no strong statements can yet be made to predict the structure of a new polymer/substrate system. An appropriately structured theoretical investigation whereby one can continuously vary film thickness, molecular weight, the strength and periodicity of polymer/surface interactions, and the strength of polymer/polymer phase separation would go a long way toward assembling a more complete picture of how commensurability affects polymer morphology. Additionally, a more facile and robust method of substrate patterning could open the door to a more complete experimental study, as noted above. Questions concerning the breadth of the window of commensurability as a function of molecular weight, the type and strength of defects as a function of film thickness and commensurability, and the strength of surface interactions needed to orient copolymer films, could be answered for a wide range of polymer/substrate systems with such an improvement in experimental technique.

Conclusion

Our understanding of polymers on heterogeneous surfaces is far from complete, a consequence of doing research on a topic that's slightly ahead of its time. This thesis took a gamble that a crude, yet effectively patterned surface could template the self-organization and phase separation of homopolymer blends and block copolymers on a molecular length scale, and fortunately paid off with some unique and elegant results. While qualitative trends have been established, the next step to take is with an experimental system whereby quantitative measurements can be made on a variety of polymer and substrate systems. The weak link is the preparation of controlled, patterned, chemically heterogeneous substrates with *consistent* molecular length scales, as no current technique fits the bill. Optimization of substrate preparation techniques will enable not only an understanding of pattern replication physics, but serve as a foundation for substrate preparation for the structuring of arrays of parallel and serial nanoscopic devices in the future. We are approaching a time in scientific history where molecular nanostructures with computing power, sensing and signaling ability, memory and gain applications, and even as yet undiscovered properties, will need controllable 'supporting-substrate' preparation techniques. Understanding the self assembly on surfaces of the block copolymer materials which are the templates for these future devices will place those in control of this knowledge at the forefront of nanostructured device assembly. From this perspective, more work on substrate patterning and copolymer self assembly is warranted with a strong focus on substrate preparation techniques.

References

1. Song, S., Mochrie, S. G. J. & Stephenson, G. B. Facetting Kinetics of Stepped Si(113) Surfaces: A Time-Resolved X-Ray Scattering Study. *Physical Review Letters* **74**, 5240-5243 (1995).

2. Song, S., Yoon, M., Mochrie, S. G. J., Stephenson, G. B. & Milner, S. T. Facetting Kinetics of Stepped Si(113) Surfaces: Dynamic Scaling and Nano-scale Grooves. *Surface Science* **372**, 37-63 (1997).

3. Chen, H. & Chakrabarti, A. Morphology of Thin Block Copolymer Films on Chemically Patterned Substrates. *Journal of Chemical Physics* **108**, 6897-6905 (1998).

4. Chakrabarti, A. & Chen, H. Block Copolymer Films on Patterned Surfaces. *Journal of polymer Science, B* **36**, 3127-3136 (1998).

BIBLIOGRPAHPY

Anastasiadis, S. H., Russell, T. P., Satija, S. K. & Majkrzak, C. F. The Morphology of Symmetric Diblock Copolymers as Revealed by Neutron Reflectivity. *Journal of Chemical Physics* **92**, 5677-5691 (1990).

Balazs, A. C., Huang, K., McElwain, P. & Brady, J. E. Polymer Adsorption on Laterally Heterogeneous Surfaces: A Monte Carlo Computer Model. *Macromolecules* **24**, 714-717 (1991).

Baumgatrner, A. & Muthukumar, M. Effect of Surface Roughness on Absorbed Polymers. *Journal of Chemical Physics* **94**, 4062-4070 (1991).

Bijsterbosch, H. D., Cohen Stuart, M. A. & Fleer, G. J. Adsorption of Graft Copolymers onto Silica and Titania. *Macromolecules* **31**, 8981-8987 (1998).

Böltau , M., Walheim, S., Mlynek, J., Krausch, G. & Steiner, U. Surface Induced Structure Formation of Polymer Blends on Patterned Substrates. *Nature* **391** (1998).

Brulet, A., Boue, F., Menelle, A. & Cotoon, J. P. Conformation of Polystyrene Chain in Ultrathin Films Obtsined by Spin Coating. *Macromolecules* **33**, 997-2001 (2000).

Chakrabarti, A. & Chen, H. Block Copolymer Films on Patterned Surfaces. *Journal of Polymer Science*, **B 36**, 3127-3136 (1998).

Chan, V. Z.-H. et al. Ordered Bicontinuous Nanoporous and Nanorelief Ceramic Films from Sefl Assembling Polymer Precursors. *Science* **286**, 1716-1719 (1999).

Chen, H. & Chakrabarti, A. Morphology of Thin Block Copolymer Films on Chemically Patterned Substrates. *Journal of Chemical Physics* **108**, 6897-6905 (1998).

Chen, W.-L. & Shull, K. R. Hydrophilic Surface Coatings from Acrylic Block Copolymers. *Macromolecules* **32**, 6298-6306 (1999).

Chou, S. Y., Krauss, P. R. & Renstrom, P. J. Nanoimprint Lithography. *Journal of Vacuum Science Technology B* **14**, 4129-4133 (1996).

Cognard, J. & Biochard, C. in Adhesion (ed. Allen, K. W.) 169-193 (Elsevier Applied Science, London/NYC, 1984).

Coulon, G., Daillant, J., Collin, B., Benattar, J. J. & Gallot, Y. Time Evolution of the Free Surface of Ultrathin Copolymer Films. *Macromolecules* **26**, 1582-1589 (1993).

de Gennes, P. G. Adsorption on Stripes. private communication (1999).

De Rosa, C., Cheolmin, P., Thomas, E. L. & Lotz, B. Microdomain Patterns from Directional Eutectic Solidification and Epitaxy. *Nature* **405**, 433-437 (2000).

Fasolka, M. J., Harris, D. J., Mayes, A. M., Yoon, M. & Mochrie, S. G. J. Observed Substrate Topography-Mediated Lateral Patterning of Diblock Copolymer Films. *Physical Review Letters* **79**, 3018-3021 (1997).

Fasolka, M. J., Banerjee, P., Mayes, A. M., Pickett, G. & Balazs, A. C. Morphology of Ultrathin Supported Diblock Copolymer Films: Theory and Experiemnt. *Macromolecules* **33**, 5702-5712 (2000).

Fetters, L. J., Lohse, D. J., Richter, D., Witten , T. A. & Zirkel, A. Connection between Polymer Molecular Weight, Density, Chain Dimensions, and Melt Viscoelastic Properties. *Macromolecules* **27**, 4639-4647 (1994).

Fink, Y., Urbas, A. M., Bawendi, M. G., Joannopoulos, J. D. & Thomas, E. L. Block Copolymers as Photonic Bandgap Materials. *Journal of Lightwave Technology* **17**, 1963-1969 (1999).

Fowkes, F. M. Additivity of Intermolecular Forces at Interfaces. I. Determination of the Contribution to Surface and Interface Tensions of Dispersion Forces in Various Liquids. *Journal of Physical Chemistry* **67**, 2538-2541 (1963).

Fukunaga, K., Elbs, H. & Krausch, G. Thin Film Phase Separation on a Nanoscopically Patterned Surface. *Langmuir* **16**, 3473-3477 (2000).

Garetz, B. A. et al. Orientation Correlations in Lamellar Block Copolymers. *Macromolecules* **29**, 4675-4679 (1996).

Green, P. F., Christensen, T. M., Russell, T. P. & Jerome, R. Surface Interaction in Solvent-Cast Polystyrene/Poly(methyl methacrylate) Diblock Copolymers. *Macromolecules* **22**, 2189-2194 (1989).

Halperin, A., Sommer, J. U. & Daoud, M. Copolymers at Striped Surfaces: Coupling Effects. *Europhysics Letters* **29**, 297-302 (1995).

Harada, K. Plasma Etching Durability of Poly(methyl Methacrylate). *Journal of Applied Polymer Science* **26**, 1961-1973 (1981).

Harrison, C., Park, M., Chaikin, P. M., Register, R. A. & Adamson, D. H. Lithography with a Mask of Block Copolymer Microstructures. *Journal of Vacuum Science and Technology B* **16**, 544-552 (1998).

Heier, J., Kramer, E. J., Walheim, S. & Krausch, G. Thin Diblock Copolymer Films on Chemically Heterogeneous Surfaces. *Macromolecules* **30**, 6610-6614 (1997).

Henkee, C. S., Thomas, E. L. & Fetters, L. J. Effect of Surface Constraints on the Ordering of Block Copolymer Domains. *Journal of Materials Science* **23**, 1685-1694 (1988).

Huang, E. Perpendicular Orientation of Microphase Separated Morphologies near Neutral Surfaces. review article section (1998).

Israelachvili, J. in Intermolecular and Surface Forces 176-213 (Academic Press, San Diego, 1992).

Karim, A. et al. Phase-Separation-Induced Surface Patterns in Thin Polymer Blend Films. *Macromolecules* **31**, 857 (1998).

Karim, A. et al. Phase Separation of Ultrathin Polymer-Blend Films on Patterned Substrates. *Physical Review E* **57**, R6273-R6276 (1998).

Kellogg, G. J. et al. Observed Surface Energy Effects in Confined Diblock Copolymers. *Physical Review Letters* **76**, 2503-2506 (1996).

Kikuchi, M. & Binder, K. Microphase Separation in Thin Films of the Symmetric Diblock-Copolymer Melt. *Journal of Chemical Physics* **101**, 3367-3377 (1994).

Kim, G. & Libera, M. Kinetic Constraints on the Development of Surface Microstructure in SBS Thin Films. *Macromolecules* **31**, 2670-2672 (1998).

Kim, G. & Libera, M. Morphological Development in Solvent-Cast Polystyrene-Polybutadiene-Polystyrene (SBS) Triblock Copolymer Thin Films. *Macromolecules* **31**, 2569-2577 (1998).

Koneripalli, N., Singh, N., Levicky, R., Gallagher, P. D. & Satija, S. K. Confined Block Copolymer Thin Films. *Macromolecules* **28**, 2897-2904 (1995).

Koneripalli, N. et al. Confinement-Induced Morphological Changes in Diblock Copolymer Films. *Langmuir* **12**, 6681-6690 (1996).

Lambooy, P. et al. Observed Frustration in Confined Block Copolymers. *Physical Review Letters* **72**, 2899-2902 (1994).

Lammertink, R. G. H. et al. Nanostructured Thin Films of Organic-Organometallic Block Copolymers: One-Step Lithography with Poly(ferrocenylsilanes). *Advanced Materials* **12**, 98-102 (2000).

Lepine, Y. & Caille, A. The Configuration of a Polymer Chain Interacting with a Plane Interface. *Canadian Journal of Physics* **56**, 403-408 (1977).

Lipatov, Y., Chornaya, V. & Todosijchuk, T. Adsorption from Two-Phase Solution of Polymer Blends. *Journal of Colloid and Interface Science* **188**, 32-38 (1996).

Mansky, P., Liu, Y., Huang, E., Russell, T. P. & Hawker, C. Controlling Polymer-Surface Interactions with Random Copolymer Brushes. *Science* **275**, 1458 (1997).

Mansky, P. et al. Interfacial Segregation in Disordered Block Copolymers: Effect of Tunable Surface Potentials. *Physical Review Letters* **79**, 237-240 (1997).

Mochrie, S. G. J., Song, S., Yoon, M., Abernathy, D. L. & Stephenson, G. B. Facetting of Stepped Silicon (113) Surfaces: Self Assembly of Nanoscale Gratings. *Physica B, Condensed Matter* **221**, 105-125 (1996).

Muller-Buschbaum, P., Vanhoorne, P., Scheumann, V. & Stamm, M. Observation of Nano-Dewetting Structures. *Europhysics Letters* **40**, 655-660 (1997).

Petera, D. & Muthukumar, M. Effect of Patterned Surface on Diblock-Copolymer Melts and Polymer Blends Near the Critical Point. *Journal of Chemical Physics* **107**, 9640 (1997).

Petera, D. & Muthukumar, M. Self-Consistent Field Theory of Diblock Copolyer Melts at Patterned Surfaces. *Journal of Chemical Physics* **109**, 5101-5107 (1998).

Pereira, G. G. & Williams, D. R. M. Diblock Copolymer Thin Films on Heterogeneous Striped Surfaces: Commensurate, Incommensurate, and Inverted Lamellae. *Physical Review Letters* **80**, 2849-2852 (1998).

Pereira, G. G. & Williams, D. R. M. Diblock Copolymer Films on Striped Surfaces: Commensurate, Incommensurate and Inverted Lamellae. *preprint* (1997).

Pereira, G. G. & Williams, D. R. M. Equilibrium Properties of Diblock Copolymer Thin Films on a Heterogeneous, Striped Surface. *Macromolecules* **31**, 5904-5915 (1998).

Pickett, G. T., Witten, T. A. & Nagel, S. R. Equilibrium Surface Orientation of Lamellae. *Macromolecules* **26**, 3194-3199 (1993).

Pickett, G. T. & Balazs, A. C. Equilibrium Orientation of Confined Diblock Copolymer Films. *Macromolecules* **30**, 3097-3103 (1997).

Puri, S., Binder, K. & Frisch, H. L. Surface effects on spinodal decomposition in binary mixtures: The case with long ranged surface fields. *Physical Review E* **56**, 6991-7000 (1997).

Reiter, G. et al. Nanometer-Scale Surface Patterns with Long-Range Order Created by Crystallization of Diblock Copolymers. *Physical Review Letters* **83**, 3844-3847 (1999).

Reiter, G. Dewetting of Thin Polymer Films. *Physical Review Letters* **68**, 75-78 (1992).

Reiter, G. & Sommer, J.-U. Crystallization of Adsorbed Polymer Monolayers. *Physical Review Letters* **80**, 3771-3774 (1998).

Reiter, G. Unstable Thin Polymer Films: Rupture and Dewtting Processes. *Langmuir* **9**, 1344-1351 (1993).

Rockford, L. et al. Polymers on Nanoperiodic, Heterogeneous Surfaces. *Physical Review Letters* **82**, 2602-2605 (1999).

Russell, T. P., Coulon, G., Deline, V. R. & Miller, D. C. Characteristics of the Surface-Induced Orientation for Symmetric Diblock PS/PMMA Copolymers. *Macromolecules* **22**, 4600-4606 (1989).

Semenov, A. N., Bonet-Avalos, J., Johner, A. & Joanny, J. F. Adsorption of Polymer Solutions onto a Flat Surface. *Macromolecules* **29**, 2179-2196 (1996).

Song, S., Mochrie, S. G. J. & Stephenson, G. B. Facetting Kinetics of Stepped Si(113) Surfaces: A Time-Resolved X-Ray Scattering Study. *Physical Review Letters* **74**, 5240-5243 (1995).

Song, S., Yoon, M., Mochrie, S. G. J., Stephenson, G. B. & Milner, S. T. Facetting Kinetics of Stepped Si(113) Surfaces: Dynamic Scaling and Nano-scale Grooves. *Surface Science* **372**, 37-63 (1997).

Steiner, U., Klein, J., Eiser, E., Budkowski, A. & Fetters, L. J. Complete Wetting from Polymer Mixtures. *Science* **258**, 1126-1129 (1992).

Walheim, S., Böltau , M., Mlynek, J., Krausch, G. & Steiner, U. Structure Formation via Polymer Demixing in Spin-Cast Films. *Macromolecules* **30**, 4995-5003 (1997).

Walton, D. G., Kellogg, G. J., Mayes, A. M., Lambooy, P. & Russell, T. P. A free Energy Model for Confined Diblock Copolymers. *Macromolecules* **27**, 6225-6228 (1994).

Wang, Q., Yan, Q., Nealey, P. F. & de Pablo, J. J. Monte Carlo Simulations of Diblock Copolymer Thin Films Confined between Chemically Heterogeneous Hard Surfaces. *Macromolecules* **33**, 4512-4525 (2000).

Wang, Q., Nath, S. K., Graham, M. D., Nealey, P. F. & de Pablo, J. J. Symmetric Diblock Copolymer Thin Films Confined between Homogeneous and Patterned Surfaces: Simulations and Theory. *Journal of Chemical Physics* **112**, 9996-10010 (2000).

Yoon, M., Mochrie, S. G. J., Tate, M. W., Gruner, S. M. & Eikenberry, E. F. Periodic Facetting of a Si (113) surface miscut towards (1-10). *Surface Science* **411**, 70-85 (1998).